Modelling the Shrinkage Behaviour of Recycled Concrete Aggregate and Cement Stabilised Materials

By

Nina Maria Agnello

Thesis presented in fulfilment of the requirements for the degree of Master of Engineering in Civil Engineering in the Faculty of Engineering at Stellenbosch University

The financial assistance of the National Research Foundation (NRF) towards this research is hereby acknowledged. Opinions expressed and conclusions arrived at, are those of the author and are not necessarily attributed to the NRF.

Supervised by:

Mrs Chantal Rudman

Prof. Kim Jenkins

March 2018

Declaration

Plagiarism is the use of ideas, material and other intellectual property of another's work and to present is as my own.

I agree that plagiarism is a punishable offence because it constitutes theft.

I also understand that direct translations are plagiarism.

Accordingly all quotations and contributions from any source whatsoever (including the internet) have been cited fully. I understand that the reproduction of text without quotation marks (even when the source is cited) is plagiarism.

I declare that the work contained in this dissertation, except otherwise stated, is my original work and that I have not previously (in its entirety or in part) submitted it for grading in this module or another module.

Date: March 2018

Abstract

Cement stabilisation of subbases is an effective method to increase the strength, permeability, stability and performance of a pavement structure. Stabilisation is used to improve marginal quality materials, by recycling the in-situ material which conserves non-renewable gravel sources and lowers transportation costs.

An alternative to stabilisation of virgin aggregates is to use Recycled Concrete Aggregate (RCA) which can have, some inherent self-cementation properties. RCA has the potential to be used as a lightly cemented material without any additional cement. RCA can be harvested from demolished buildings or old concrete pavements through crushing of the concrete and forming concrete aggregates. This saves quarrying for natural aggregate and reduces associated costs. Other environmental benefits include fewer landfills and the reduction in cement usage. Cement production is estimated to contribute 5% of global CO_2 emissions, (Worrell et al., 2001).

The primary failure of a stabilised layer is load induced fatigue cracking and shrinkage cracking. As RCA has some self-cementing properties due to the active latent cement particles present, there is potential for RCA to undergo similar failure mechanisms.

The challenge with RCA is that it can be considered an inconsistent material in comparison with natural aggregates. Factors such as parent material mineralogy, time and environment of construction, and level of hydration of the material vary from different RCA sources. This can lead to difficultly in properly characterising the material.

This study focuses on the characterisation tests and cylindrical shrinkage tests of a stabilised Malmesbury Hornfels and Metamorphic Andesite, as well as RCA. RCA contains a significant percentage of active latent cement which influences the properties of the material. It is an objective of this study to evaluate the active latent cement content of RCA and equate that to an equivalent stabilised granular material. It is difficult to accurately quantify the amount of active latent cement present. Therefore, the extent of active latent cement content was analysed by comparing a RCA that has undergone some exposure through a repeated wetting and drying procedure. This exposure activates some of the active latent cement and decreases the self-cementing properties. The preliminary tests provide the characteristics of the material needed for causal analysis associated with

the cylindrical shrinkage tests. The maximum axial shrinkage is addressed and compared. The influence of cement, host material, aggregate size and humidity on shrinkage of RCA and Cement Treated Material (CTM) is evaluated and compared to literature. As drying shrinkage cracking is the common failure mechanism of CTM, the study sets out to predict the shrinkage crack pattern i.e. the width and spacing of cracks within a RCA and CTM pavement layer.

A shrinkage cracking model for concrete pavements was established by Houben (2008). The model estimates shrinkage crack widths and spacing. It includes variables such as time and temperature variations, tensile and compressive strengths of materials, stress relaxation and friction between pavement layers. The Houben model works on the basis that cracks form when there is a build-up of tensile stresses from the fluctuations in temperature and humidity. Cracks will form when the tensile strength of the material is less than that of the tensile stresses developed (Houben, 2008).

Three materials are modelled with an adapted Houben Shrinkage Crack Model, namely Andesite (2%), Unexposed RCA (0%) and Exposed RCA (0%). It is found that the Unexposed RCA showed higher levels of self-cementation than the Exposed RCA. However, the potential for shrinkage cracking of Unexposed RCA is a reality and must be taken into consideration when designing.

Opsomming

Sementstabilisering van stutlae is effektief daarin om die sterkte, duursaamheid, deurlaatbaarheid, stabiliteit en gedrag van 'n plaveiselstruktuur te bevorder. Stabilisasie word gebruik om grensgehalte materiale te verbeter deur die in-situ materiaal te herwin. Sodoende bly nie-hernubare gruisbronne behoue, en vervoerkoste en kweekhuisgasvrystellings word verlaag.

'n Alternatief vir die stabilisering van gruisaggregaat is om Herwinde Betonaggregaat (RCA) met inherente self-sementeringseienskappe, te gebruik. RCA het soms die potensiaal om as 'n gedeeltelike gesementeerde materiaal, sonder toevoeging van addisionele sement, gebruik te word. RCA kan vanaf gesloopte geboue of ou betonplaveisellae verkry word, deur die beton af te breek om aggregaat te vorm. Die behoefte aan steengroewe vir natuurlike aggregate en die gepaardgaande koste word dus verminder. Ander omgewingsvoordele sluit minder stortingsterreine en die vermindering van sementverbruik in. Daar word beraam dat sementproduksie 5% aan die globale vrystelling van CO_2-bydra (Worrell et al., 2001).

Gestabiliseerde lae word dikwels ontwerp vir sterkte en nie noodwendig vir duursaamheid nie. Dit lei tot die primêre faling van lasgeïnduseerde vermoeiings- en krimpkrake. ‘n Uitdaging van RCA is dat die samestelling as wisselvallig in vergelyking met natuurlike aggregate, beskou kan word. Faktore soos die mineralogie van die oorsprongmateriaal, tyd en omgewing van konstruksie, en hidrasie van die materiaal verskil van verskillende RCA-bronne. Dit kan dus uitdagend wees om die materiaal te karakteriseer.

Hierdie studie fokus op die karakteriseringstoetse en silindriese krimptoetse van gestabiliseerde Malmesbury Hornfels en Metamorphic Andesite, sowel as RCA. RCA bevat 'n beduidende persentasie latente sement wat die eienskappe van die materiaal beïnvloed. Dit is 'n doelwit van hierdie studie om die latente sementinhoud van RCA te evalueer en te vergelyk met 'n ekwivalente gestabiliseerde gruismateriaal. Weens die uitdaging om die hoeveelheid latente sement teenwoordig akkuraat te kwantifiseer, is die teenwoordigheid daarvan ontleed deur RCA wat aan herhaalde benatting- en

drogingsprosesse blootgestel is, te vergelyk. Hierdie blootstelling aktiveer van die latente sement en verminder die self-sementeringseienskappe. Die voorlopige toetse bepaal die eienskappe van die materiaal wat benodig word vir oorsaaklike analise in verband met die silindriese krimptoetse. Die maksimum aksiale krimp word aangespreek en vergelyk. Die invloed van sement, gasheermateriaal, aggregaatgrootte en humiditeit op krimping van RCA en CTM word geëvalueer en vergelyk met literatuur. Aangesien drogingskrimpkrake 'n algemene oorsaak van faling vir CTM is, is daarop gefokus om die krimppatroon, dws die wydte en spasiëring van krake binne 'n RCA- en CTM-plaveisellaag, te voorspel.

‘n Model wat die wydte en spasiëring van krimpkrake vir betonplaveilsels beraam, is deur Houben (2008) ontwikkel. Dit sluit veranderlikes vir onder andere tyd en temperatuur, trek- en druksterkte, spanningsontlading en wrywing tussen plaveisel lae, in. Die Houben-model veronderstel dat krake as gevolg van spannings wat opbou, veroorsaak deur ’n verandering in temperatuur en humiditeit, vorm. Krake vorm indien die trekspannings wat ontstaan, die treksterkte van die materiaal oorskry. (Houben, 2008).

Drie materiale, naamlik Andesite (2%), nie-blootgestelde RCA (0%) en blootgestelde RCA (0%), is gemodelleer met 'n aangepaste Houben-Model. Daar is bevind dat die nie-blootgestelde RCA hoër vlakke van self-sementering as die blootgestelde RCA toon. Die potensiaal vir krimpkrake van nie-blootgestelde RCA is egter 'n realiteit en moet in die ontwerp in ag geneem word.

Acknowledgments

I would like to thank the following people who helped to turn this study into a reality:

→ Firstly Mrs Rudman and Prof Jenkins for their unwavering guidance, support and encouragement.

→ Dion and Oom Johan for their patient assistant in the workshop.

→ Gavin, Collin and Eric for their help in the laboratory.

→ Riaan for organisation and help in the laboratory.

→ The NRF for finances and opportunity to further my studies.

→ My office mates Elaine, Ricki-Lee and Zaandre for the comradery and friendship which made this experience all the more enjoyable.

→ My parents for their unconditional love and support.

→ Leo for always believing in me.

Contents

List of figures

List of tables

Nomenclature

α	Coefficient of thermal expansion
c_1	Hydration Coefficient
$\Delta\varepsilon$	Reduction in tensile strain midway between two cracks
$\Delta\sigma$	Reduction of tensile stress [MPa]
Δw	Crack growth [mm]
E	Elastic Modulus [MPa]
ε	Maximum tensile strain
ε_S	Shrinkage strain
ε_T	Thermal strain
f_{ck}	Characteristic average compressive strength [MPa]
f_{cm}	Average compressive strength [MPa]
f_{ctm}	Average tensile strength [MPa]
γ	Coefficient of sliding friction 3.8 (Mbaraga, 2015)
g	Gravity at 9.8m / sec^2
L_a	Breathing length [m]
L_w	Distance between cracks [m]
ρ	Material density [kg/m^3]
R	Relaxation factor
S	Maximum shrinkage
σ(t)	Induced tensile stress due to shrinkage at time t in hours
t	Time
$T_{ampyear}$	Annual average air temperature amplitude [°C]

$T_{aveyear}$	Average annual temperature [°C]
$T_{climate}$	Climate dependant temperature [°C]
T_{daily}	Daily average minimum temperature [°C]
$T_{hydration}$	Hydration temperature [°C]
T_{road}	Road temperature [°C]
$T_{seasonal}$	Average seasonal temperature [°C]
$w_{friction}$	Crack width due to friction [mm]
w_i	Initial crack width [mm]
$w_{shrinkage}$	Crack width due to shrinkage [mm]

Abbreviations

AASHTO	American Association of State Highway and Transportation Officials
ANDE	Andesite
ASR	Alkali Silica Reaction
BSM	Bitumen Stabilised Materials
C	Cement
CDW	Concrete Demolition Waste
CSM	Cement Stabilised Materials
CSH	Calcium Silica Hydrate
CTE	Coefficient of Thermal Expansion
CTM	Cement Treated Materials
CTMG	Cement Treated Mix Granulates
DC	Degree of Compaction
FWD	Falling Weight Deflectometer
HORN	Hornfels
HVS	Heavy Vehicle Simulation
ICC	Initial Consumption of Cement
ITS	Indirect Tensile Strength
JCP	Joint Concrete Pavement
LL	Liquid Limit
M	Masonry Content
MDD	Maximum Dry Density
NC	New Concrete
OMC	Optimum Moisture Content

PI	Plastic Index
PL	Plastic Limit
PVC	Polymerizing Vinyl Chloride
RCA	Recycled Concrete Aggregate
RCA.E	Exposed Recycled Concrete Aggregate
RCA.U	Unexposed Recycled Concrete Aggregate
RMA	Recycled Masonry Aggregate
RH	Relative Humidity
SANS	South African National Standards
SL	Shrinkage Limit
UCS	Unconfined Compression Strength
XRD	X- Ray Diffraction

Chapter 1

Introduction

1.1 Overview

Cement stabilisation of subbases is an effective method to increase the strength, durability, permeability, stability and performance of a pavement structure. Apart from the benefits associated with stabilised layers, the material does not come without its challenges.

Paige-Greene (2008) refers to the experience in the South African environment which summates to number of decades but additionally also highlights the numerous problems that have increasingly emerged in recent years due to stabilisation of layers, including the manifestation of cracking due to shrinkage of the layers.

Stabilisation of granular material has been implemented successfully in pavements for many years. Moreover, good quality granular material such as crushed stone aggregates is however a non-renewable resource and will run out at some stage in the future.

Countries such as the Netherlands have already experienced serious shortages, and have implemented a solution of using Recycled Concrete Aggregates (RCA) as a supplementary material. RCA has proved to be an adequate substitute in other countries, however in South Africa it is still largely perceived as Recycled Concrete Waste (RCW). These perceptions are rapidly changing and recent utilisation of alternative materials gained increased focus. Many questions still remain on the performance of this material, not only for potential use as a stabilised layer (with the addition of cement), but also in its "natural" form without the addition of cement. Would an RCA layer pose the same inherent challenges as a stabilised granular layer? How does the shrinkage of RCA compare to that of a stabilised material?

Research on the performance and durability of RCA is necessary to be able to benchmark the application of this material. This study investigates the shrinkage cracking behaviour

of RCA and how it compares to Cement Treated Material (CTM). This is achieved though laboratory testing of RCA and CTM and further modelling of these results. The model provides an indication of the potential crack widths and spacing within a layer which can be used as benchmarking conclusions on the durability and performance of the research materials.

1.2 Problem Statement

RCA has the potential to be used as an equivalent granular material. However, industry remains wary of utilising this as a material in road construction practices. This is due to lack of specifications and knowledge that encourage the implementation. Shrinkage plays a large role in the ultimate durability of a pavement. Therefore, the shrinkage of RCA used as a stabilised material (with the addition of stabiliser) needs to be further investigated. A clear understanding of the potential challenges due to its self-cementing properties (no addition of stabiliser) also need to be considered.

1.3 Research Objectives and Motivation

The primary objective of this study is to achieve an understanding of the engineering properties that govern the performance of RCA. In particular the mechanisms that govern the manifestation of durability aspects such as shrinkage. This will enable the benchmarking of RCA against granular and cemented materials.

The secondary objectives of this study include:

→ *To gain an understanding on the variables that influence the durability behaviour of stabilised materials such as cement content, moisture content, curing period, material density, plasticity and host material in order to understand how this manifests into shrinkage cracking.* The influence of cement has a significant effect on shrinkage due to hydration. The additional effect of parent/host material could have an influence on shrinkage due to the aggregate mineralogy and grading which contributes to packing and density.

→ *To evaluate the active latent cement content of RCA and equate that to an equivalent stabilised granular material.* Depending on the source, RCA may

contain active latent cement which influences the properties of the material. It is difficult to accurately quantify the amount of active latent cement present in RCA and therefore we cannot predict its behaviour as accurately as with a granular material. By performing the same characterisation tests on both stabilised granular material and RCA, it is possible to get a better understanding of the material through comparison.

→ *To predict the shrinkage crack pattern i.e. the width and spacing of cracks within a RCA and CTM pavement layer.* The laboratory shrinkage test data can be modelled and be used in an adapted version of the Houben Shrinkage Crack Model (2008). Through modelling of the crack pattern, conclusions can be drawn with regards to the long-term performance and durability of a pavement.

1.4 Scope and Limitations

This research focusses on the shrinkage and consequential shrinkage cracking for cement stabilised granular materials and RCA. The granular research materials included a Metamorphic Andesite and Malmesbury Hornfels, which differ slightly in plasticity. In order to analyse the influence of the latent cement percentage present in RCA, exposed and unexposed versions of the same RCA were considered.

This study investigated each research material at two different cement percentages. The Andesite and Hornfels were stabilised at 2% and 4%, while both RCAs were investigated at 0% and 2% additional cement. The characterisation tests included ICC, pH of suspended soils, Atterberg Limits, UCS and ITS tests. These tests were used to determine the characteristics of each material.

The shrinkage cracking is modelled for Metamorphic Andesite, Unexposed and Exposed RCA. The crack spacings and widths are determined and are compared, as well as the time to initial cracking.

Due to time and material restrictions:

→ Only 28–100 days of shrinkage data could be collected, unlike Xuan (2012) who collected data for 360days.

→ The five materials tested were only stabilised at two percentages of cement. Whereas other research has tested at three different percentages of cement, (Mbaraga, 2015; Semugaza, 2016).

→ Assumptions such as the Elastic Modulus, relaxation and friction factors, thermal coefficient and temperatures were made in order to further develop the Houben shrinkage model (2008).

1.5 Thesis Layout

Chapter 2 Materials:

Chapter 2 and 3 form part of a two-part Literature Study. This chapter discusses the research materials investigated namely, RCA and CTM. An overview of each material is provided as well as a brief introduction to its shrinkage cracking potential.

Chapter 3 Shrinkage Cracking:

This chapter explains the concept of physical shrinkage mechanisms of soils and granular materials. The various types of shrinkages are explained namely autogenous, drying, thermal and carbonation. The effect that shrinkage has on cracking in a pavement layer is further discussed. The influencing factors on shrinkage cracking are addressed in detail. Literature on previous laboratory testing is considered and used as a basis for the development of an experimental framework for this study.

Chapter 4 Experimental Framework:

The experimental framework provides background on how the research materials (CTM and RCA) were acquired and prepared. This chapter also discusses the preliminary characterisation tests and the development of the cylindrical shrinkage tests performed.

Chapter 5 Test Results and Discussion:

This chapter provides and discusses all material characterisation tests results such as the ICC, pH of suspended soils, Atterberg Limits, UCS and ITS. The results of the various materials tested are compared and conclusions are drawn. Furthermore, the shrinkage trends of the research materials are discussed in relation to the cement content, host

material, aggregate size and humidity. Finally, these results are compared with that of previous research.

Chapter 6 Overview of Shrinkage Crack Model*:*

This chapter explains a shrinkage crack model that predicts the crack width and spacing for cement stabilised material. The original model was by Houben (2008) and was adapted to suit the material characteristics of this study.

Chapter 7 Modelling of Shrinkage Results:

This chapter discusses the results of the shrinkage crack model. The results are used to analyse how the research materials will behave and benchmark the potential for cracking against that of standard granular stabilised materials.

Chapter 8 Conclusions and Recommendations:

This final chapter provides a summary of the findings of this study. Insights and improvements are suggested for further research in this field.

Chapter 2

Materials

Chapters 2 and 3 form a two-part Literature Study. This chapter provides the fundamental understanding of the building blocks/materials and the attributes that govern the behaviour of CTM and RCA as well as the performance and challenges. Thereafter Chapter 3 provides detail into the mechanism of shrinkage in particular.

This chapter discusses the research materials that are investigated in this study. Cement stabilisation of soils or aggregates is industry's primary solution to improve the strength and durability of an unbound layer in a pavement structure. CSM has been thoroughly researched over the years, with standards and specifications endorsing confident usage. RCA is a renewable and recyclable material. Although it is relatively new and unfamiliar in South Africa, it is a material that could perform as a supplementary or equivalent granular material. This study investigates the potential shrinkage cracking behaviour of RCA and how it compares to CTM.

2.1 Cement Treated Base

2.1.1 Overview

The aim of stabilisation is to increase the strength, permeability and stability of a material, (Li, 2014). By mixing a stabiliser, such as cement with a soil or aggregate, it becomes a bound material. Cement stabilisation is often used in subbases as it provides structural rigidity, improves load spreading and reduces stresses imposed on the subgrade. Because the layer is solid and stiff, it serves as an "anvil" for the compaction of a granular base layer, and therefore increases the ability to withstand deformation, (TRL, 2003).

From Figure 2-1 the typical South African pavement structure as well as the critical stress/strain parameters per layer are observed. The pavement consists of a granular base

layer, following a cemented subbase layer. The critical parameter for a granular layer is shear safety factor, while a cemented layer is vulnerable to tensile strain at the bottom of the layer, (SANRAL, 2014a)

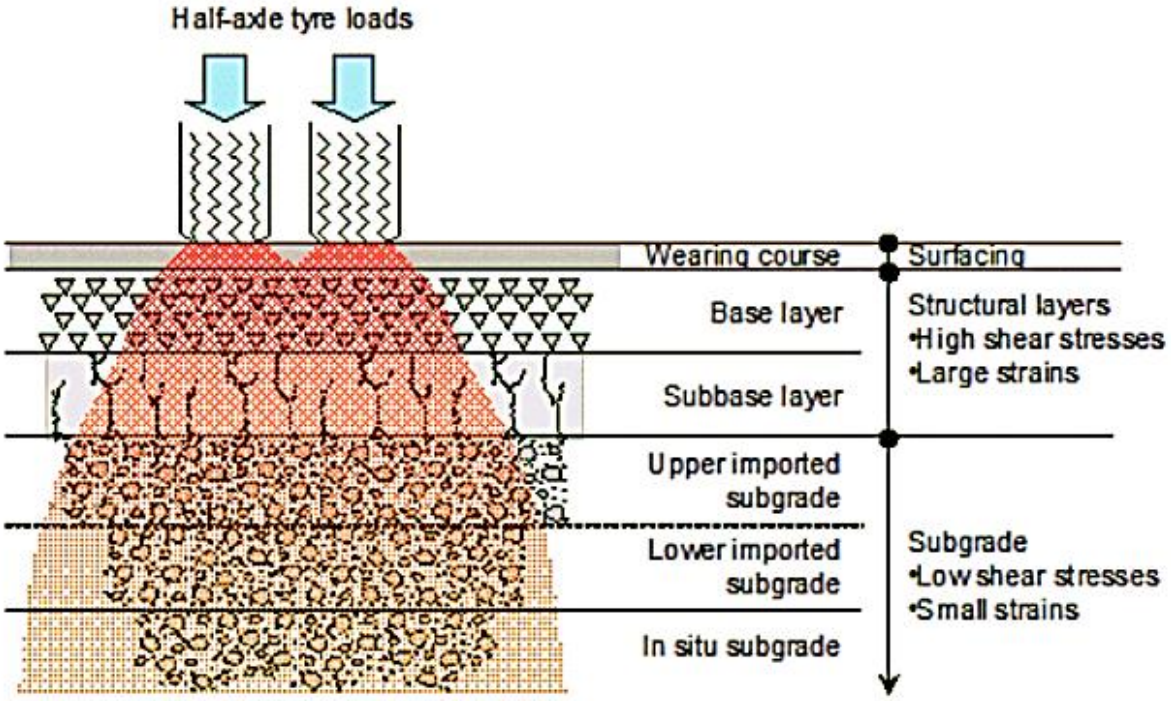

Figure 2-1: Analysis positions for critical stress/strain parameters for South African pavement structures, (SANRAL, 2014a)

2.1.2 Benefits and Challenges

With increasing axle load limits, increasing tyre inflation pressures and a general increase in traffic, pavements with higher structural capacities are needed. Cement stabilisation provides a more resilient, uniform and water resistant material compared to an unstabilised material. Stabilisation is used to improve marginal quality materials, by recycling the in-situ material which conserves non-renewable gravel sources, lowers transportation costs and lowers greenhouse gas emissions, (Paige-Green 2008, Mbaraga 2015).

According to SAPEM (2014a), problems associated with loss of stabilisation are generally related to the materials not meeting the required ITS before carbonation. SAPEM therefore recommends to take into account the ITS and not only prioritise UCS strengths when considering appropriate stabiliser content. However, the failure mechanism of a

stabilised layer is tensile strain. By adding large quantities of cement to satisfy the ITS leaves the pavement vulnerable to shrinkage and fatigue cracking in the layers. Fatigue cracks start from the bottom of the layer and are linked to traffic loading and material strength and stiffness. Shrinkage cracking on the other hand begins at the surface of the layer and are related to volume change, (George, 1990).

Traffic and environmental effects influence the Elastic Modulus of a cement stabilised layer. Freeme (1984) explains how a pavement progresses through three phases with traffic loading, see Figure 2-2.

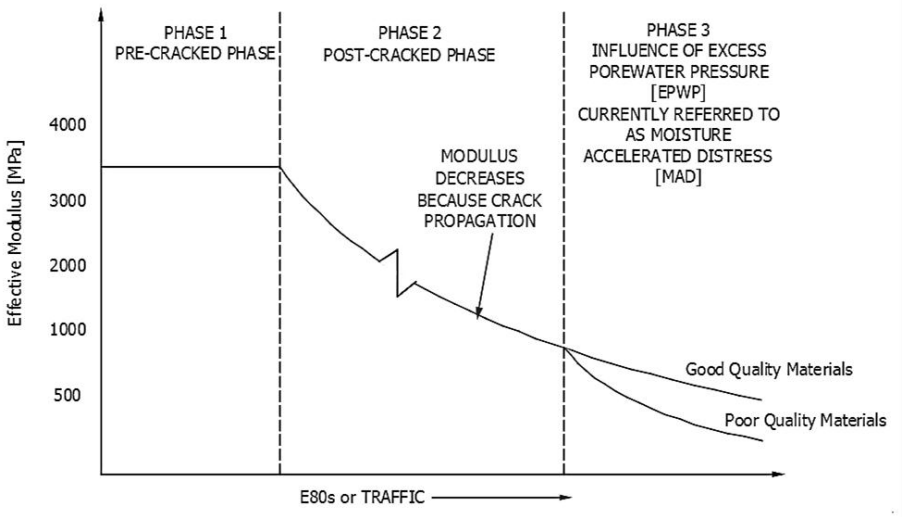

Figure 2-2: Change in Elastic Modulus of a cement stabilised layer, (CSIR, 2015)

In Phase 1, see Figure 2-3, the Elastic Modulus is relatively high and the stabilised layer is intact. At this stage shrinkage cracking will occur due to the properties of the material and environmental factors. Shrinkage cracking in combination with repetitive loading reduces the Elastic Modulus of the layer. In Phase 2 the Elastic Modulus continues to decrease due to crack propagation and the material can be classified as an equivalent granular material. During the final phase, water could ingress through the propagated cracks. This may cause increased pore-water pressure and layer instability, (Freeman & Little, 1998).

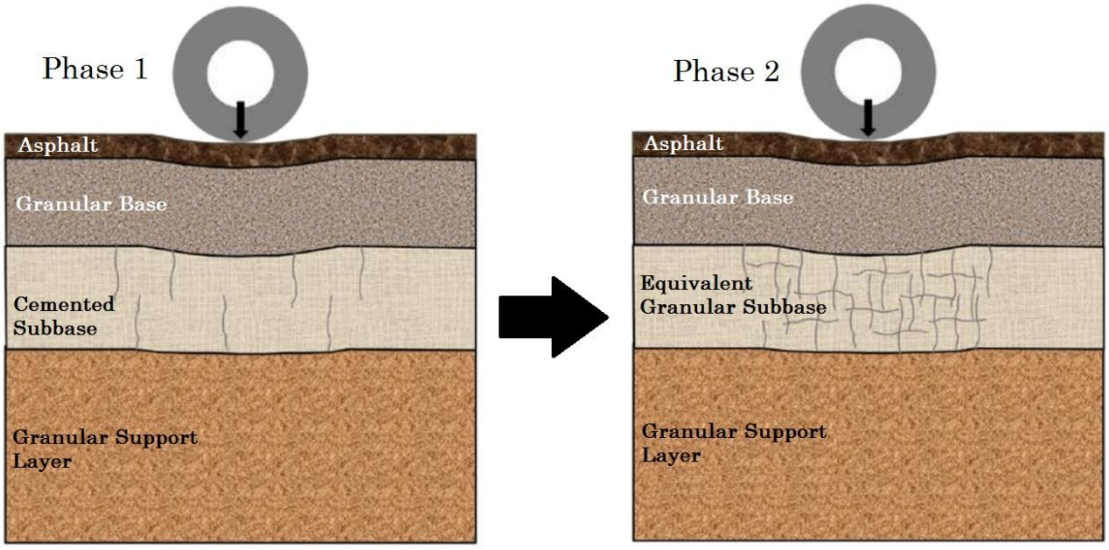

Figure 2-3: Change from lightly cemented layer to equivalent granular, (SANRAL, 2014a)

As mentioned, fatigue cracking is a primary mode of failure for CTM. Theyse (1996) explains that at the end of the effective fatigue life, the stabilised layer is assumed to behave as an equivalent granular material. As the maximum tensile strain increases, the number of loading cycles decreases and ultimately reduces the pavement life, see Figure 2-4.

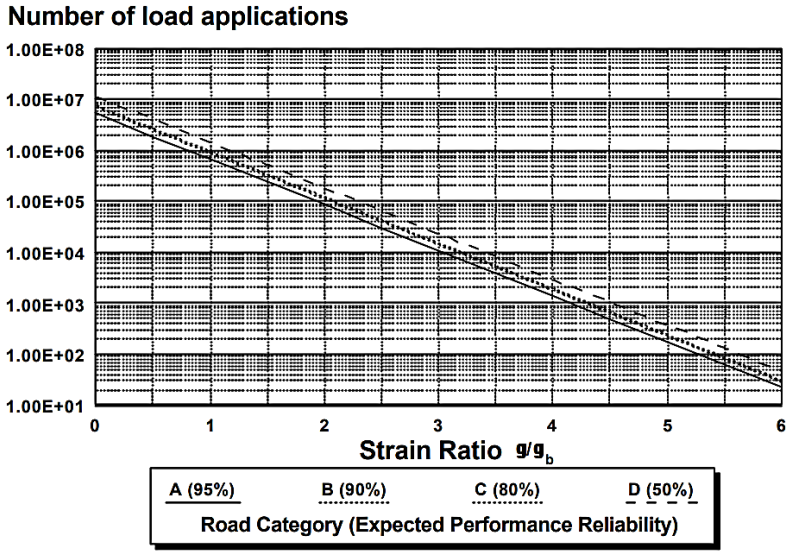

Figure 2-4: Effective fatigue life transfer functions for cemented material, (Theyse et al., 1996)

2.1.3 Shrinkage Cracking of CTM

Although there are many benefits of cement stabilisation, the main challenge is shrinkage cracking. Shrinkage cracking in CTM are caused from changes in moisture and temperature, and cannot be avoided. The degree of cracking is dependent on various factors, but in general the stronger the material, the wider the cracks at larger crack spacing, (TRL, 2003). Shrinkage cracks, especially in a base layer, can propagate through to the asphalt layer. Should these resultant cracks remain unsealed, they could lead to water ingress and would be detrimental to the underlying pavement structure. To seal these cracks can be expensive, effect the riding quality of the surface and looks unattractive, (George, 1968).

Micro shrinkage cracking in subbases are caused from restraints from layers above and below, which lead to an increase in tension stresses. If these stresses exceed that of the tensile strength of the material, shrinkage cracking will form. These cracks may not propagate through a granular base to the asphalt layer, but cause disintegration of the subbase layer itself. This would decrease effective load spreading and cause damage to the subgrade, (Mbaraga, 2015).

As mentioned, shrinkage cracking occurs when the induced tensile stress exceeds the tensile strength of the material. According to the TRH13 (1986), cracking generally forms rectangular patterns. Shrinkage cracking can occur at any time within a few days of construction up to 4 months after construction. The crack spacing and widths are determined by the rate of strength development relative to rate of shrinkage stress development. If the tensile stress exceeds the tensile strength for material with low tensile strength, the cracks will be more frequent and widths will be narrower and more closely spaced, see Material A in Figure 2-5. These cracks vary from hair line cracks to 1mm and can be up to 2m apart, (TRH13, 1986).

If the tensile stress exceeds the tensile for a material with relatively high tensile strength, the cracks will be spaced further part and will be less frequent and wider, see Material B in Figure 2-5. These cracks can be 2-3mm wide and 4-6m apart.

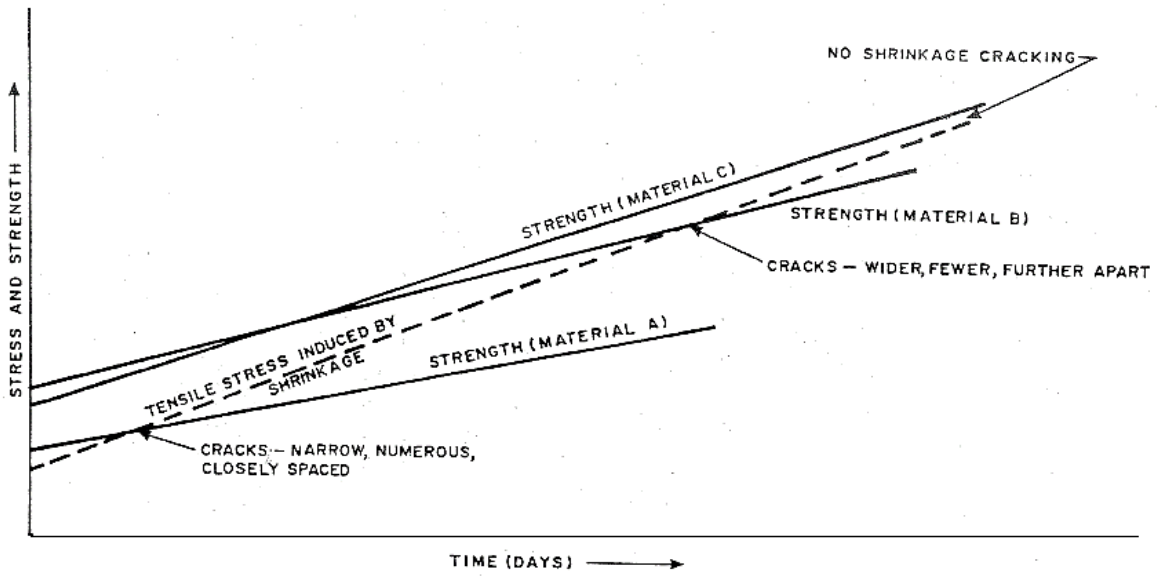

Figure 2-5: Cracking as a result of the interrelationship between shrinkage stress, strength and time (TRH13, 1986)

2.2 Recycled Concrete Aggregate

2.2.1 Overview

Recycled concrete aggregate is more commonly known as concrete demolition waste. However, concrete demolition waste can be divided into two materials: RCA and Recycled Masonry Aggregate (RMA). This study focuses on RCA which excludes any masonry particles. It is true that the origin of this material is seen as waste, however countries such as Netherlands, USA, UK, China and Australia have implemented this material in their base (our equivalent subbase) layers. Currently South Africa has no specified design standards that can guide industry. However there has been a Working Group established for the writing of "Guidelines" towards the application of RCA and RMA in pavement layers, and the insight gained in this research will feed into these guidelines, (Tawine, 2017).

2.2.2 Benefits and Challenges

RCA can be harvested from demolished buildings or old concrete pavements through crushing of the concrete and forming concrete aggregates. This saves quarrying for natural aggregate and reduces associated costs. Other environmental benefits include fewer landfills and the reduction in cement usage. Cement production is estimated to contribute 5% of global CO_2 emissions, (Worrell et al., 2001).

The challenge with RCA is that it can be considered an inconsistent material in comparison with natural aggregates. Factors such as parent material mineralogy, time and environment of construction, and level of hydration of the material vary from different RCA sources, see Figure 2-6. This can lead to difficulty in properly characterising the material. It is also impossible to remove 100% of impurities such as steel reinforcing and soil, (Tawine, 2017). Therefore, characterisation tests such as unconfined compression tests, indirect tensile tests, and initial consumption of cement tests are essential to understand how a specific RCA performs.

Figure 2-6: Different RCA sources

2.2.3 Recycling Process

The recycling process of concrete demolition waste normally involves a primary and secondary crushing stage. Jaw crushers, which are used in the primary stage, produce aggregates that are somewhat flat and sharp, but have the best grain-size distribution. Impact and cone crushers are often used in the secondary stage. Cone crushers produce more spherical particles. Impact crushers provide good grain-size distribution and lower the flakiness index. The size and shape specifications of the coarse aggregates can be met by adjusting the aperture of the crusher. However, the fine aggregates are inclined to be more angular and coarse than the standard sands used in the production of concrete, (Silva et al., 2014).

2.2.4 Density

Bulk Density is an indicator of the packing capacity of a material. This influences the water requirement and in turn effects the permeability, drying shrinkage and durability. For a given particle relative density, the higher the bulk density, the lower the water required and hence the lower permeability and drying shrinkage, (Owens G, 2012).

As mortar is less dense than natural aggregates, the more cement paste present on the surface of the RCA fractions, the lower the particle relative density of those fractions. As recycling/crushing process may consists of many stages, the cement paste or mortar on the aggregate surface will break down resulting in an increase in particle relative density and quality of the coarse recycled aggregate. The fine fractions will however decrease in particle relative density with each processing level as it could consist primarily of mortar. Therefore, the recycling processes should not be too few in order to achieve adequate quality and size of coarse aggregates. However, it should be approached with caution due to a decrease in quality of the fine fractions, (Silva et al., 2014).

However, if there is a breakdown of the original stone in the concrete and not only the mortar on the aggregates' surface, then this could potentially change the particle relative density and quality of the fines, as it is not all mortar. The ability to breakdown the original stone would depend on the type of crusher used, the amount of mortar on the aggregates' surface and the number of recycling/crushing stages.

Molenaar and van Niekerk (2002) investigated the influence of composition, grading and degree of compaction on the mechanical characteristics of unbound recycled aggregates. It was found that a continuous grading with sufficient fines performed better than a gap grading. The fines provide the friction between the larger particles that provide the strong matrix structure, see Figure 2-7. It was also found that with an increase in compaction, the particles orientate themselves into a tighter packing matrix which ultimately increased bulk relative density of a layer. Further detail on how density influences shrinkage cracking can be found in Section 3.4.4.

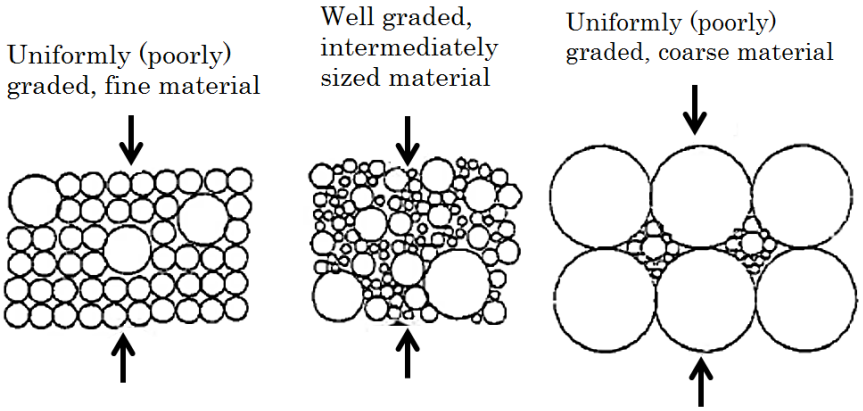

Figure 2-7: Skeleton of poorly and well-graded materials (van Niekerk & Huurman, 1995)

2.2.5 Water Absorption

The findings of Poon et al (2006) and Silva (2014) showed that the particle relative density of RCA was lower than that of natural aggregates. This was due to the higher water absorption of RCA from the latent cement/mortar present that consumed the moisture for hydration. The increase of porosity of RCA also contributes to the water absorption due to the recycling process.

Silva (2014) confirms that the water absorption of natural aggregates are between 0.5% - 1.5% and that precautions need to be taken as recycled aggregates will almost always have greater porosity. The extent of porosity can vary depending on the various factors such as: recycling procedure, quality of original material and size and shape of the aggregates. From Table 2-1, Poon (2006) exhibits an increase in water absorption for RCA in comparison to natural aggregates. This is due to the same reasons mentioned by Silva.

Table 2-1: Water absorption of natural aggregates and RCA (Poon et al., 2006)

		Aggregate size			
		40 (mm)	20 (mm)	10 (mm)	< 5 (mm)
Water Absorption (%)	Natural Aggregates	1.06	0.57	0.59	3.51
	RCA	3.17	2.17	2.29	10.3

The same findings were observed by Barisanga (2014), where the water absorption increases with an increase in fine particles. The fine particles have larger surface area, and therefore absorb more water. This is seen as a constant amongst all his research materials, see Figure 2-8.

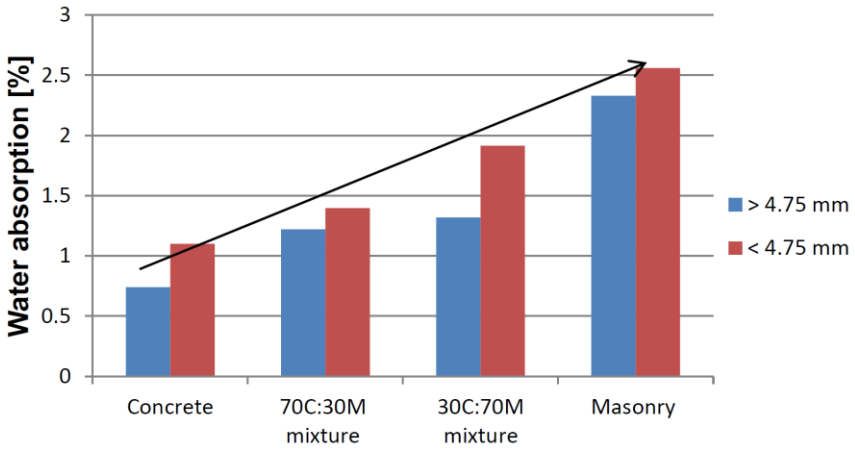

Figure 2-8: Water absorption,(Barisanga, 2014)

2.2.6 Self-Cementation

RCA can be used as granular substitutes with additional self-cementing properties. The fines content of RCA consists mostly of hydrated and potentially un-hydrated cement particles. Self-cementation occurs when active residual or latent cement particles react with water and produce hydrate compounds. These hydration compounds increase the stiffness, (Tawine, 2017).

Tawine (2017) performed XRD (X-Ray Diffraction) testing on the 0.075mm and the 1.18-2.36mm fractions. Higher levels of active CSH was found in the 0.075mm fraction, see Figure 2-9.

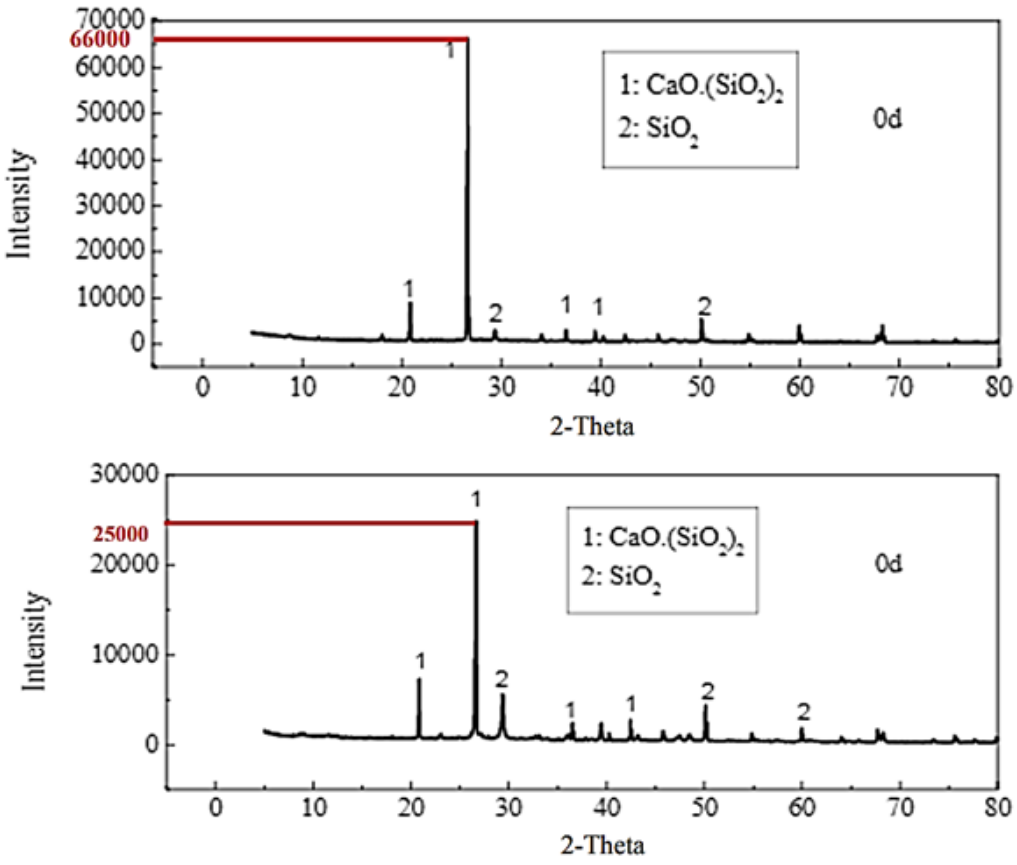

Figure 2-9: XRD results for 0.075mm and 1.18-2.36mm concrete fines, (Tawine, 2017)

According to Poon et al. (2006) the majority of active latent cement is present in the fractions smaller than 0.15mm and in between 0.3 – 0.6mm fractions, see Figure 2-10. This was found through XRD, where higher levels of C_2S and $C_3H_2S_3$ (CSH) was found. This agrees with the findings of Tawine.

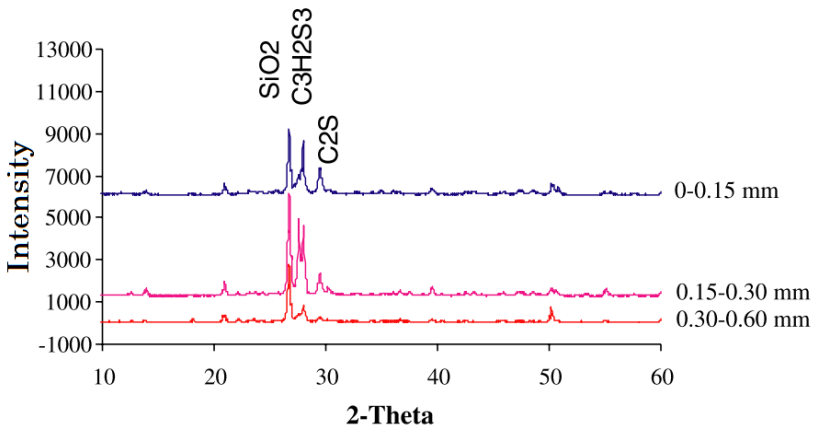

Figure 2-10: X-ray diffraction patterns of different size fractions of Fine RCA, (Poon et al., 2006)

Chai et al. (2009) presents a case study of a road where re-cementation of a base material was observed from a test pit. This was discovered as hydrochloric acid was sprayed onto the material, which indicated the presence of old cement. While on the same material phenolphthalein was also sprayed and turned magenta. This signified un-carbonated cement with a pH greater than 10, see Figure 2-11.

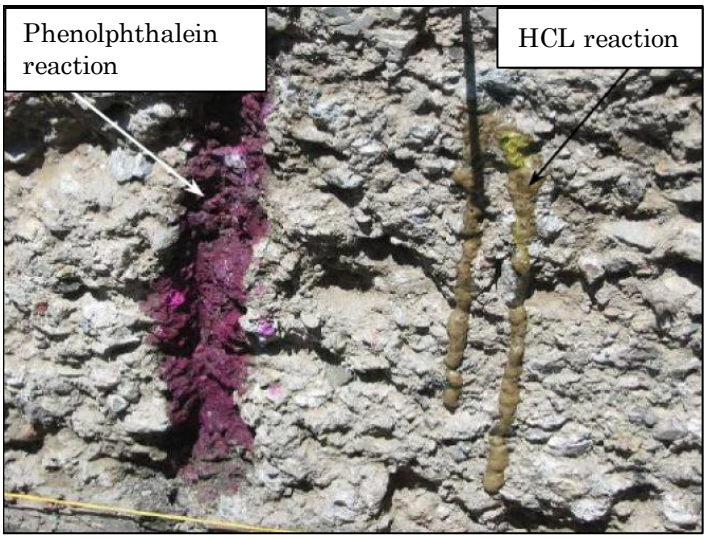

Figure 2-11: Phenolphthalein and hydrochloric acid reaction on base material (Chai et al., 2009)

2.2.7 Pavement Behaviour

Tawine (2017) explains that the self-cementation can be a hindrance for a base course as it increases in stiffness which can lead to cracking that can propagate through to the asphalt surface. However, it would work effectively as a semi stabilised subbase. Self-cementation be considered a positive if accounted for in the design.

A general problem with a cemented base, as Tawine mentioned, is shrinkage cracking which can propagate through to the asphalt layer. Furthermore a granular base was adopted as a solution to stop crack propagation, due to its unbound nature as seen in a typical South African pavement structure in Figure 2-1. As RCA acts as a lightly stabilised material, if it is considered for base layer application, one must be aware if the potential challenges, (Tawine, 2017).

Chai et al. (2009) investigated a case study where two Heavy Vehicle Simulations were performed on a base layer that contained recycled material including crushed Portland cement concrete. The Elastic Moduli were recorded over 7 years through FWD back calculations, see Figure 2-12. In between the first and second HVS, the back calculations

showed that the Elastic Moduli increased from 1000 – 4000 MPa over approximately five years. The layer experienced no truck loadings, only light car traffic during this time. It was suggested that the increase in stiffness was attributed to the re-cementation of the recycled concrete aggregates, (Chai et al., 2009). There was however no mention of any comparison between the initial and 5 year compaction density. It is possible that there was an assumption that no consolidation occurred due to traffic.

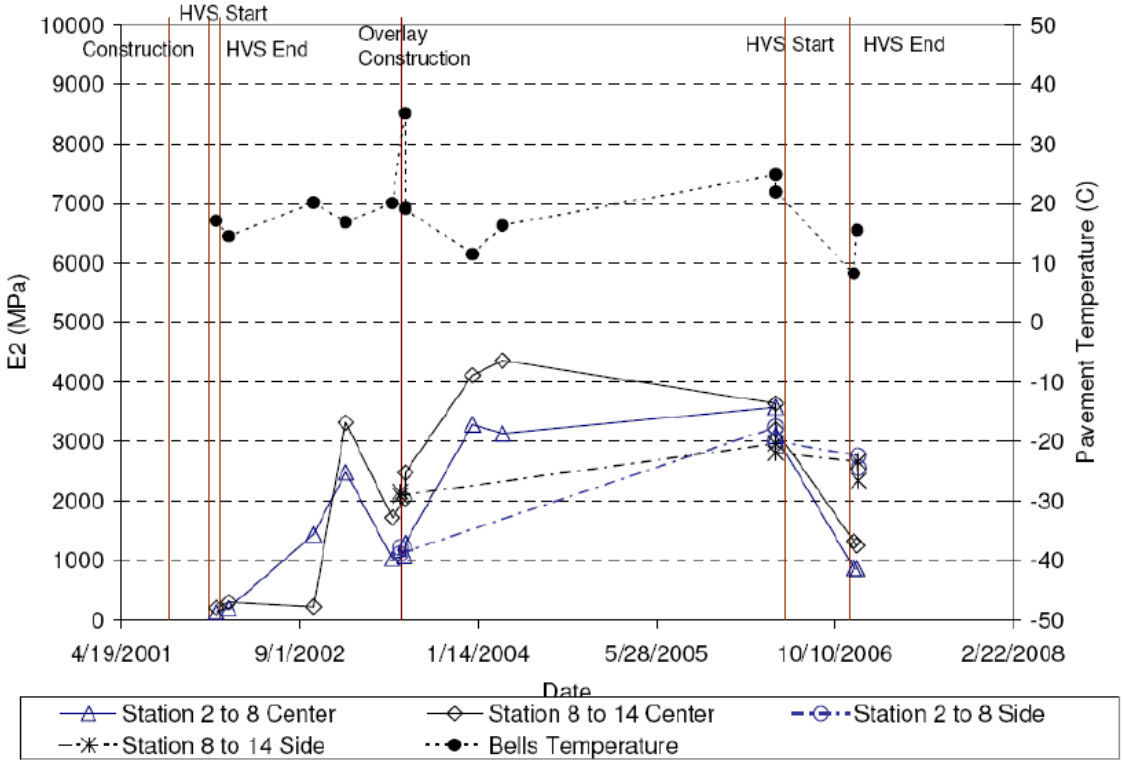

Figure 2-12: Elastic Moduli of recycled aggregate base from FWD measurements versus time, (Chai et al., 2009)

2.2.8 Shrinkage of RCA

Shrinkage of a RCA layer is expected to be more than that of a layer consisting of high quality natural aggregate, due to the active latent cement particles present. Reason being that there are additional hydration reactions taking place, causing an increase in stiffness of the layer. The total shrinkage therefore consists of chemical and drying shrinkage.

Depending on the source of the RCA, when considering CDW the original aggregates in concrete are generally of high quality and could potentially cause less shrinkage when compared to a poor quality natural aggregate.

When comparing RCA and Recycled Masonry Aggregate (RMA), the factors to consider are quality of material, as well as quantity of active latent cement present on the aggregates' surface. Xuan (2012) performed cylindrical shrinkage tests on materials that contained RMA and RCA at various percentages. Xuan defines shrinkage in the positive direction, see Figure 2-13. The material with 0% masonry has 100% RCA and vice versa. Figure 2-13 shows that the material with the least RCA and therefore the most masonry (M100C4DC101) experiences the least shrinkage. Even though the RMA is expected to be of lesser quality due to its porosity and lack of strength, it shrinks less than the RCA. It is suspected that the RCA in question contained high amounts of active latent cement on the aggregates' surface, which lead to an increase in shrinkage.

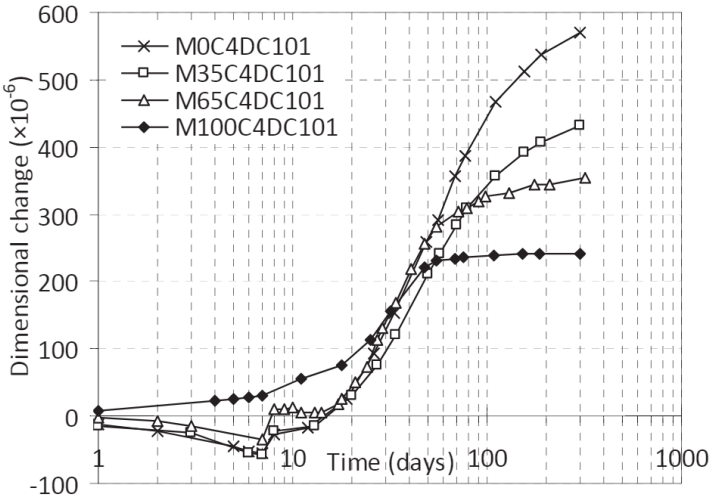

Figure 2-13: Cylindrical shrinkage test results of RMA and RCA, (Xuan, 2012)

2.3 Conclusion

Stabilisation is used to increase the stiffness and durability of a layer. CTMs are most commonly used in subbases, as stabilised base layers tend to cause cracking problems that propagate through to the asphalt layer. RCA can be used as an equivalent granular material with additional self-cementing properties that increase the stiffness. RCA could therefore also potentially act as a lightly stabilised layer; hence the self-cementation is discussed. It is important to perform characterisation tests to determine how much self-cementation can occur. If properly designed for, RCA can save on costs and positively impact the environment.

Chapter 3

Shrinkage Cracking

There are four main types of shrinkages discussed: autogenous, drying, thermal and carbonation. Each type of shrinkage has its own mechanisms and have different influencing factors. This chapter discusses the two main mechanisms of shrinkage, capillary tension and hydration, different types of shrinkages and the main influencing factors of drying shrinkage.

3.1 Shrinkage Mechanisms Concepts

There are many different types of shrinkages defined by their own mechanisms. The main mechanistic concepts are Surface Tension, Capillary Tension Theory and movement of interlayer water and hydration.

3.1.1 Surface Tension and Capillary Tension Theory

Surface tension is due to the intermolecular hydrogen bonds between neighbouring water molecules. The molecules on the surface have no neighbouring molecules to bond with and therefore enforce stronger bonds with molecules to the sides, see Figure 3-1. This causes the surface molecules to be unbalanced. The molecules try to minimise the surface area and therefore form a drop, known as a meniscus, (EdInformatics.com, 1999)

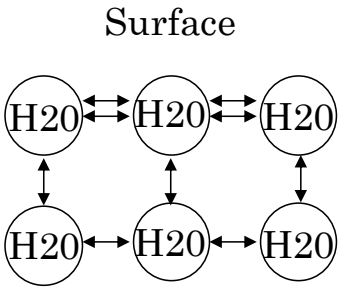

Figure 3-1: Surface Tension

The capillary tension occurs when evaporation takes place and the pore water forms a meniscus between particles due to the water tension. As the drying continues, due to evaporation, the tension at the meniscus in the capillary increases as the radius of the meniscus becomes progressively smaller (George, 1968). This principle is demonstrated in Figure 3-2. This tension force can also be referred to high matric suctions or negative pore pressures as seen in Figure 3-3, (Morris, 2005). This causes the walls of the capillaries to pull together and cause volumetric changes, (Mbaraga, 2015).

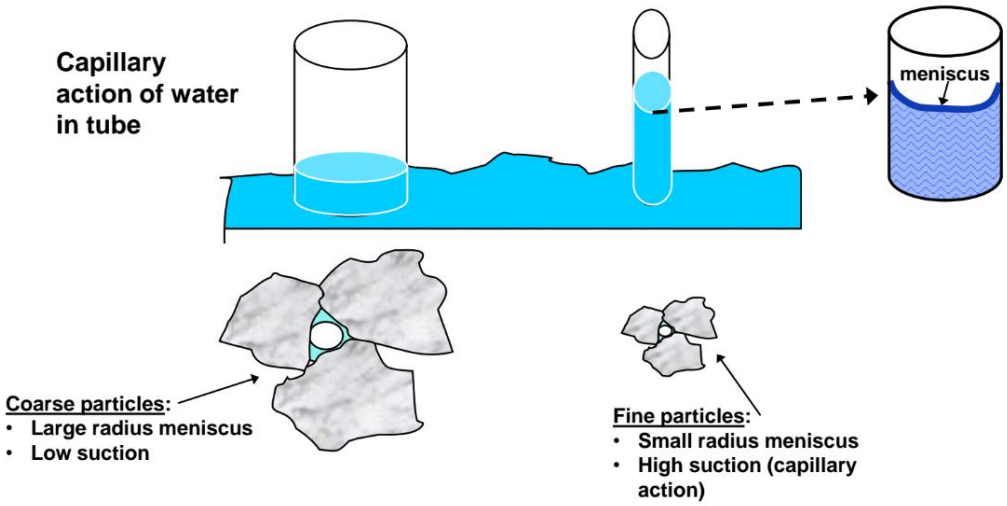

Figure 3-2: Principle of capillary action, (SANRAL, 2014b)

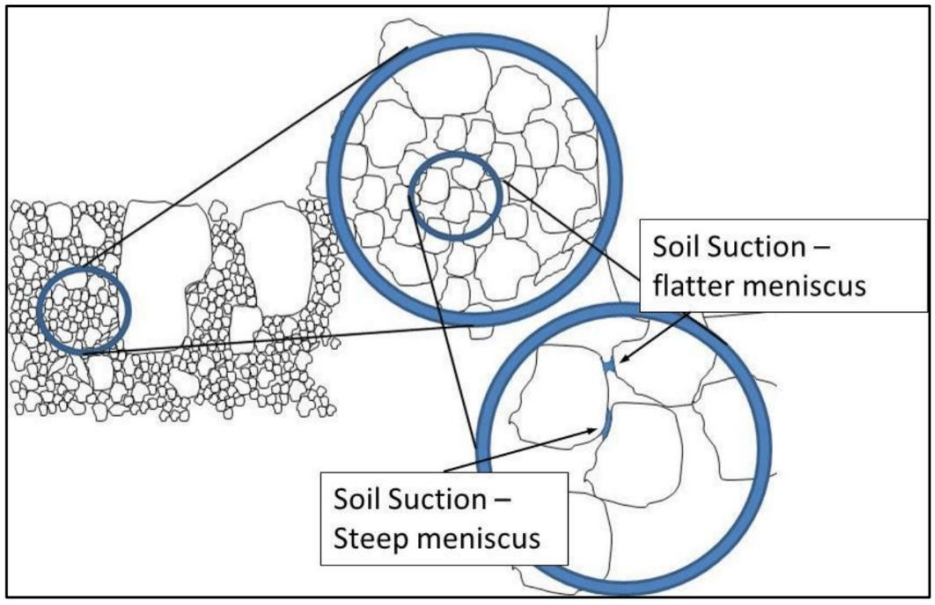

Figure 3-3: Capillary action in partially saturated soils creating suction forces, (SANRAL, 2014b)

3.1.2 Movement of Interlayer Water

The moisture loss due to evaporation is largely dependent on the exposed surface area and the moisture migration pathways, (Semugaza, 2016). This has to do primarily with the porosity and degree of compaction. The more compact the layer, the fewer voids available for water to move around. Porosity increases the water movement as more water can be retained due to the porous nature of the aggregates.

3.1.3 Hydration

The main constituents of cement are calcium silicates, aluminates and calcium oxides. With the presence of water, these constituents form hydrated compounds, which harden and form a strong, binding cemented matrix around the aggregate. These compounds are in a gel form called calcium silicate hydrates (CSH). The gel is where the most of the strength and low permeability properties arise from, (Mbaraga, 2015).

Hydration initially a fast-exothermic reaction, and slows down with time. Most soils or gravels can be stabilised with cement. Exceptions include materials that have a high organic content which retards the hydration process. Soils with high clay content prevent even mixing of the soil and cement. (Gourley, Greening 1999, Paige-Green 2008, Mbaraga 2015)

The basic principles of cementation reactions are similar for cement or lime stabilisation. Stabilisation with lime includes a hydration reaction between aluminates in the soil and calcium hydroxide, which is a pozzolanic component. Cement stabilisation is very similar; cement already contains the calcium, silicates and aluminates, only water needs to be added to begin the reaction (Paige-Green, 2016).

3.2 Shrinkage Types

3.2.1 Autogenous Shrinkage

Autogenous shrinkage is due to the hydration reaction between the water molecules and the unhydrated cement molecules. During hydration the volume of the hydrate, which is

the product the hydration, is smaller than the volume of the water and the unhydrated cement before the hydration reaction, see Figure 3-4. This is referred to as *Le Chatelier contraction* (Tazawa et al., 1995). Autogenous shrinkage is the macroscopic volume reduction due to hydration, without any loss or gain of moisture to and from the specimen at constant temperature, (Tazawa et al., 1995; Li, 2014).

Although this shrinkage does not lose or gain any moisture to and from a specimen, the hydration does consume moisture internally and causes drying of the specimen. According to Neithalath et al. (2005), concrete with lower water to cement ratios will experience more autogenous shrinkage. The degree of autogenous shrinkage is linked to the degree of hydration that has taken place. Due to the low percentages of cement used in CTM versus concrete, autogenous shrinkage is not considered as critical as drying shrinkage.

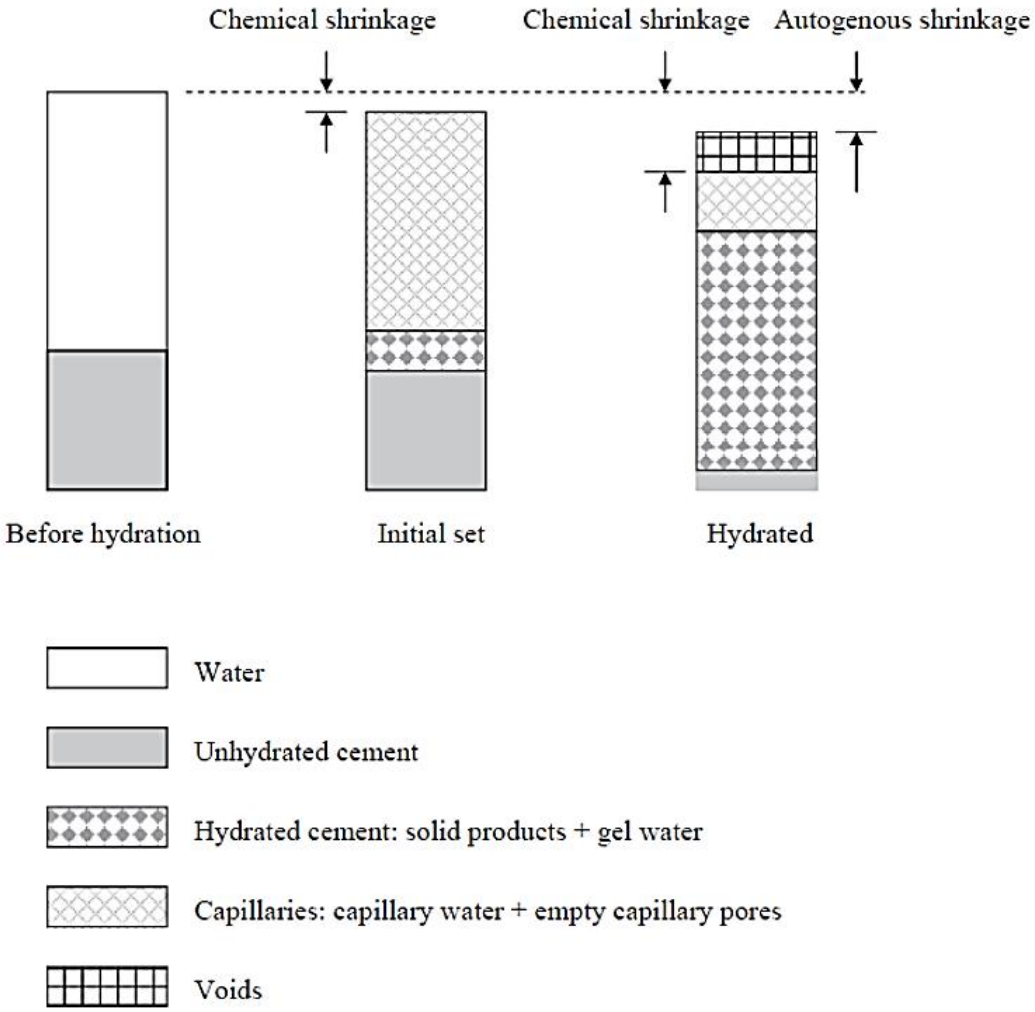

Figure 3-4: Schematic representation of autogenous and chemical shrinkage of hydrating cement paste, (Brooks, 2015)

3.2.2 Drying Shrinkage

Drying shrinkage or plastic shrinkage is due to the loss of moisture. This occurs when the moisture within the specimen tries to reach equilibrium with the surrounding environment through evaporation, (Bhandari, 1975; Morris, 2005; Neithalath et al., 2005). As the moisture in the capillaries is expelled, the tension forces increase in the material as mentioned in the capillary tension theory. The rate of drying shrinkage depends on the exposed surface area, the drying environment and the materials internal structure, (Chakrabarti & Kodikara, 2006).

Xuan (2012) performed drying shrinkage tests, looking specifically at influencing variables such as RMA content, cement content and degree of compaction. His findings concluded that RMA content was the dominating factor with regards to shrinkage crack control. Degree of compaction had the least contribution on shrinkage.

3.2.3 Thermal Shrinkage

Thermal shrinkage or volume change occurs when the material experiences temperature fluctuations. As the temperature of the material rises it undergoes thermal expansion. This happens to concrete during early age hydration as the reaction is exothermic. When the temperature cools the concrete will contract, (Holt, 2001). The increase in temperature from the surrounding environment can accelerate the hydration reaction, also referred to as early setting or flash setting, (George, 1968). In CTM the heat generated by hydration is dependent on the cement content and corresponding hydration rate, (Li, 2014).

Mbaraga (2015) performed shrinkage testing with accelerated curing conditions at 70 ºC for 3 days. His study exhibited initial thermal expansion which caused initial swelling of the material within the first 4hours. This heat potentially accelerated the hydration reaction.

During the early stage of CSM hydration when there is relatively low strength or strain capacity, temperature fluctuations from night to day can have significant effect on shrinkage cracking, (Li, 2014). After the expansion and contraction of hydration, the only temperature effect is from the environmental temperature fluctuations such as seasonal changes, at which stage drying shrinkage is the most important factor in CTM layers, (George, 1969).

3.2.4 Carbonation Shrinkage

The mechanism of carbonation of concrete or CTM begins when the material is exposed to air that contains carbon dioxide. The calcium hydroxide in lime reacts with the CO_2 and forms calcium carbonate ($CaCO_3$). This means that the stabilising agent (lime) reverts to its original form (limestone) and therefore loses its pozzolanic/stabilising properties. Once carbonated the pH at the surface of a stabilised material lowers and begins to penetrate inwards. As mentioned previously, stabilisation with lime is similar to that of cement, and therefore carbonation is not only confined to lime stabilised materials, (Netterberg & Paige-Green, 1984). Carbonation leads to the drying out and decomposition of the CSH gel and causes volumetric changes, (Chen et al., 2006). Figure 3-5 displays the calcite crystals (calcium carbonate, $CaCO_3$). The formation of these crystals cause expansion and cracking.

Figure 3-5: Optical microscope view of calcite crystal development associated with cracks (±100x) left and (±200x) right, (Chai et al., 2009)

3.2.5 Concluding Remarks

All the shrinkage types mentioned have detrimental effects on concrete. As this study focuses on CTM and RCA, which have much lower cement contents and much higher water to cement ratios, the shrinkages related to hydration are not as applicable. Drying shrinkage plays the largest role in the shrinkage of CTM and RCA, (Chakrabarti & Kodikara, 2006).

3.3 Shrinkage Cracking

Cement stabilisation can be the cause of shrinkage cracking. Cracking shows potential for deterioration and not necessarily a significant deterioration. Secondary cracks may form due to traffic action and could eventually lead to server distress.

According to Halsted (2010), shrinkage cracking in a stabilised base layer can cause reflective cracking through to the asphalt layer. If the reflective cracks are < 3mm wide, there will still be sufficient load spreading due to adequate aggregate interlock. For these narrow cracks, moisture ingress can be considered minimal and non-problematic. Furthermore, Halsted explains that cracks > 6mm can result in moisture intrusion, poor load transfer and increase stress in the asphalt layer and base deterioration. Pumping of the subgrade material is not a direct cause of the cracks, however cracks could lead to increased stresses and moisture which could cause pumping.

This is however in contrast with the TMH9 (1992), where block cracking is caused by shrinkage of a stabilised pavement layer and are not only restricted to the wheel paths. The block cracks consist of longitudinal and transverse cracks and have a definite block pattern. According to the TMH9, the spacing of block cracks depend on:

→ Type of material

→ Type and quantity of stabilising/modifying agent

→ Degree of secondary distress such as spalling of cracks

The TMH9 rates the severity of the cracks from 1 to 5, see Table 3-1. Here the TMH9 describes cracks at about 3mm to be considered moderately severe and precautions should be taken.

Table 3-1: Description of degrees of block/stabilisation cracks, (TMH 9, 1992)

Degree	Description
1	Faint cracks.
3	Distinct, open cracks (≈ 3mm) with significant spalling, deformation or secondary cracking at corners in the form of triangles.
5	Open cracks (> 3mm) with significant spalling, secondary cracking or deformation evident around open cracks, or wide open cracks (>10mm) with little or no secondary defects

The TMH9 also addresses crack spacing as it is related to the crack activity. It also gives an indication of the severity of type of distress. The severity rating can be seen in Table 3-2. Cases where block cracking has deteriorated to very narrow spacing, can be classified as crocodile cracks.

Table 3-2: Spacing categories for block/stabilisation cracks, (TMH 9, 1992)

Category	Spacing in direction of travel [m]
Narrow	< 0.5
Medium	0.5 to 2.5
Large	>2.5

There are 3 damage modes that can be seen in Figure 3-6. The critical mode of failure will depend on the pavement structure, shape and characteristic of the cracks as well as the type of loading or stresses that are applied onto the pavement. Mode 1 shows shrinkage cracking due to volume changes and induced tension stresses in the stabilised layer. Mode 2 corresponds to shearing, this commonly occurs when the shrinkage cracks propagate through to the asphalt due to trafficking. Modes 1 and 2 are the main damage modes and can cause poor load distribution and poor riding quality to the pavement, (Xuan, 2012).

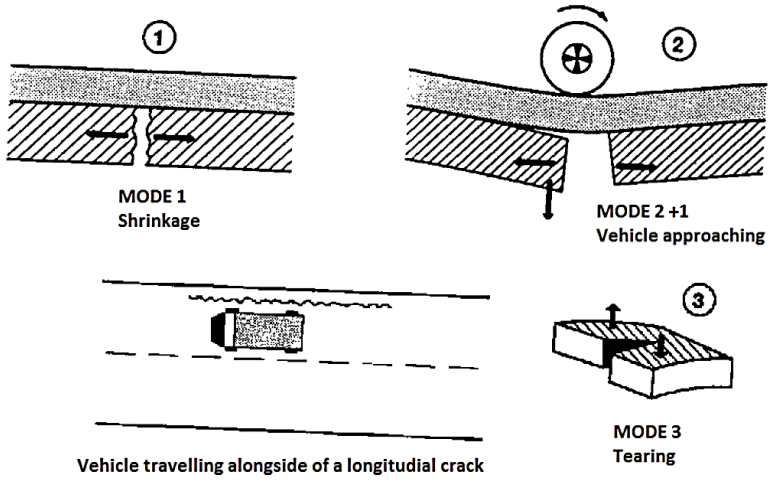

Figure 3-6: Three damage modes of a pavement, (Irwin, 1957)

Shrinkage cracks are a result of volume change (shrinkage) and induced tension stresses in the stabilised layer. As soon as the tension stresses exceed the tensile strength of the material, a crack will form as a mechanism to release of stress, (Houben, 2008). As

mentioned shrinkage can be due to cement hydration, drying through evaporation and temperature change, (George, 1968). However, studies have illustrated that cracks in CTM wider than 6mm are primarily due to drying shrinkage or water loss, rather than hydration or temperature, (Halsted, 2010).

3.4 Factors Influencing Shrinkage Cracking

3.4.1 Cement Content

The primary reason for shrinkage is the loss of moisture. George (1968) studied the influence of cement hydration on shrinkage and self-desiccation. The experiment involved a soil-cement beam that was covered with wax which prevented any moisture loss due to evaporation. The hydration shrinkage contributed 17% of the overall shrinkage. This illustrates that hydration can play a role in shrinkage and self-desiccation. The more cement content, the more paste/gel particles can be formed as a product of hydration. George (1968) mentioned that cement hydration is "robbing" the material of the water. Li (2014) agrees in saying that the risk of shrinkage cracking increases with the increase in cement content.

According to Xuan (2012), cement content, as an influencing factor of drying and thermal shrinkage, is second to that of the host material. It was found however, that there was an increase in both drying and thermal shrinkage with an increase in cement content, see Figure 3-7.

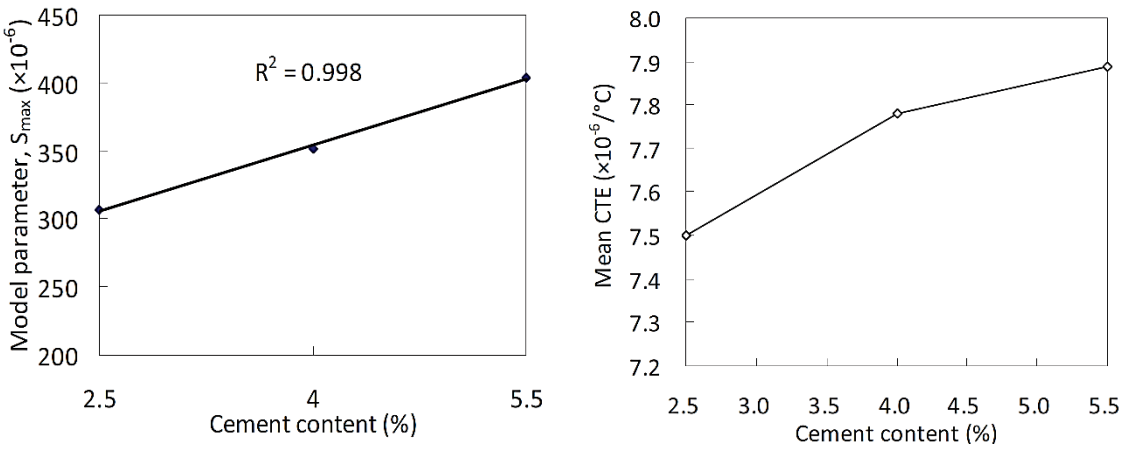

Figure 3-7: Influence of cement content on drying shrinkage (left) and thermal shrinkage (right), (Xuan, 2012)

3.4.2 Moisture Content

The optimum degree of compaction of CSM should be done at optimum moisture content. Too much moisture in the mix creates opportunities for large shrinkage cracks. The more moisture present the more can evaporate and cause shrinkage, (George, 1968; Norling, 1973; Halsted, 2010). In Figure 3-8 George shows that a decrease in compaction achieved negatively effects the shrinkage. Shrinkage is governed by the matrix interlock which is related to degree of compaction. The degree of compaction is a direct product of the percentage moisture and dry density. At higher moistures, lower densities can be achieved. The lower the moisture the higher the dry density. This is only true until a point. At low moistures, the material will compact with difficulty as there is not enough moisture for the particles to move into place. This leads to poor aggregate interlock and low densities, (George, 1968).

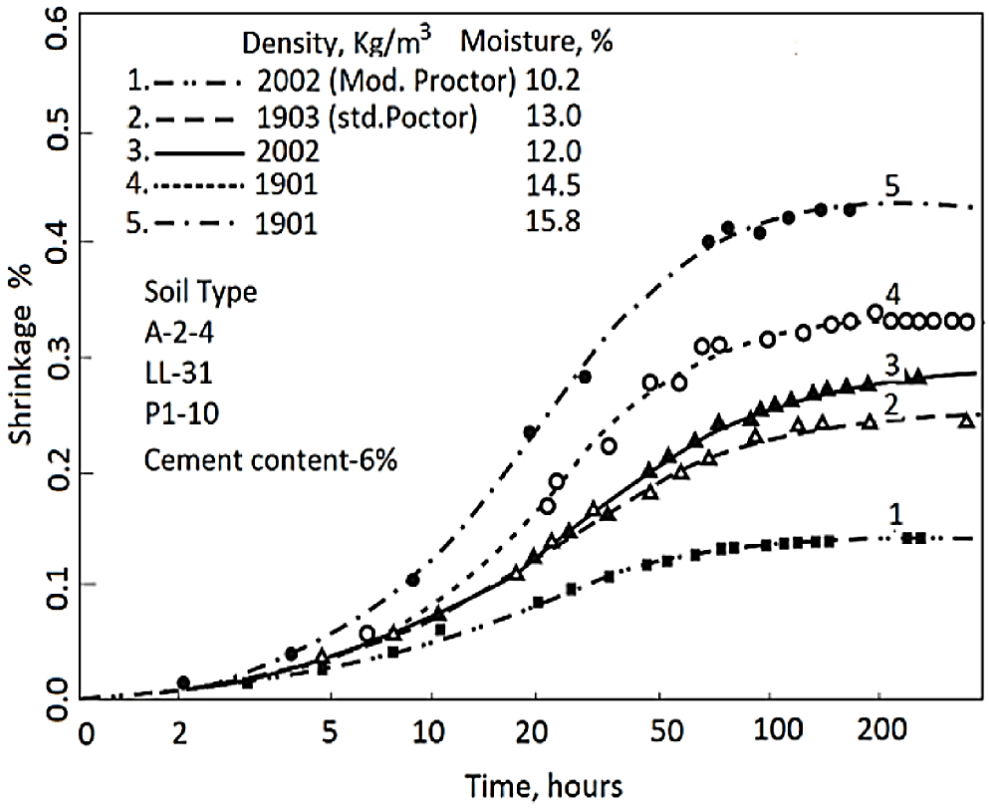

Figure 3-8: Influence of density and moisture on shrinkage, (George, 1968)

3.4.3 Curing Period

There are many curing methods for concrete, which seal in the moisture and prevent evaporation. This is done so that there is water available for full hydration to take place. The longer the curing process at 100% Relative Humidity (RH) the higher the proportion of CSH gel that will form. This will increase strength and stabilising effects, however it will increase the change in volume, (George, 1968). The humidity and temperature conditions of curing can greatly influence the shrinkage.

3.4.3.1 Humidity and Temperature

According to George (1968), temperature has a large influence on shrinkage. George found shrinkage problems occurred more frequently in hot weather than in cooler weather. This was discovered by pre-heating the soil increased the shrinkage. His reasoning was that the increased temperature of the mix resulted in increased setting time. This is known as early set or "flash" setting which accelerates the potential for volume change. Increasing temperature would also increase the rate of evaporation, therefore it is discouraged to construct a cement stabilised layer in peak summer temperatures.

Contrastingly George (1968) and Mbaraga (2015) also experienced that curing at high temperatures, which is considered accelerated curing, assists in the development of cementitious hydrated particles. In the case of Mbaraga it caused initial swelling of the material which is considered shrinkage retardation.

Humidity has a direct influence on the level of shrinkage. The lower the humidity, the less moisture in the air. An equilibrium is reached between the environment and the material. Therefore moisture is lost through evaporation at low humidities. Evaporation causes suction pressures to be built up in the material and causes the particles to pack more tightly, resulting in volume decrease. Ma et al., (2007) performed a study investigating the influence of relative humidity on relative drying shrinkage for cement-based materials. It was found that capillary tension was the dominant mechanism in the 45 – 90% RH range, due to the evaporation as explained in Section 3.1, see Figure 3-9.

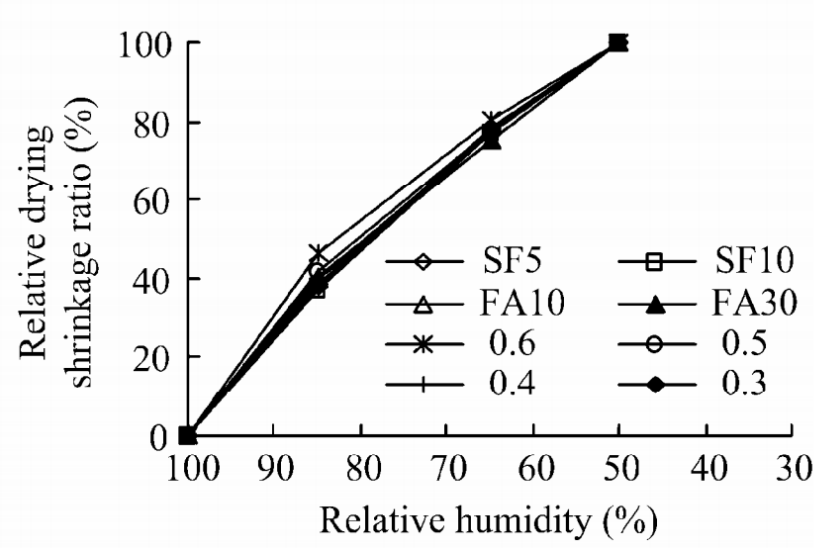

Figure 3-9: Effect of relative humidity on relative drying shrinkage ratio, (Ma et al., 2007b)

3.4.4 Material Density

It is a general finding that an increase in compaction energy results in a higher bulk density and therefore leads to a possible decrease in shrinkage, (George, 1968). This could be due to better packing and aggregate interlock, which reduces void size and increases suction. The grading has a direct influence on packing and therefore bulk density. A good grading consists of a range of large aggregates floating in a fine matrix, see Figure 3-10.

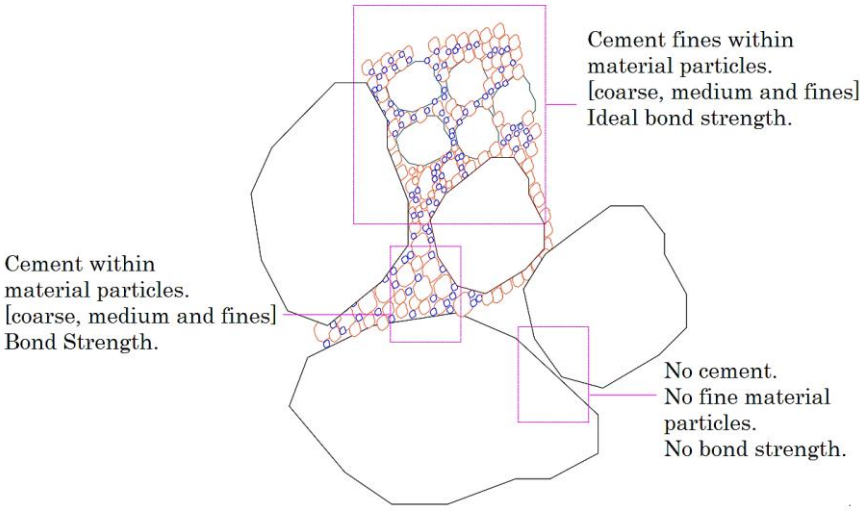

Figure 3-10: Aggregate interlock and cement stabilisation (Mbaraga, 2015)

Better packing leads to better aggregate interlock, as all the particles are touching and creating traction off one another. In terms of cracking, it is more advantageous to have a continuous grading as the absence of larger coarse aggregates can lead to larger crack widths, see Figure 3-11. As cracks form around aggregates, it would therefore require more energy for a crack to form around larger aggregates than smaller aggregates. Thus a gap grading creates an easier path for cracks to form. The larger aggregates provide better interlock of the matrix after the crack has already formed and prevents further widening of the crack.

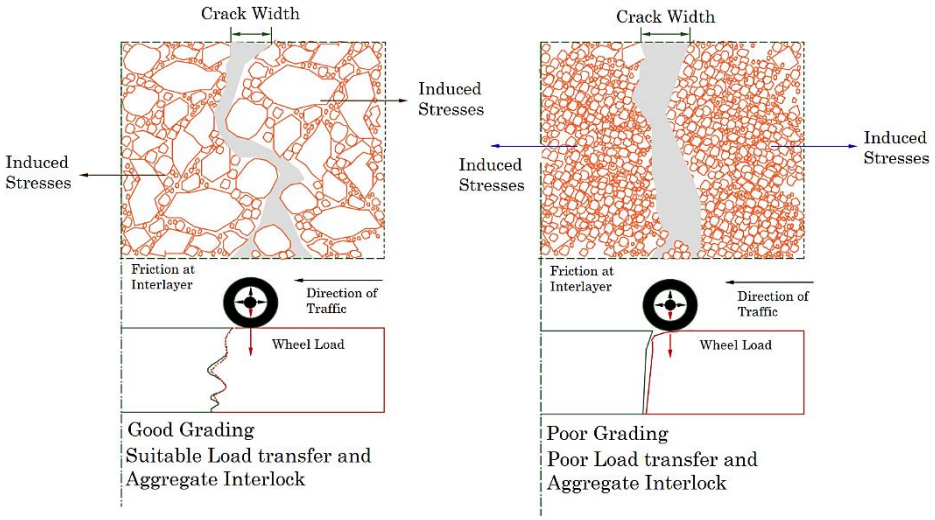

Figure 3-11: Important of good aggregate interlock (Mbaraga, 2015)

3.4.5 Clay Content

Cement reacts with various soils in different ways. According to THR13 (2015), soils with high active clay contents are less effectively stabilised with cement. In order to stabilise a clayey soil with a PI greater than 10, it should first be treated with a small percentage of lime to reduce the plasticity and therefore improving the workability. Clay materials tend to hold more water when compared to other materials and need to be compacted at higher moisture contents which leads to a high shrinkage potential, (Halsted, 2010).

Norling (1973) confirmed that granular soil-cements with low clay content shrink less than soil-cements that are fine grained soils. This can also be confirmed with Mbaraga's work where he achieved a higher level of shrinkage with a Ferricrete (PI 3) than a Hornfels (non-plastic) as seen in Figure 3-12, (Mbaraga, 2015).

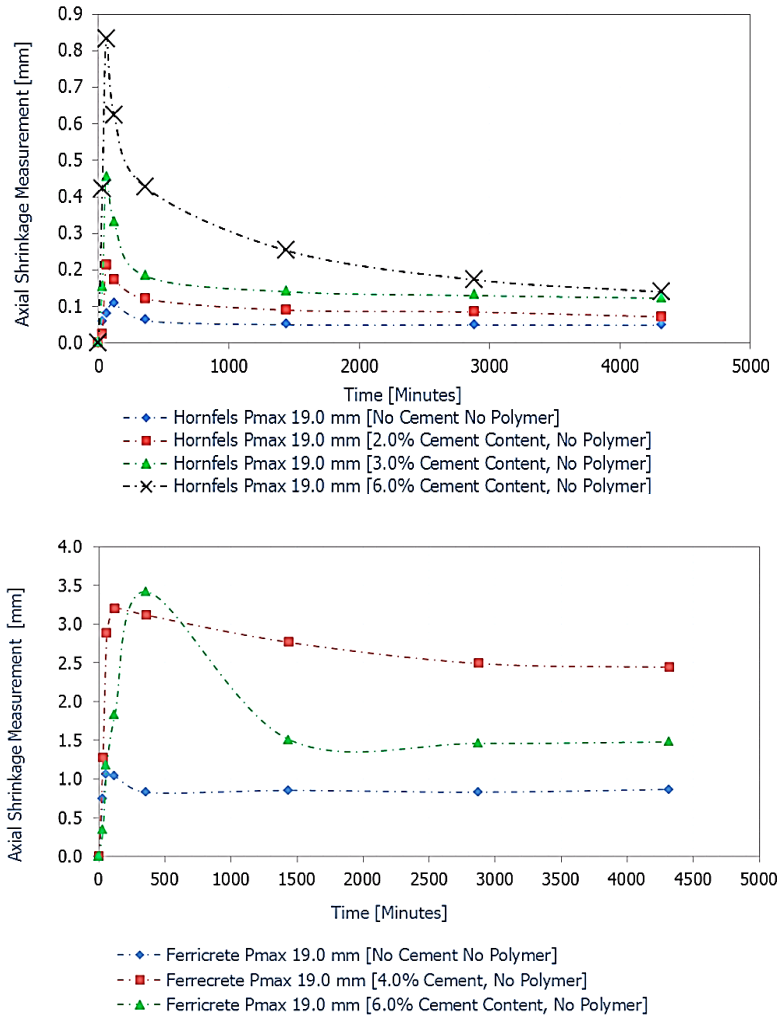

Figure 3-12: Influence of PI on shrinkage of Hornfels and Ferricrete, (Mbaraga, 2015)

3.5 Cylindrical Shrinkage Test

The cylindrical shrinkage test has been implemented in previous research such as Semugaza (2016), Mbaraga (2015), Campher (2015) and Xuan (2012) for RCA, CTM and BSM. The reason that the cylindrical shrinkage test is favourable compared to the beam tests is as follows:

→ Higher Density

The cylindrical tests exhibit higher densities due to the thicker compaction layers which allow for a more realistic aggregate packing, (Campher, 2015). The vibratory hammer orientates the particles and leaves fewer voids, see Figure 3-13.

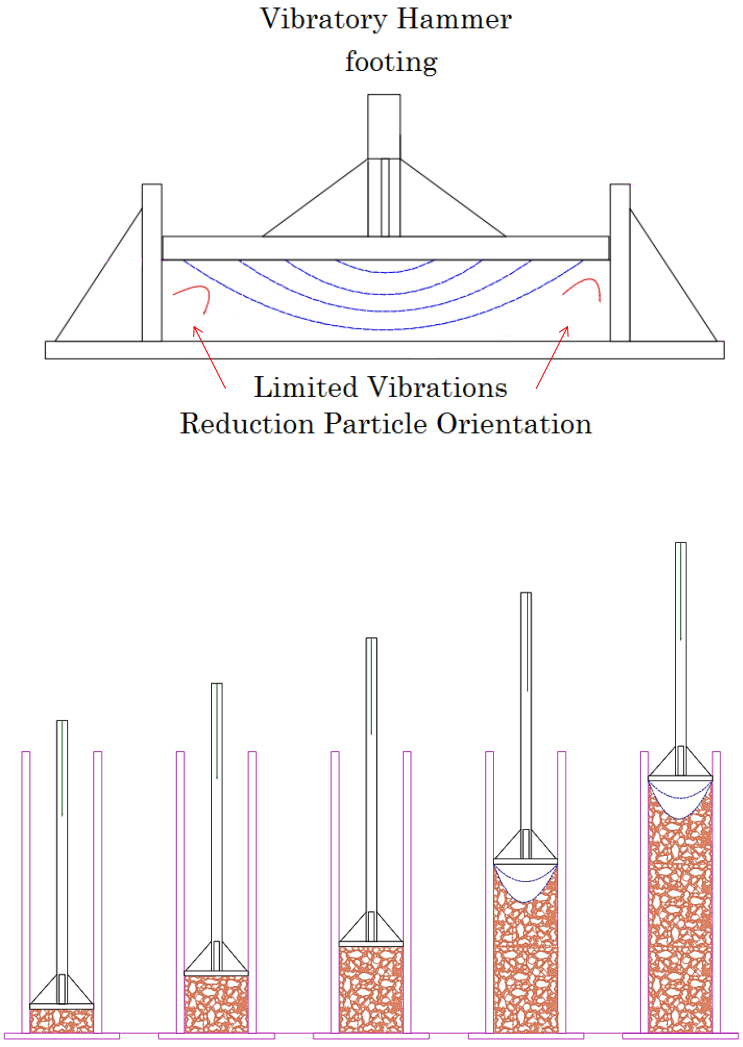

Figure 3-13: Beam (above) and cylindrical (below) shrinkage test compaction (Mbaraga, 2015)

→ Surface Area

The cylindrical shrinkage test has a larger exposed surface area than the beam test, and therefore has more consistent overall shrinkage.

→ Easy and Repeatable

The split moulds are much easier to use and clean than the beam moulds and is more repeatable.

The geometry of the beam test best simulates how a layer is compacted on site (vertically), while the shrinkage is measured horizontally. The horizontal tensile stresses that occur induce shrinkage cracks. In practise shrinkage is therefore measured perpendicularly to the direction of compaction, see Figure 3-14.

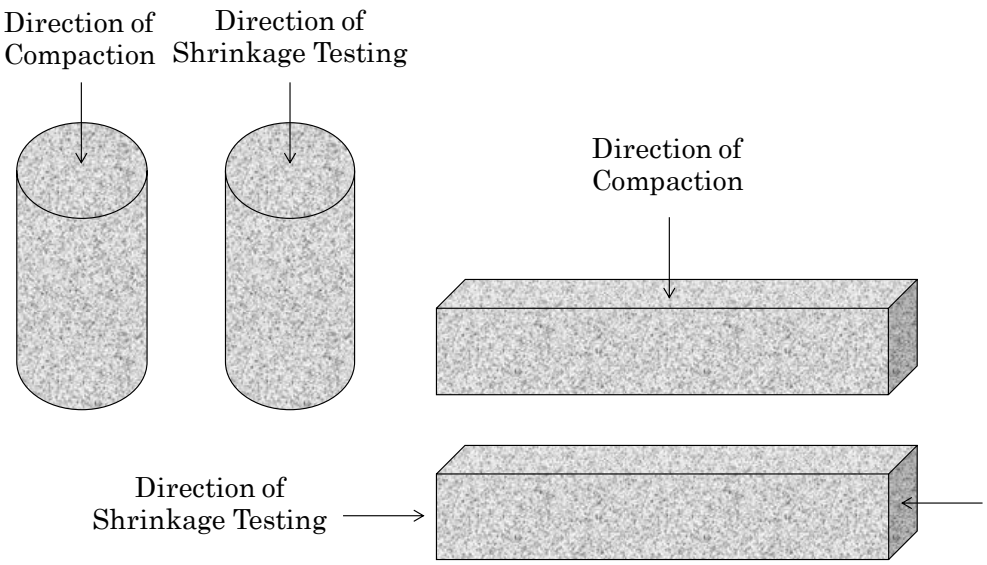

Figure 3-14: Direction of shrinkage and compaction

Based on the findings of Mbaraga (2015), the beam shrinkage tests exhibited an increase in restraint of shrinkage in comparison with the cylindrical shrinkage, see Figure 3-15. This is due to the geometry of the beam vs cylinder. There is a large friction build up on the interface of the base plate and the beam which hinders shrinkage. The surface area of the cylindrical geometry allows for even distribution of moisture loss and therefore shrinkage.

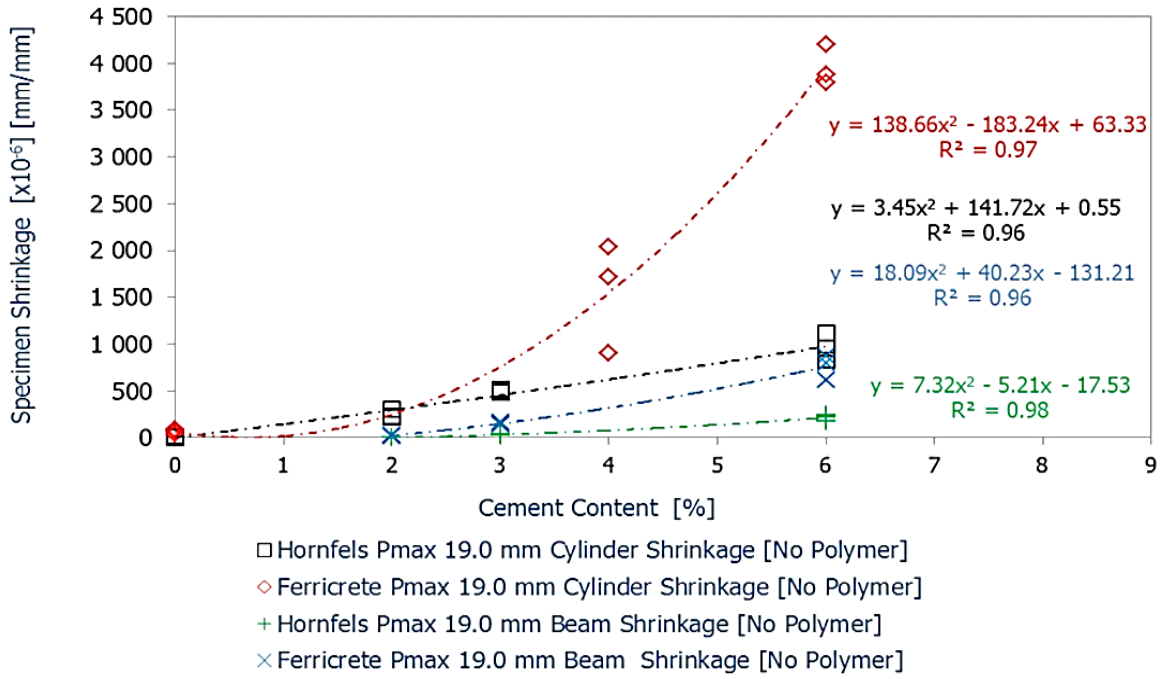

Figure 3-15: Beam vs cylinder shrinkage [Effect of friction, specimen size and shape], (Mbaraga, 2015)

3.5.1 Shrinkage Crack Modelling

3.5.1.1 Houben Shrinkage Crack Behaviour Model

The Houben Model is designed specifically to evaluate the crack behaviour in concrete pavements. The basis of the model is that as soon as the induced occurring tensile stress in the material exceeds the tensile strength of the material, transverse cracks will form. These cracks act as stress relief for the pavement, and are referred to as primary cracks.As the material experiences temperature variations and undergoes further chemical transformations, tensile stresses will again build up in the material until it exceeds the tensile strength of the material. It is assumed that the secondary cracks will form half way between two primary cracks. This procedure will repeat itself until the tensile stress in the material does not exceed the tensile strength of the material. The Model makes use of this crack behaviour principle and various other equations and assumptions to analyse the crack width and crack interval length of the cracks.

3.5.1.2 Model Adaptions

As mentioned, the Houben Model was originally designed for concrete pavements. Xuan (2012) and Mbaraga (2015), have made adaptions to the model in order to model Cement Treated Mix Granulates (CTMG) with Recycled Masonry and Concrete; and CTM respectively. Both authors made assumptions and simplifications for various input coefficients and equations. Variables such as time, temperature seasonal changes, hydration and thermal expansions, friction, material properties etc. all influence the model and are explained in detail in Chapter 6.

3.5.1.3 Concluding Summary

Shrinkage cracking is mainly a result of drying shrinkage of the stabilised material. As the material loses moisture, there is an increase in capillary tension which causes suction forces, which leads to induced tensile stresses. Once this tensile stress exceeds the tensile strength of the material, a crack will form in order to release some of the built-up tension. Other factors such as the environmental influences and cement and moisture content will also contribute to the magnitude of the total deformation.

Chapter 4

Experimental Framework

This chapter introduces the materials investigated, the testing setup and programme. The testing preparations and procedures for the preliminary and shrinkage tests are explained. The material characterisation tests and preparations include the wet sieve analysis, maximum dry density and optimum moisture content, initial consumption of cement, Atterberg Limits, pH of soil suspension, unconfined compressive strength and indirect tensile strength. These preliminary tests provide the characteristics of the material needed for causal analysis associated with cylindrical shrinkage tests, see Figure 4-1 for a schematic overview of the experimental study.

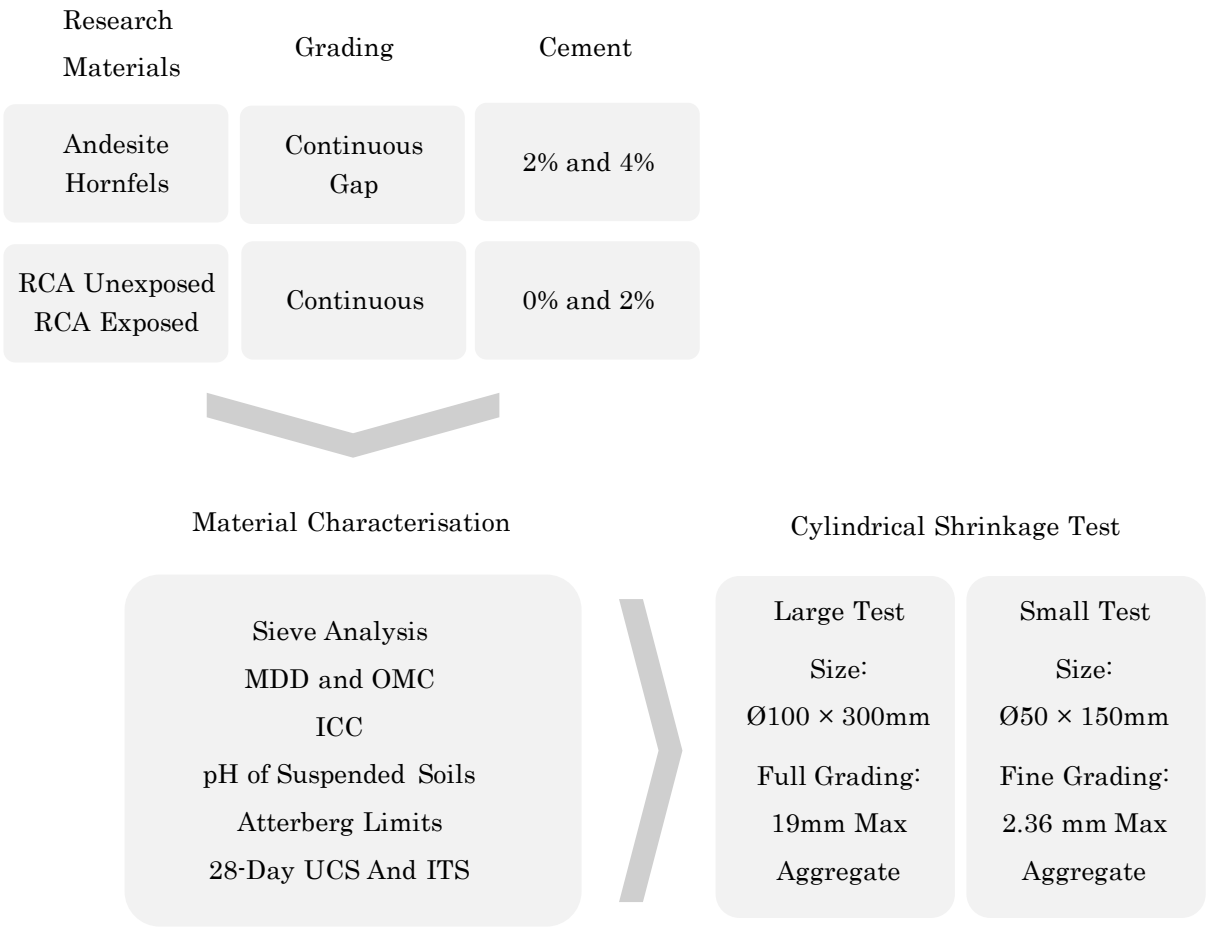

Figure 4-1: Experiment layout

4.1 Research Material Background

The research materials used included:

→ Granular materials that were cement stabilised

→ RCA which was un-stabilised and cement stabilised.

4.1.1 Granular Materials

The materials supplied by Aurecon included two G5 crushed stone aggregates, which were sourced from quarries in Brewelskloof and Contermanskloof. The Brewelskloof crushed stone is a grey metamorphic Andesite and the Contermanskloof crushed stone is a brown Malmesbury Hornfels. Both materials were sieved into fractions and stored in bags, see Figure 4-2.

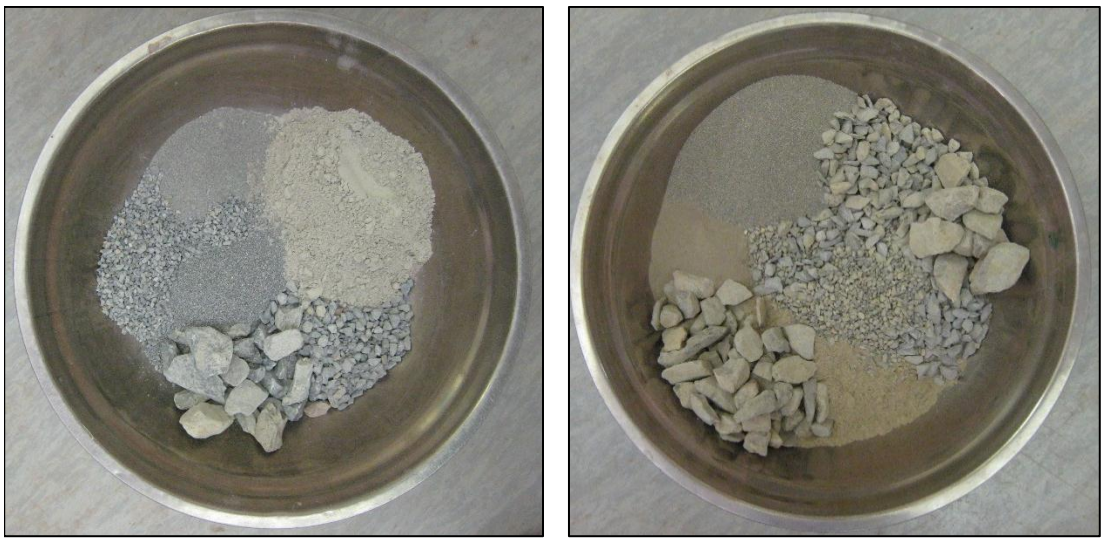

Figure 4-2: Andesite (left) and Hornfels (right)

4.1.2 Recycled Concrete Aggregate

The RCA was obtained from the demolition of a strip of concrete road on the N2 in Cape Town between Borcherds Quarry Road and the R300. The N2 comprised of a Jointed Unreinforced (Plain) Concrete Pavement (JCP). The pavement was originally constructed

between 1971 and 1972. Shortly after construction severe surface cracking was observed along the contraction joints. It was discovered that the cracks were a result of an Alkali Silica Reaction (ASR), (Strauss & Van der Walt, 1989).

ASR is a chemical reaction between the alkaline hydroxides in the pore water and active silica which can be found in mineralogy of certain aggregates, such as the Malmesbury Hornfels which was used. The product of this reaction is a gel which destroys the bond between the hardened cement paste and the aggregates. The gel absorbs water and swells significantly. This causes disruptions in the concrete and can lead to excessive cracking, (Domone & Illston, 2010).

In 1986 it was attempted to constrain the crack development/expansion as well as to restore the integrity of the pavement structure. It was reasoned at the time that the contraction joints were already in a state of compression, due to the expansive nature of the ASR and therefore, only the severely damaged joints would be addressed. To prevent further continuation of the ASR, it was decided to seal off the entire length and width of the concrete pavement with a bitumen rubber seal and a bitumen rubber open graded asphalt surfacing. This prevented exposure to moisture and allowed the concrete to dry out to a humidity of <75%, (Strauss & Van der Walt, 1989). SANRAL Pavement Management Systems, the current deteriorated state of the N2 has justified periodic maintenance project over 10 years, (Western Cape Goverment, 2016)

The project began in January 2016 and that was when Stellenbosch University acquired its first batch of RCA material. The RCA from this site was crushed with a jaw crusher at Stellenbosch University and then sieved into fractions and stored in bags until further use, Figure 4-3.

In terms of material storage and use, it is quite possible that two scenarios could exist on site after demolition i.e. the material is crushed and used immediately or stored in stockpiles while being exposed to the elements. The RCA that is crushed and used immediately has a high potential for self-cementation, while the exposed and stockpiled RCA has lower potential for self-cementation. The experimental plan considers both alternatives.

The exposed situation was simulated by wetting and drying the crushed and sieved RCA fractions repeatedly for a week. This gave the active latent cement present in the unexposed material time to react with the water molecules. This material was then considered exposed and was also tested for shrinkage.

Figure 4-3: RCA material processing

4.1.3 Sieve Analysis and Grading

A wet sieve analysis was executed on the two granular sources. Each source had a continuous grading and in order to compare them the material was reconstituted i.e. with consolidating individual fractions as an average of the two. Based on this common continuous grading, a gap grading was also arbitrarily chosen to analyse the effect of

packing and density. The gap grading considered has a lower percentage of large aggregates and a higher percentage of mid-size fractions than the continuous grading. The gap grading was only applied to the Brewelskloof Andesite. The gap grading was considered as a third comparator to the two original sources (Brewelskloof and Contermanskloof) with the continuous gradings.

A typical continuous RCA grading was based on the research study of Semugaza (2016). The grading of the granular materials and RCA are both continuous however are slightly different. Typical continuous gradings were selected for granular and RCA respectively to be in line with industry.

Both granular and RCA material was reconstituted based on the respective typical grading established, see Section 4.2.1 and 4.2.2 for further details regarding fraction sizes and grading reconstituted methods.

4.1.4 Cement Content

The cement content of the granular materials (2 and 4%) was decided based on the ICC test, which is discussed further in Section 4.2.4. As RCA already has active latent cement present, only a 0% and 2% additional cement content was considered as part of the experimental setup. IDM general purpose cement with 32.5N strength was used as stabilising agent. Other researchers have used higher strength cement (42.5N), however this was due to a lack of production of 32.5N at the time. For the application of this research the lower strength cement is sufficient and is in line with what is specified for roads.

4.1.5 Material Identification

All the previously mentioned variables are considered as part of the experimental plan, and are summarised in Table 4-1. A systematic code was developed to identify each combination of material, grading and cement content.

Table 4-1: Codes for various CTM and RCA samples.

Material Code	Material	Grading	Cement (%)
ANDE - C2	Andesite	Continuous	2
ANDE - C4	Andesite	Continuous	4
ANDE - G2	Andesite	Gap	2
ANDE - G4	Andesite	Gap	4
HORN - C2	Hornfels	Continuous	2
HORN - C4	Hornfels	Continuous	4
RCA.U - C0	RCA - Unexposed	Continuous	0
RCA.U - C2	RCA - Unexposed	Continuous	2
RCA.E - C0	RCA - Exposed	Continuous	0
RCA.E - C2	RCA - Exposed	Continuous	2

4.2 Preliminary Material Characterisation Tests

4.2.1 Sieve Analysis

A wet sieve analysis according to TMH1 (1986) Method A1, was performed on the Andesite and Hornfels, in order to establish the natural grading/particle size distribution of each granular material. An average continuous grading was determined by taking the average of each particle fraction, see Figure 4-4.

The averaged continuous grading was applied to both materials, by manually reconstituting the fractions. This was done to exclude the grading as a variable between the granular materials. As mentioned previously, a gap grading was arbitrarily selected and can be seen in Figure 4-4.

A material's grading greatly influences the density and packing, and ultimately the engineering properties. In having said this, a typical continuous RCA grading was selected as it would be a better representation of what would occur in industry. This does limit the comparison between CTM and RCA, however both are continuous and based on Figure 4-5 are very similar.

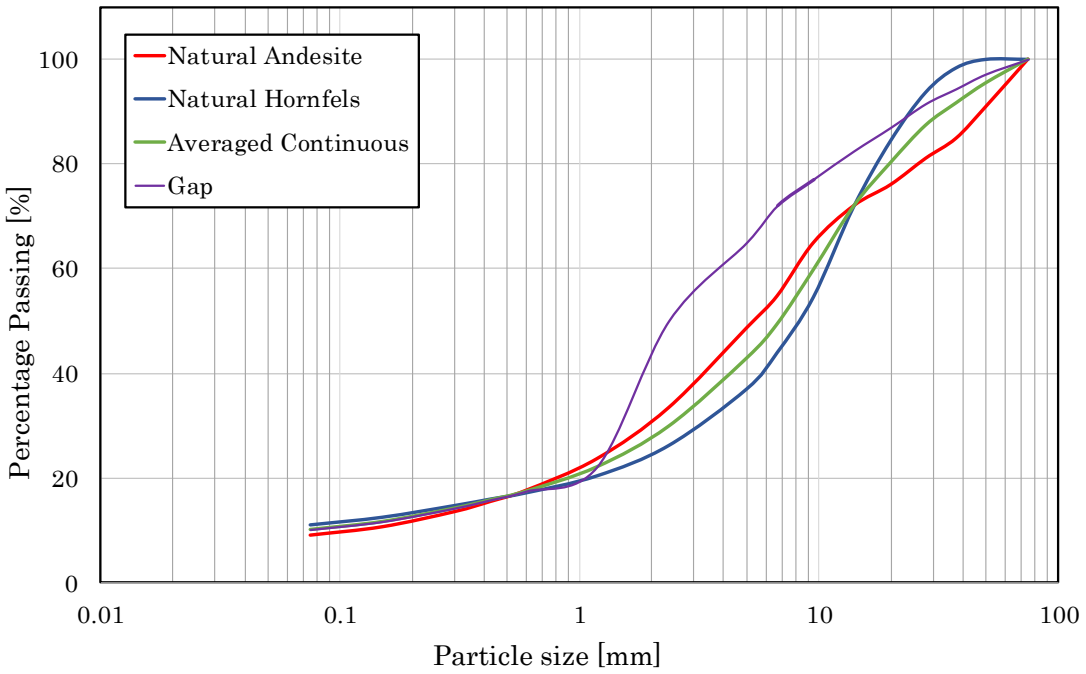

Figure 4-4: Averaged continuous and gap grading

4.2.2 Grading

The experimental plan included shrinkage tests on both large and small samples. This required scaling of the grading, where a full and fine grading i.e. 19mm and 2.36mm maximum aggregate sizes were used respectively. The full grading was determined with the scalp add-back method and the fine grading was determined with the scalp method. For exact grading used see Table 4-2and Table 4-3.

4.2.2.1 Scalp add back method for full grading

Boundary conditions effect the behaviour of the material and is dependent on the specimen size. The maximum aggregate size of 19mm was selected based on the balance between maximum aggregate size in relation to specimen geometry. Maximum aggregate size of 19mm was based on the recommended minimum $ds_{specimen}/ d_{max\text{-}particle}$ ratio of 6-7, (Van Zyl, 2015). The grading therefore needed to be reduced to a maximum stone size of 19mm. The scalp add back method was applied to the full grading in order for the effect of the larger aggregates to be taken into account. This required the total mass of stones larger than 19mm to be added as 13.2mm retained fraction. The scalp add back grading

of the RCA was a typical continuous grading used in Semugaza (2016) research, see Figure 4-5.

Table 4-2: Full average continuous and gap grading of Andesite, Hornfels and RCA

Sieve size [mm]	CTM Averaged Continuous [% passing]	RCA Averaged Continuous [% passing]	Andesite Gap [% passing]
19	100	100	100
13.2	71.9	67.0	82.4
9.5	59.7	60.0	77.1
6.7	49.4	52.0	72.0
4.75	42.9	45.0	65.0
2.36	29.9	35.0	50.0
1.18	22.1	26.0	22.1
0.6	17.5	20.0	17.5
0.425	15.8	17.5	15.8
0.3	14.2	15.0	14.2
0.15	11.6	10.5	11.6
0.075	10.1	8.0	10.1
<0.075	0	0	0

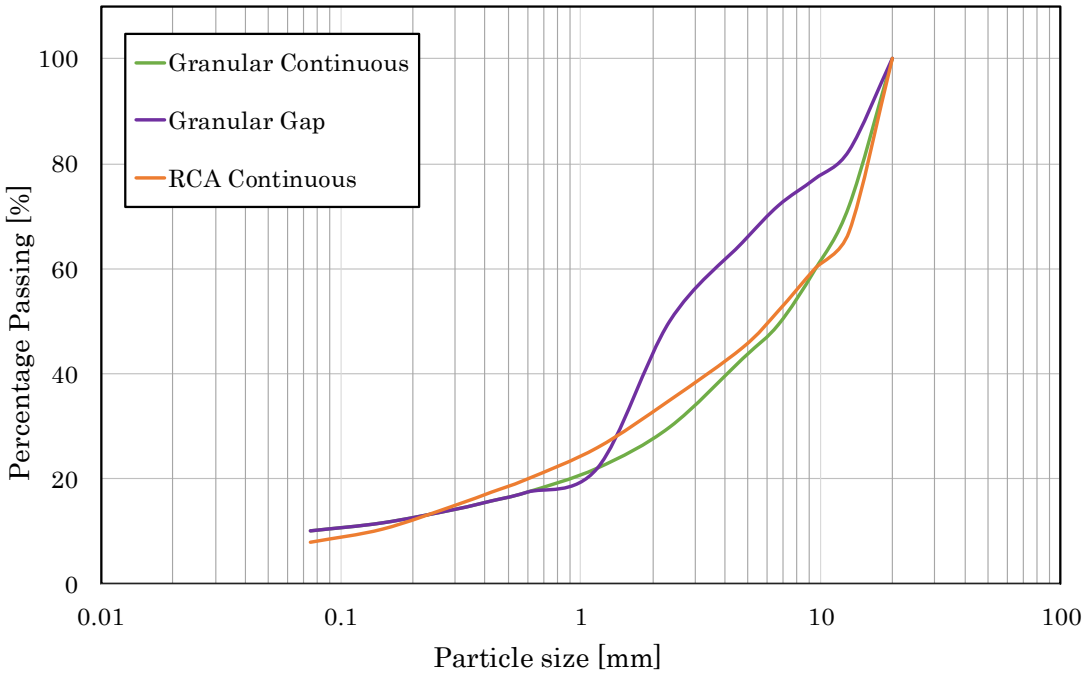

Figure 4-5: Scalp add back full grading

4.2.2.2 Scalp method for fine grading

The purpose of the fine grading was to monitor the shrinkage contribution of the finer material. Therefore, the ratio of finer material needed to remain consistent with that of the full grading and seemed unnecessary to apply the scalp add back method. The largest stone size for the small grading was 2.36mm. The material larger than 2.36mm was simply scalped. This changed the percentage passing, but the ratio on a mass basis remained unchanged.

The maximum stone size was decided on through trial and error. It was important to try keep the maximum particle size as small as possible. The first attempt was a maximum particle size of 0.425mm. This was impractical as the material lacked aggregate interlock and strength. Compaction of these samples through vibratory hammer could not be achieved. The samples would split in half when removed from the split mould after compaction. The procedure was repeated with an increasing particle size with each attempted and eventually succeeded with a maximum particle size of 2.36mm. The moisture content/ density and MOD tests results are further discussed in the next section.

Table 4-3: Fine average continuous grading for CTM and RCA

Sieve size [mm]	CTM Fine grading [% passing]	RCA Fine grading [% passing]
4.75	100	100
2.36	69.6	77.8
1.18	51.5	75.8
0.6	40.8	44.4
0.425	36.9	38.9
0.3	33.1	33.3
0.15	27.2	23.3
0.075	23.6	17.8
<0.075	0	0

4.2.3 Maximum Dry Density and Optimum Moisture Content

The Maximum Dry Density (MDD) and Optimum Moisture Content (OMC) are standard tests as described in the TMH1(1986) Method A7. This standard test defines the optimum relationship between moisture and density of a material when prepared and compacted, according to the Modified AASHTO compaction effort. The MDD is achieved by varying moisture contents. The moisture content which gives maximum dry density is the OMC. The OMC and MDD is determined for each material for the full and fine grading. Even though this method of compaction was not used for compacting the UCS, ITS and shrinkage samples, it was performed as it is an industry comparative.

4.2.3.1 Proctor Hammer

Stellenbosch University makes use of the Proctor Hammer to achieve the standard 100% Mod AASHTO compaction. The test requires a standard mould of Ø152 ×152mm and a tamper of 4.54kg which falls freely on the sample 11 times per layer. Each layer experiences 8 blows to the outside circumference and 3 blows to the centre. Each of the 5 layers should be between 25mm and 30mm thick. The densities and corresponding moisture contents are then plotted and the MDD and OMC are read off. This method was implemented on the full grading of the continuous and gap graded Andesite and the continuous graded Hornfels Table 4-4 and Figure 4-6.

Figure 4-6: Proctor hammer, Wirtgen Vibratory hammer and Bosch Vibratory hammer

4.2.3.2 Vibratory Hammer

All samples were compacted with the double shaft frame with the Bosch GSH 11 E ® Vibratory hammer, see Figure 4-6. Since the vibratory hammer provided a much higher compaction energy, the MDDs and OMCs of the granular materials were adjusted to take this into account. The adjusted MDDs and OMCs were then tested with the vibratory hammer to ensure that the adjusted values were achievable, see Table 4-4 for results.

Table 4-4: MDD and OMC results of granular materials with full gradings

Material	MDD [kg/m^3]	OMC [%]	Adjusted MDD	Adjusted OMC
ANDE - C	2372	5.9	2380	5.6
ANDE - G	2326	6.1	2335	5.8
HORN - C	2340	5.8	2355	5.7

The maximum dry densities and optimum moisture contents for the RCA materials were previously performed on the Wirtgen WLV1 Vibratory hammer by Master's student Z. Bredenkamp, see Figure 4-6. Because of a material shortage, it was not possible to perform a Proctor Mod on the RCA material as previously done with the granular materials. It was then decided to adjust the Wirtgen MDD and OMC, which was done at a higher compaction energy, to account for the reduction in compaction energy of the Bosch hammer, see Table 4-5

Table 4-5: MDD and OMC results of RCA with full gradings

Material	MDD [kg/m^3]	OMC [%]	Adjusted MDD	Adjusted OMC
RCA.U - C	2120	6.8	2100	7.5
RCA.E - C	2160	6.8	2136	7.5

4.2.3.3 MDD and OMC of Fine Grading

The fine grading is not standard, therefore the adjusted MDD was used as with the full grading for a consistent comparison. A Mod AASHTO with the Proctor hammer would have required a large amount of fine material, which seemed wasteful as there was a

shortage of material. Specimens were compacted with the Bosch hammer in a small mould, see section 4.3.3.1, in 3 layers of 50mm each.

Due to the vast increase in surface area, it was assumed that a larger amount of additional moisture would be needed as a beginning moisture content for a vibratory hammer MOD. An initial target density was also difficult to estimate due to the fineness of the material. Many attempts at achieving an MDD were performed and were achieved, however the samples broke during demoulding. This suggested that there was not enough moisture present. The moisture content was determined through trial and error. It was decided to assume the same density as the large samples, however slightly higher moisture contents were required for stable demoulding, see Figure 4-7.

Figure 4-7: Fine grading with max stone size 1.18mm (left), fine grading with low moisture content (middle) and first successful trial specimen with fine grading and maximum stone size 2.36mm (right)

The same principle was applied to RCA; however, the required height was not achievable and therefore the density was adjusted accordingly. When demoulding the specimens split down the middle, therefore moisture was increased in 1% intervals until the specimens could be demoulded without damage, see Table 4-6.

Table 4-6: MDD and OMC of fine grading

Material	MDD [kg/m^3]	OMC [%]
ANDE - C	2380	6.0
HORN - C	2355	6.0
RCA.U - C	2010	9.0
RCA.E - C	2010	9.0

4.2.4 Initial Consumption of Cement

The initial consumption of cement (ICC), SANS 3001 – GR57 (2014), test was performed to determine the percentage of cement required to introduce pozzolanic activity in the granular material. Should there be insufficient cement present in the mix, the material would not provide free lime and could lead to durability issues. The test measures the pH of the sample. With each increasing percentage of cement, it is expected that the pH will increase, as the pH of cement is 12.4 and is generally higher than that of granular material. SANS (2014) considers sufficient stabilization of a material at a pH of 12. The optimum percentage cement was recorded at this pH level. This test is also used to determine the level of carbonation. As cemented materials get exposed to CO_2 in the environment, the pH of the cementitious material drops, as explained in Chapter 3.

4.2.4.1 Sample Preparation and Testing

According to SANS, samples of 200g with full gradings (max stone size 19mm) are prepared with varying percentages of cement, 0%, 1%, 2%, 3%, 4%, 5% and 6%. The guidelines for the amount of distilled water to be added are unclear. SANS recommends adding sufficient distilled water until the mixture is over-saturated, i.e. when water has filled the pores of the material and free water collects when a hollow is made in the material. The mixture must be stirred every 10min for 60min to allow for the cement to hydrate adequately, see Figure 4-8.

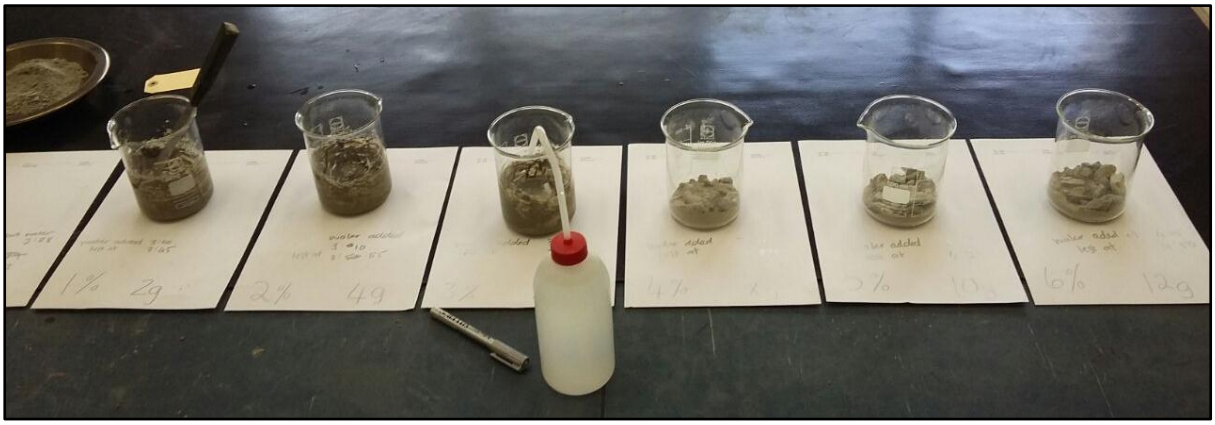

Figure 4-8: ICC test preparations

Meanwhile the pH and temperature probes are calibrated with buffer solutions. Both probes are then carefully submerged in the sample, and a reading is taken after 3 minutes. The process is repeated a second time. If the difference between the readings is more than 0.02, it is required to take an additional reading in which case the average must be calculated.

Usually a material is considered sufficiently stabilised when a pH of 12.4 is reached. According to the SANS test procedure a material can be considered stabilised at a pH of 12 for this test, see Figure 4-9.

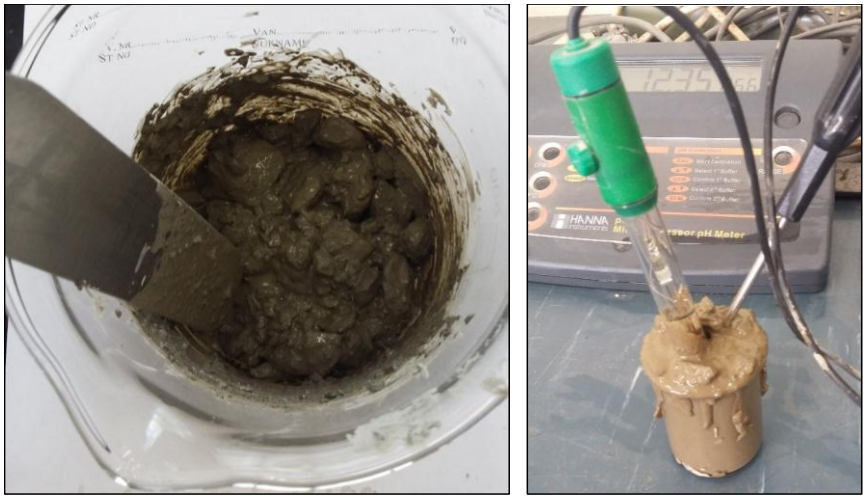

Figure 4-9: ICC reading procedure

4.2.5 Electrometric Determination of the pH Value of Suspended Soils

The pH values of the various materials were determined with method A20 in the TMH1 (1986), with a calibrated pH meter, see Figure 4-10. Material of at least 30g was prepared where the maximum stone size was less than 0.425mm. The material was added to 75ml of distilled water and was stirred. The solution was covered and left to rest overnight. Readings were taken the following day after stirring the solution again and ensuring that the material was sufficiently suspended. The mean of three readings were taken.

Figure 4-10: Electrometric determination of the pH value of suspended soils test setup

4.2.6 Atterberg Limits

The Atterberg limits considered were the liquid limit and plastic limit as well as the linear shrinkage. Plasticity explains the ability of a material to undergo permanent deformation without cracking or crumbling. Generally, a material can be in a liquid, plastic, semi solid or solid state depending on the water content. The water content is defined as a ratio of mass of water within the soil to the mass of the solid particles.

The liquid limit (LL) is the minimum amount of water added to a material for it to become a liquid. The LL is expressed as the water percentage of the oven dried mass at the boundary of the material being classified as a liquid or plastic material, see Method A2 from TMH1(1986).

The linear shrinkage test assesses the shrinkage potential of a material, at the LL water content. A 15cm bar container is filled with material, and placed in the oven. The water in the material evaporates and causes shrinkage. The new length of the specimen is then measured, see Method A4 from TMH1(1986).

The plastic limit (PL) is the minimum amount of water in the material before it becomes brittle and crumbles. The method involves rolling the material into threads of 3mm in diameter at the minimum moisture content without the treads crumbling, see Method A3 from TMH1 (1986). In Figure 4-11 it can be seen that PI is equal to the difference between the LL and the PL.

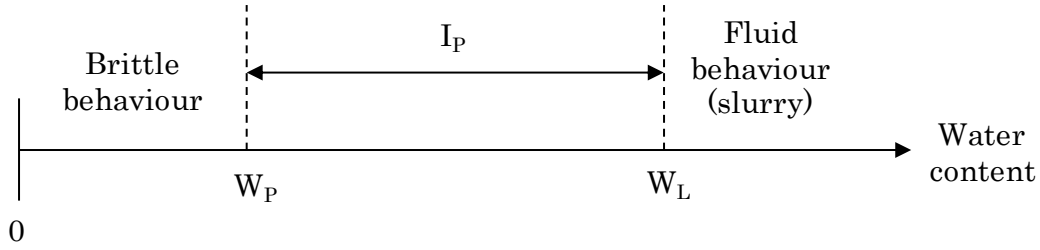

Figure 4-11: Atterberg limits (Knappett & Craig, 2012)

4.2.7 Material Strength Tests

The Unconfined Compression Strength (UCS) test and Indirect Tensile Strength (ITS) test form part of the standard mix design process for stabilised materials. The tests give indications of whether a sufficient quantity of cement has been added in order to achieve the required strengths. It is also widely used on site for quality control purposes during construction (SANRAL, 2014c). The UCS sample dimensions were assumed as (Ø100 ×150mm) and a standard loading rate of 150kN/min was applied. The ITS sample dimensions were assumed as (Ø100 ×100mm) with a standard loading rate of 40kN/min. The material preparation procedure is the same as for the shrinkage tests in Section 4.3.4. Based on the specimen geometry, mass per layer was calculated and weighed off. The UCS samples were compacted in 3 layers of 50mm each and the ITS samples were compacted in 2 layers of 50mm each. Three repeats were executed for both UCS and ITS per material and cement percentage, see Figure 4-12. The specimens were cured for 28 days.

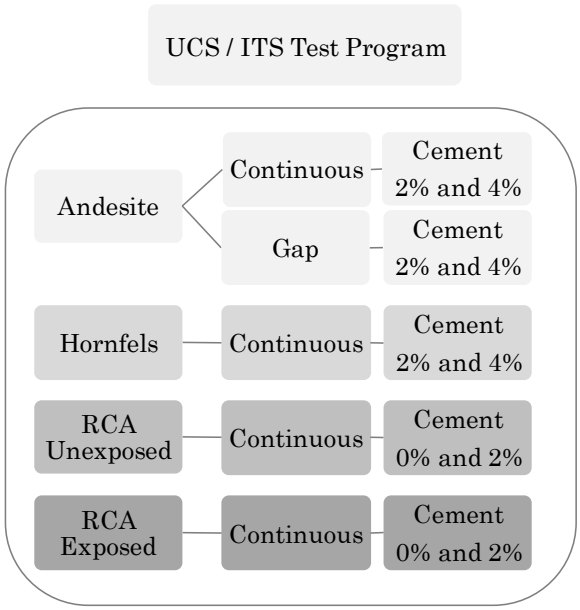

Figure 4-12: UCS and ITS testing program

4.3 Cylindrical Shrinkage Tests

Cylindrical shrinkage tests were performed to measure the axial shrinkage behaviour. This test involved the monitoring of axial displacement over time for compacted cylindrical specimens. Large and small shrinkage tests were performed on Andesite, Hornfels, unexposed and exposed RCA at various cement contents. See Figure 4-13 for a breakdown of shrinkage tests done.

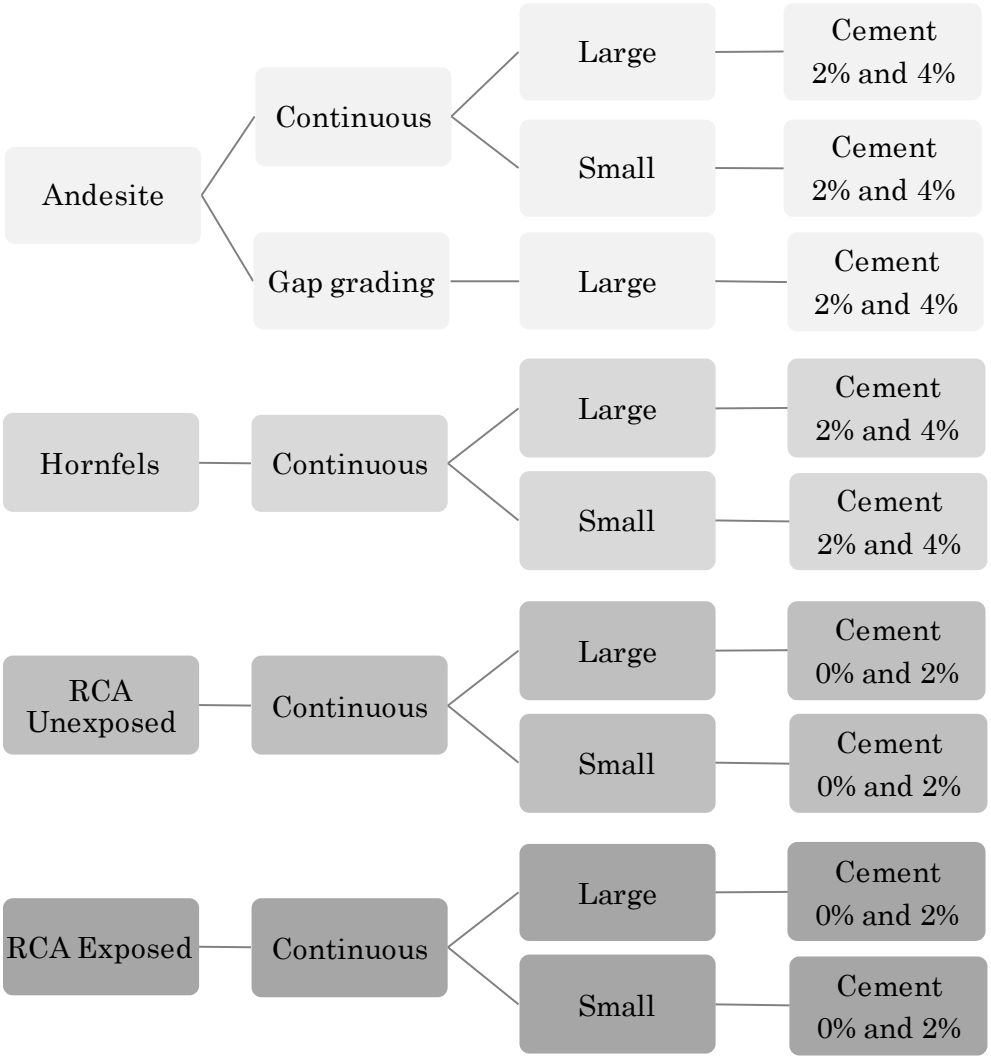

Figure 4-13: Schematic overview of shrinkage testing program

4.3.1 Specimen Size and Cement Percentage

The cylindrical shrinkage test made use of a large sample size of Ø100 × 300mm, with a maximum aggregate size of 19mm. A diameter to length ratio of 3 was chosen to minimise the effect of friction from both ends of the sample (Van Niekerk, 2002), see Figure 4-14.

The majority of shrinkage occurs in the finer particles; therefore a smaller sized cylindrical shrinkage test was designed (Ø50 × 150mm) with maximum stone size of 2.36mm. As with the large specimens a diameter to length ratio of 3 was chosen to minimise the effect of friction from both ends of the samples.

Figure 4-14: Small and large small shrinkage test samples

As previously discussed the cement percentages of 2% and 4% were chosen for the granular materials base on the ICC tests. The 0% and 2% cement percentages for RCA were chosen based on ICC tests, but also based on literature.

4.3.2 Material Identification and Shrinkage Test Program

Large and small shrinkage tests were carried out on all materials, gradings and cement contents, as previously outlined. The only exception was Andesite gap grading, where the fine grading was the same as the continuous fine grading, see Table 4-7 for the specimen identification codes.

Table 4-7: Specimen identification code

Code	Material	Grading	Cement (%)	Size
ANDE - C2L	Andesite	Continuous	2	Large
ANDE - C2S	Andesite	Continuous	2	Small
ANDE - C4L	Andesite	Continuous	4	Large
ANDE - C4S	Andesite	Continuous	4	Small
ANDE - G2L	Andesite	Gap	2	Large
ANDE - G4L	Andesite	Gap	4	Large
HORN - C2L	Hornfels	Continuous	2	Large
HORN - C2S	Hornfels	Continuous	2	Small
HORN - C4L	Hornfels	Continuous	4	Large
HORN - C4S	Hornfels	Continuous	4	Small
RCA.U - C0L	RCA - Unexposed	Continuous	0	Large
RCA.U - C0S	RCA - Unexposed	Continuous	0	Small
RCA.U - C2L	RCA - Unexposed	Continuous	2	Large
RCA.U - C2S	RCA - Unexposed	Continuous	2	Small
RCA.E - C0L	RCA - Exposed	Continuous	0	Large
RCA.E - C0S	RCA - Exposed	Continuous	0	Small
RCA.E - C2L	RCA - Exposed	Continuous	2	Large
RCA.E - C2S	RCA - Exposed	Continuous	2	Small

4.3.3 Experiment Apparatus Design

This research project benefitted from the previous developmental work regarding the apparatus such as the moulds and frames.

4.3.3.1 Moulds for Shrinkage Tests

Large split moulds were used to make the Ø100 × 300mm. These moulds have been used in previous research by Mbaraga,(2015) and Semugaza,(2016). The small samples required a small split mould (Ø50 × 200mm) and Ø50mm tamping foot to be designed and manufactured. A removable base of Ø300mm was manufactured to comply with the hammer and to secure the split mould, see Figure 4-15.

Figure 4-15: Moulds for compaction

4.3.3.2 Frame for Shrinkage Tests

Once compacted, the shrinkage specimens (1) needed to be placed into a suitable frame, see Figure 4-16, where the dial gauges could measure the vertical displacement. The original frames were designed for the 300mm samples, and therefore needed to be modified to fit the additional small specimens that were also tested. Additional holes (2) were punched into the vertical steel members for easy adjustment depending on the height of the specimen.

The base of the frames (3) were made from timber and were painted with water proof sealer. This prevented any swelling or movement of the wood from the surrounding moisture. Two 3mm thick Perspex disks (4) were cut to size to fit underneath and on top of each specimen. This provided a smooth and even surface for the dial gauge to rest on. The dial gauges (10mm stroke) came with lug backs that were fastened to Ø10mm steel pins. The pins were held in place by PVC plastic strips (5) attached to frames with screws. A 2mm slit was cut into the side of each PVC plastic strip, and thread was manually tapped into the holes that were drilled. The screws tightened the gap in the slit and secured the dial gauges. This also made it easier to remove the dial gauges after use, see Figure 4-17.

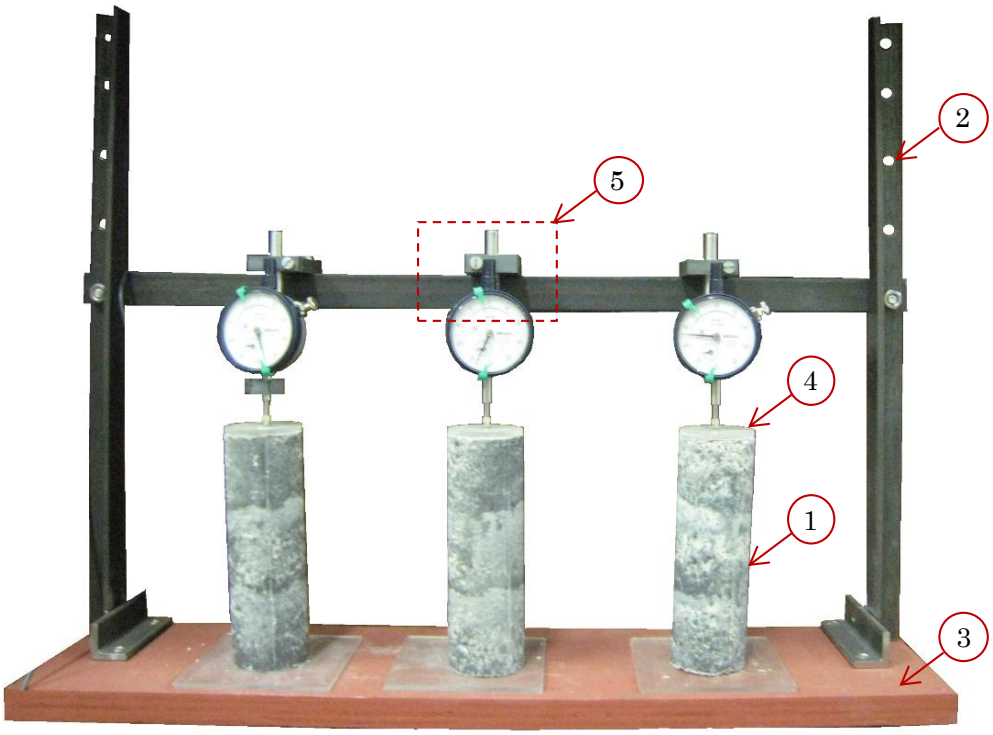

Figure 4-16: Adjustable shrinkage frame

Figure 4-17: Dial gauge connection (5)

4.3.3.3 Shrinkage Chamber

A chamber was designed from a wooden frame with glass sliding doors. This provided a more protected housing against environmental changes such as concentrated air flow from the air-conditioning and against heat from direct sunlight. The vertical design allowed for smaller areas between specimens where environmental conditions could be controlled. The original frames were modified to fit into the chamber. The frames were placed in a staggered manner to take readings from dial gauges more easily. Caster wheels with stoppers were added to the bottom of the chamber for quick and easy manoeuvring, see Figure 4-18.

Figure 4-18: Shrinkage chamber

Humidity control was carried out using a statured solution of humidity salts as recommended by Winston and Bates, (1960). Small computer fans were installed on adjustable shelves that would circulate the air within the theoretically closed system. The gap between the glass doors would have been sealed with duct tape to simulate a closed system. This however could not be implemented as the glass doors did not open and close smoothly leading to disturbance of the dial gauges. The second attempt at a closed system included the use of clear plastic sheeting that could be lifted when inserting samples,

however it was difficult to take accurate readings off the dial gauges that were further to the back. A constant humidity was impossible to be attained due to opening and closing of the sheeting. The humidity and temperature were documented with meters at every reading instead. It should however be mentioned that due to the setup a good degree of control could be attained and as all measurements were taken it was possible for these variables to be quantified.

4.3.4 Specimen Preparation for Shrinkage Tests

As mentioned, two sizes of samples were tested, namely a large (Ø 100 × 300) and small sample (Ø 50 × 150). The following specimen preparation was performed for both sizes:

→ Together with the maximum dry density and sample height, it was possible to estimate a mass for the sample and reconstitute the grading.

→ The cement content was calculated as a percentage of the dry aggregate.

→ The water was calculated using the adapted OMC percentage of the dry mass.

→ All the constituents were added in a pug mixer, firstly the aggregate, then the cement and then while mixing the water was slowly added.

→ The mass of each layer was weighed out into plastic bags for the sample.

→ The large specimens were compacted into 5 layers of 60mm each, while the small samples consisted of 3 layers of 50mm each, see Figure 4-19.

Figure 4-19: Sample preparation

→ The split moulds and base plates were properly cleaned, dried and sprayed with "Spray and cook" to minimise friction on the sides and base.

→ The Bosch GSH 11 E ® vibratory hammer was used for compaction, where the mould was properly secured to the base plate.

→ A circular paper disk was placed at the bottom on the mould to ensure no loss of material.

→ Each of the pre-weighed out layers were poured into the mould and compacted to the specified height of the layer.

→ After compaction, each layer was scarified using a drill with a long nose drill bit. This was done to loosen the top 1cm of the material for better bonding of the next layer.

→ Once compacted, the specimen was removed from the mould and wrapped in 5 – 6 layers cling wrap to ensure no moisture loss.

→ A Plexiglas was placed at the bottom and on top of the specimen to ensure a stable footing for the dial gauge apparatus.

→ The specimen was placed into the shrinkage frame and the dial gauges were adjusted and secured.

4.3.5 Shrinkage Test Procedure

As soon as the specimens were secured in the frame, the first reading was recorded and used as a reference reading. An increase in reading indicated shrinkage and a decrease in reading indicated swelling. The difference was calculated as the dimensional change. Strain was determined by dividing the dimensional change by the height of the compacted sample. The assumption is made that the strain is constant over the height of the sample. This is not entirely the case, because of the boundary conditions (at the bottom) and due to other factors.

For the first 7 days readings were taken every 6 to 12 hours. For the next 21 days readings were taken daily. After 28 days the shrinkage more or less stabilised and readings were taken every 3-4 days.

4.3.6 Application of Results

The preliminary material tests results are discussed in detail in Section 5.1. These results help to characterise the material in terms of cement content, host material and strength performance.

The shrinkage results obtained will be plotted against time. In Section 5.2, the shrinkage trends of each material are compared and analysed while considering the influence of the following on shrinkage:

→ Cement content and host material on large and small samples individually

→ Aggregate size

→ Humidity

The shrinkage data as well as the preliminary tests are used in Chapter 6 and Chapter 7 to model the shrinkage crack behaviour of the material when used in a road. The model is based on the Houben model, which was initially for a concrete pavement. However, this model has been adapted for CTM and RCA.

4.4 Concluding Summary

This chapter presented a detailed description of research materials and the necessary characterisation tests performed. The materials discussed included Hornfels, Andesite, unexposed and exposed RCA. The characterisation tests included a sieve analysis, OMC and MDD, ICC, pH of suspended soils, Atterberg Limits, UCS and ITS tests. These tests are all standard tests and were performed according to the TMH1 (1986).

Two sizes, large and small, cylindrical shrinkage tests were discussed. This was to investigate the influence of aggregate size on shrinkage. This chapter includes the material preparation, apparatus developments and, test set up and procedures. These tests are not standard and were based on previous research.

Chapter 5

Test Results and Discussion

This chapter deals with the results of the preliminary tests as described in the previous chapter. Shrinkage tests are discussed and compared in terms of cement content, host material, aggregate size and humidity.

5.1 Material Characterisation

The results from the ICC, pH of Suspended Soils, Atterberg limits, UCS and ITS tests are presented and discussed in this section. These tests provide an indication of the material characteristics and will be used to give insight on the shrinkage behaviour.

5.1.1 ICC

The ICC test is performed on the full gradings with maximum aggregate sizes of 19mm. Materials tested: Andesite (continuous and gap graded); Hornfels (continuous) and both exposed and unexposed RCAs (continuous), see Table 5-1 and Figure 5-1. SANS (2014), specifies that sufficient stabilisation can be considered at a pH of 12 and not 12.4 which is the pH of cement.

Table 5-1: ICC test results

Materials	pH						
Cement (%)	0	1	2	3	4	5	6
ANDE - C	8.25	11.63	12.15	12.24	12.47	12.47	12.47
ANDE - G	8.06	11.46	11.87	12.04	12.18	12.25	12.4
HORN - C	8.34	12.00	12.18	12.20	12.37	12.4	12.44
RCA.U - C	12.83	12.83	12.83	12.83	12.83	12.83	12.83
RCA.E - C	9.45	11.53	11.86	12.05	12.20	12.30	12.40

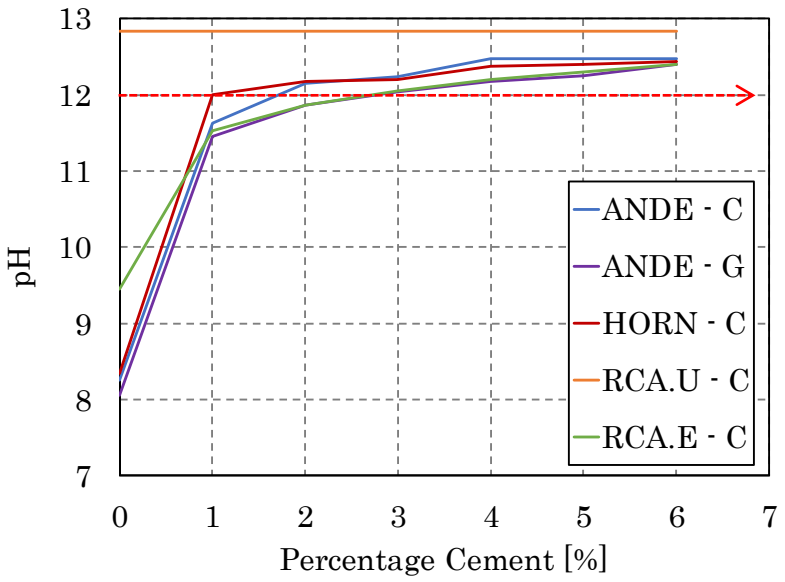

Figure 5-1: ICC test result

5.1.1.1 Granular Materials

The continuous grading of Hornfels requires the lowest percentage of cement to stabilise (1%), while the continuous Andesite requires 2%. The gap grading Andesite required 2.5% for stabilisation. It was decided to select 2% as the minimum cement percentage for all materials despite not meeting the stabilisation requirements for the gap grading by 0.5%. This was substantiated as a gap grading is less likely to be used in industry in comparison to a continuous grading. It would also be considered an unnecessary addition of cement for the Hornfels. The gap grading considered has a lower percentage of large aggregates and a higher percentage of mid-size fractions than the continuous grading. It has the same fine fractions percentages. This suggests that grading could have an influence on the percentage cement needed to stabilise. Therefore, to be cost efficient it is beneficial to use a continuous grading.

5.1.1.2 RCA

The unexposed RCA reached a pH of 12.83 with 0% additional cement. This indicates a high concentration of active latent cementitious product even in the crushed form. According to the ICC specifications, unexposed RCA does not need any additional cement for stabilisation. The exposed RCA has an initial pH of 9.45 which is higher in comparison

with the granular materials, however is much lower than the unexposed RCA. This is a possible indication that the exposure through wetting and drying has reduced the amount of active latent cement particles present. This could be due to carbonation during the exposure. The exposed RCA follows a similar rate of increase in pH as the granular material and is considered stabilised at 2.5%, see Figure 5-1.

5.1.1.3 Conclusion

The ICC test was performed to confirm the required quantities of cement for stabilisation and further shrinkage testing. To ensure adequate cement stabilisation, 2% was selected as the lower limit for granular materials. This could be argued to be too low for the stabilisation of gap graded Andesit. However, an ICC is rarely performed on site, as the required cement percentage is usually based on UCS strength. The UCS results of the gap graded Andesite were in line with the standards of a C2, see Section 5.1.4, and therefore 2% would have been acceptable on site. Typically, 4% would be excessively high for site, however for research purposes and a sensitivity analysis a higher percentage cement was included. The ICC was also performed to compare the pH of CTM and RCA. This was to obtain an indication of how much active latent cement was present in the RCA in comparison to the virgin granular aggregate.

The unexposed RCA has a high concentration of active cement as seen with the high pH reading. Whereas the exposed RCA resulted in pH behaviour similar to that of granular material. It was therefore concluded to use 0% and 2% as the cement contents for further shrinkage testing of RCA.

5.1.2 pH of Suspended Soils

The pH of suspended soils method differs from the ICC method due to the smaller maximum aggregate size (less than 0.425mm). The ICC represents the actual material by taking into account the full grading. This method looks at the contribution of the fine fractions where, one could argue that this is acceptable as activity occurs in the finer fractions. The pH results can be seen in Table 5-2 and Figure 5-2.

Table 5-2: pH results

Materials	pH				
Cement (%)	0	1	2	3	4
ANDE	8.46	11.65	12.06	12.34	12.40
HORN	8.82	11.61	12.17	12.28	12.40
RCA.U	12.40	12.40	12.40	12.40	12.40
RCA.E	10.00	10.66	11.05	11.30	11.50

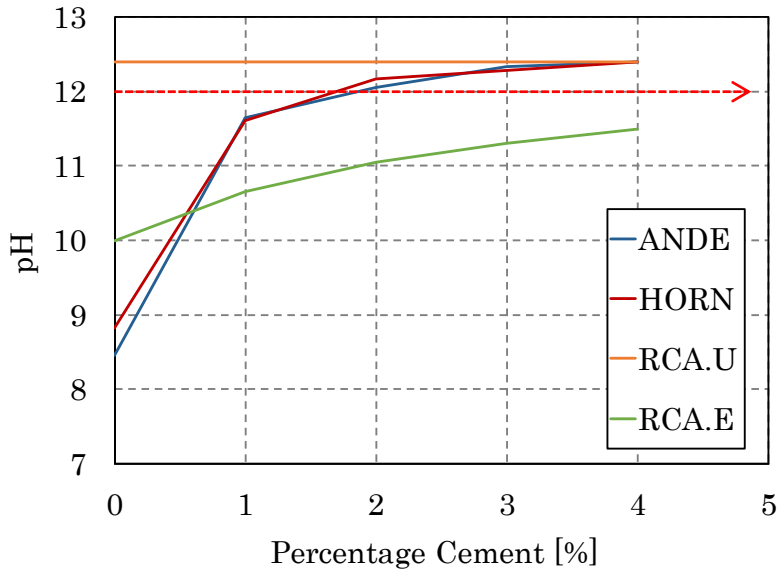

Figure 5-2: pH of suspended soil results

5.1.2.1 Granular Materials

The Andesite and Hornfels perform similarly to the ICC test, and the same conclusions can be drawn.

5.1.2.2 RCA

As with the ICC, the results indicate that unexposed RCA has a significant percent of active latent cement as it has a pH of 12.4 without any additional cement added. Unfortunately, it is very difficult to quantify the exact amount of active latent cement present, however it is possible to estimate at least a minimum percentage. It is possible that the unexposed RCA could be equivalent to at least a 2% stabilised Andesite or Hornfels. Bearing I mind that stabilisation is considered at a pH of 12. The equivalent

percentage cement could be higher however, the pH level would not indicate this as it would remain at 12.4 after the initial stabilised limit has been reached.

The exposed RCA shows conflicting results in comparison to the ICC test. At increasing percentages of cement the RCA.E does not follow the same increasing rate as the granular materials. This is despite its higher initial pH reading of 10. The exposed RCA does not meet the required pH of 12, no matter the increase in cement percentage. It is predicted that according to this test stabilisation would only occur at much higher cement percentages. This shows again that the unexposed RCA has a higher percentage active latent cement than the exposed RCA due to the exposure.

5.1.2.3 Conclusion and Synthesis

The influence of grading is only noted through the ICC test, as the pH of suspended soil test only considers maximum aggregate size of 0.3mm. The ICC results between the gap and continuous grading of the Andesite indicated that the gap grading would need additional cement for stabilisation. This suggests that there is an increase in surface area due to the absence of the larger aggregates and would require more cement for sufficient stabilisation.

Based on the comparison between the two tests, the results of the RCA.E and RCA.U suggest that there could be active filler on the surface of the large aggregates that contribute to the stabilisation more so than in the fine fractions.

This interpretation is supported by Tawine (2017) who performed pH and Phenolphthalein tests on various individual fractions of crushed and sieved new and old RCA fines, see Table 5-3 for Tawine's pH test results.

Table 5-3: pH test results for RCA fine material for new and old concrete, (Tawine, 2017)

Fraction Size [mm]	pH of New Concrete	pH of Old Concrete
0.3	13.5	13.34
0.15	13.54	13.05
0.075	13.54	13.31
Pan	9.2	10.44

The above mentioned pH results indicated that for the 0.300 - 0.075mm fractions the material gave pH readings ranging from 13.05 – 13.54. However, the pan fractions were much lower ranging from 9.20 – 10.44. A possible reason for this is that the majority of the pan consists of crushed mortar, which forms the paste around the large aggregates. This mortar has already reacted with water molecules and is active anymore. However, the bigger fractions may have fine active latent cement particles that cling to the surface of the aggregate.

A Phenolphthalein test involves a Phenolphthalein indictor solution that turns basic solutions magenta. The higher the pH the brighter the colour. The test involves spraying the material and monitoring the colour intensity. Tawine performed these tests on the 0.300mm, 0.150mm, 0.075mm and pan fractions. The 0.300 – 0.075mm fractions showed magenta, while the pan fractions did not. This confirmed that the pan fraction held the least cementing agent. Phenolphthalein was also sprayed onto the 9.5mm aggregates, which indicated magenta. This suggests that in addition to the pH tests performed on the adhered material there are self-cementing particles coating the large aggregates, (Tawine, 2017).

The pH of suspended soils test, as well as the ICC test are equally appropriate tests as they provide different perspectives. The ICC explains the influence of the large aggregates on stabilisation and cement consumption, while the pH of suspended soils test highlights the potential for stabilisation in the fine fractions.

5.1.3 Atterberg Limits

The plastic index of Andesite and Hornfels are 4 and 5 respectively. According to Mukherjee (2014) both PIs can be considered slightly plastic, see Table 5-4 and Table 5-5.

Table 5-4: Plasticity ranges (Mukherjee, 2014)

PI Range	Plasticity
0-3	Non Plastic
3-15	Slightly Plastic
15-30	Medium Plastic
>30	Highly Plastic

Both unexposed and exposed RCA were non plastic. This correlates with the assumption that RCA contains some cementitious product. According to SAPEM, lime is added to clayey material to reduce the plasticity. This occurs as the calcium ions from the hydrated lime coat the clay particles and displace water and other ions.

Table 5-5: Atterberg Limit results

Materials	Shrinkage Limit (%)	Liquid Limit (%)	Plastic Limit (%)	Plastic Index
ANDE	1	19.92	15.97	4
HORN	2	22.82	18.07	5
RCA.U		Non Plastic		
RCA.E		Non Plastic		

Mbaraga investigated Hornfels and Ferricrete with PIs as non-plastic and 2.8 respectively. Hornfels which was non-plastic gave a higher compacting density than Ferricrete. Similarly with this study, Andesite with the lower PI gave slightly higher densities than the Hornfels. This could be due to the different mineralogy characteristics such as clay minerals. Materials with higher PI tend to hold more moisture and need to be compacted at higher moisture levels, (Mbaraga, 2015). This also links in with the classification of the material. The higher the classification, the lower the PI specification therefore achieving higher compaction densities, (TRH14, 1985).

5.1.4 Material Strength Test Results

The UCS and ITS tests form part of South Africa's material classification procedure which is stipulated in TRH14 (1985). CTM and RCA are generally stronger in compression than in tension. The influence of cement and host material on UCS and ITS strengths is the focus of this section. The bulk densities, moisture contents and strengths of each UCS and ITS sample tested can be seen in Table A - 1 and Table A - 2 in Appendix A.

In Figure 5-5 - Figure 5-9, the left bar reports the 28-day UCS and the right bar shows the 28-day ITS. The ITS results are always much lower than the UCS strengths. This is a consequence of the materials failure mechanism and the boundary conditions of the tests. The 2% increase in cement improves the ITS and UCS strength due to the

stabilising effect of the cement. The percentage increase in strength is displayed in the last column for UCS and ITS in Table 5-6.

The percentage increase in strength of the UCS is consistently lower than the increase of the ITS for CTM and RCA. This suggests that a 2% cement increase has more influence on ITS than on the UCS. The UCS strength works on the "stone column effect", where the compression strength can be carried by the larger particles. Its compression strength is based on the interlock of the particles and the cement bonds between the particles assist this mechanism. The ITS is based on the tensile strength of the material. The tensile strength is related mainly to the cement bonds between particles that hold the specimen together. Therefore it makes sense for the ITS to benefit more from the increase in cement than the UCS.

Table 5-6: 28-day UCS and ITS strength results

	UCS Strength [MPa]			ITS Strength [MPa]		
CTM	2%	4%	Increase	2%	4%	Increase
ANDE - C	3.6	5.3	47%	0.9	1.8	100%
ANDE - G	3.5	6.5	86%	0.8	2	150%
HORN - C	4.2	6.4	52%	1.1	2	82%
RCA	0%	2%	Increase	0%	2%	Increase
RCA.U - C	4.9	7.7	57%	0.8	1.7	113%
RCA.E - C	1.1	8.7	691%	0.1	2.4	2300%

The target and actual moisture contents and bulk densities for the UCS and ITS are stated in Table 5-7 and Table 5-8. The actual and target bulk densities for the materials are displayed in Figure 5-3 and Figure 5-4. From these figures, it is seen that the actual bulk densities are much higher than the target bulk densities. The bulk densities are consistently higher for the CTMs than the RCA materials, for both UCS and ITS. This would indicate that granular materials are more compactable. This is confirmed when analysing the actual moisture contents, as RCA has double the moisture than the that of the CTM. The RCA has a high percentage of residual moisture which is observed when comparing the target to the actual moisture. This is likely due to high porosity of the RCA. It must be noted that the moisture for the RCA.U – C2 was not recorded correctly, and therefore an average between 11 and 12% was chosen.

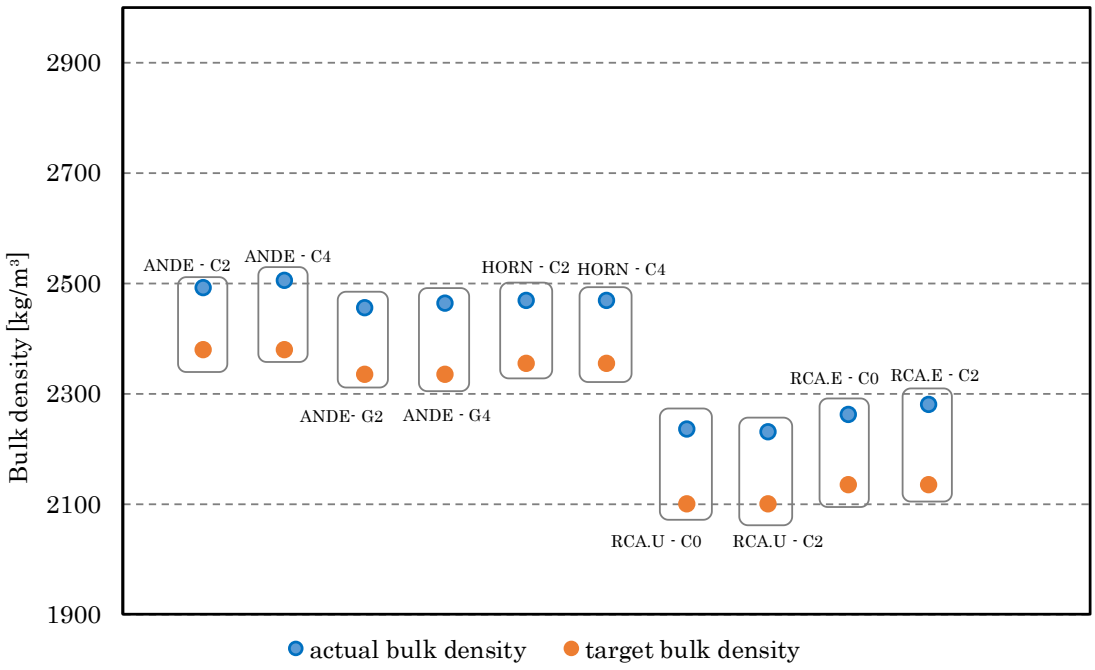

Figure 5-3: Actual vs target bulk density of UCS

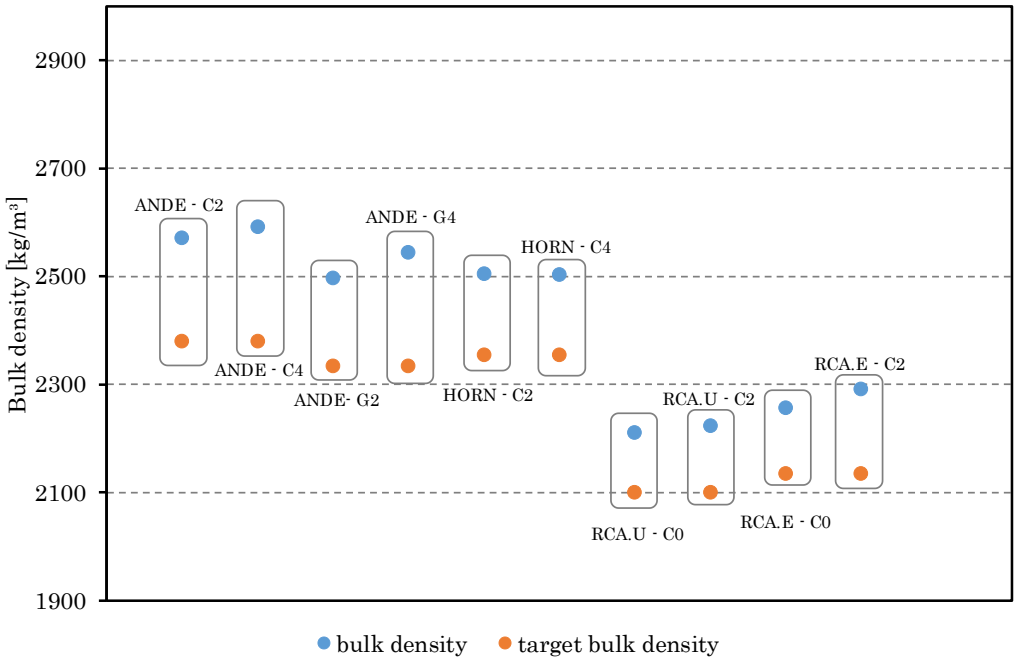

Figure 5-4: Actual vs target bulk density of ITS

Table 5-7: Moisture content and bulk densities of UCS

Material	Target Moisture [%]	Target Bulk Density [kg/m^3]	Actual Moisture [%]	Bulk Density [kg/m^3]
ANDE - C2	5.6	2380	5.6	2493
ANDE - C4	5.6	2380	5.5	2505
ANDE- G2	5.8	2335	5.7	2457
ANDE - G4	5.8	2335	5.4	2465
HORN - C2	5.7	2355	6.0	2470
HORN - C4	5.7	2355	5.5	2469
RCA.U - C0	7.5	2100	11.1	2236
RCA.U - C2	7.5	2100	11.5	2232
RCA.E - C0	7.5	2136	12.1	2263
RCA.E - C2	7.5	2136	10.8	2282

Table 5-8: Moisture content and bulk densities of ITS

Material	Target Moisture [%]	Target Bulk Density [kg/m^3]	Actual Moisture [%]	Bulk Density [kg/m^3]
ANDE - C2	5.6	2380	5.3	2571
ANDE - C4	5.6	2380	5.2	2592
ANDE- G2	5.8	2335	5.7	2497
ANDE - G4	5.8	2335	5.5	2545
HORN - C2	5.7	2355	5.5	2505
HORN - C4	5.7	2355	5.5	2504
RCA.U - C0	7.5	2100	11.1	2211
RCA.U - C2	7.5	2100	11.5	2224
RCA.E - C0	7.5	2136	12.1	2257
RCA.E - C2	7.5	2136	10.8	2292

5.1.4.1 CTM

All CTM 2% and 4% material have comparable UCS and ITS strengths, see Table 5-6. The difference between gap and continuous Andesite UCS and ITS strengths for 2% cement is not significant. This indicates that this gap grading does not play a large role in UCS and

ITS strength at 2% cement. However, there is a 22.67% difference in compression strength between ANDE-C4 and ANDE-G4. When comparing the actual bulk densities, it shows that the ANDE-C4 has the higher bulk density while ANDE-G4 has the lower bulk density. This is counterintuitive as a higher bulk density should indicate a higher strength due to better aggregate packing and fewer voids. Random variability is therefore assumed.

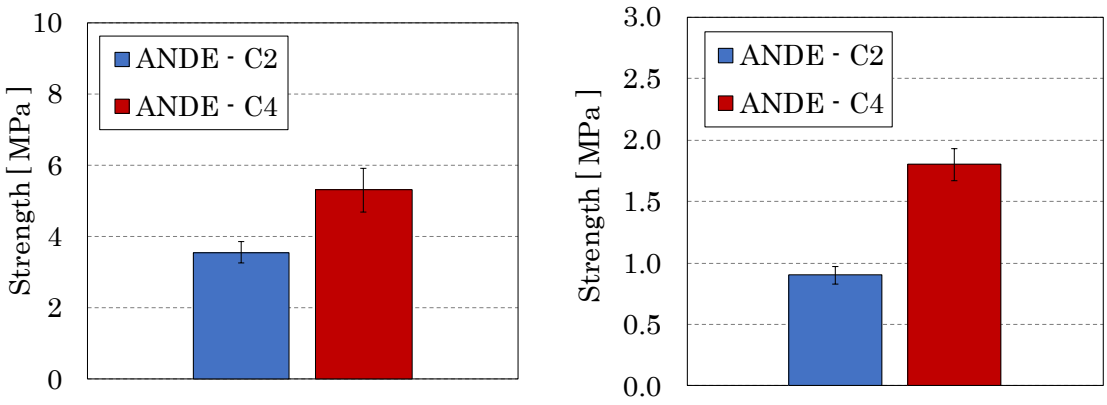

Figure 5-5: UCS (left) and ITS (right) results of continuously graded Andesite

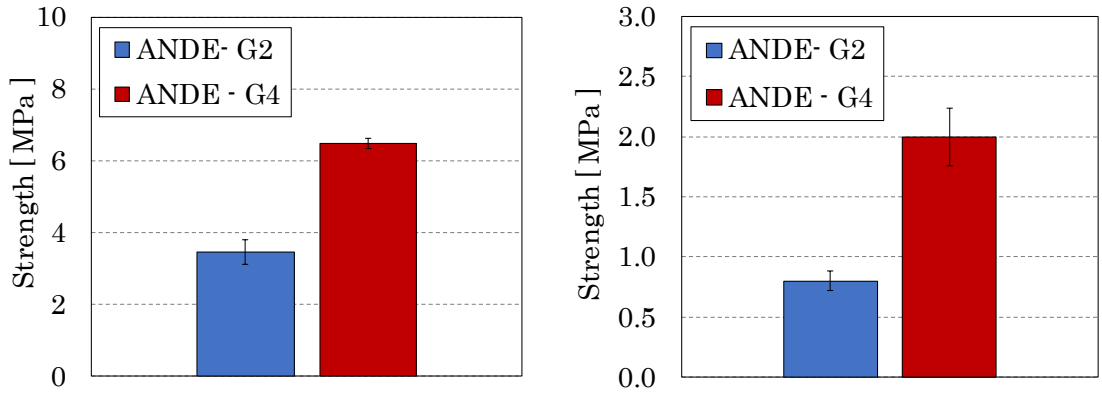

Figure 5-6: UCS (left) and ITS (right) results of gap graded Andesite

The difference in strength between Andesite and Hornfels is slight. The Hornfels shows slightly higher UCS and ITS strengths. This again is counterintuitive as the Andesite, for both percentages of cement, have higher bulk densities and lower or equal moisture contents. This should suggest lower strengths for the Hornfels. However, it is possible that the difference in pH could have an influence. From the ICC test results, it showed that the Hornfels stabilised at lower percentage cement (1%) than the Andesite (2%). This could suggest that the due to the additional moisture content it was possible for the Hornfels to gain more strength through the addition of cement.

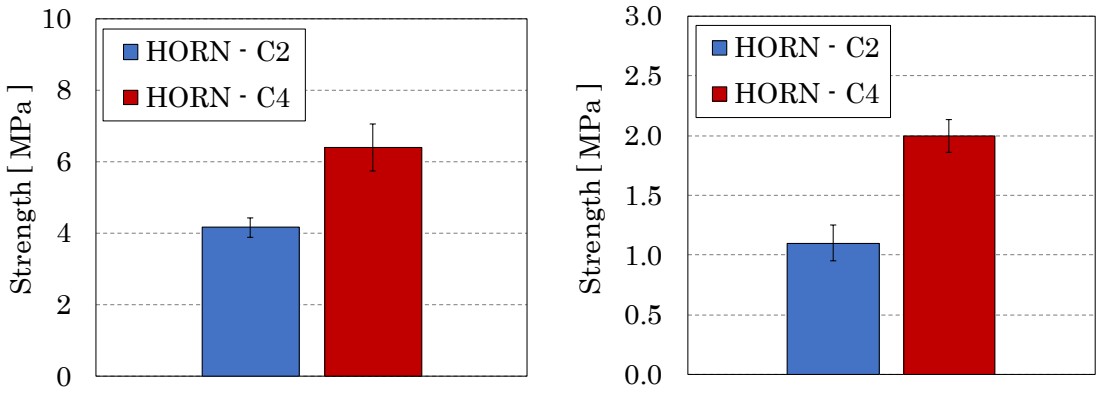

Figure 5-7: UCS (left) and ITS (right) results of continuously graded Hornfels

5.1.4.2 RCA

It is clear from the Figure 5-8 and Figure 5-9 that the exposed RCA yields much lower UCS and ITS results at 0% cement content than the unexposed RCA. As with the ICC test results, the low pH reading of 10 for RCA.E shows that the material has low cementing properties which contributes to the low strength. The additional 2% cement significantly improves the UCS and ITS of the exposed material by 691% and 2300% respectively.

Table 5-9: 28-day UCS and ITS results of unexposed and exposed RCA

	UCS Strength [MPa]			ITS Strength [MPa]		
RCA	0%	2%	Increase	0%	2%	Increase
RCA.U - C	4.9	7.7	57%	0.8	1.7	113%
RCA.E - C	1.1	8.7	691%	0.1	2.4	2300%

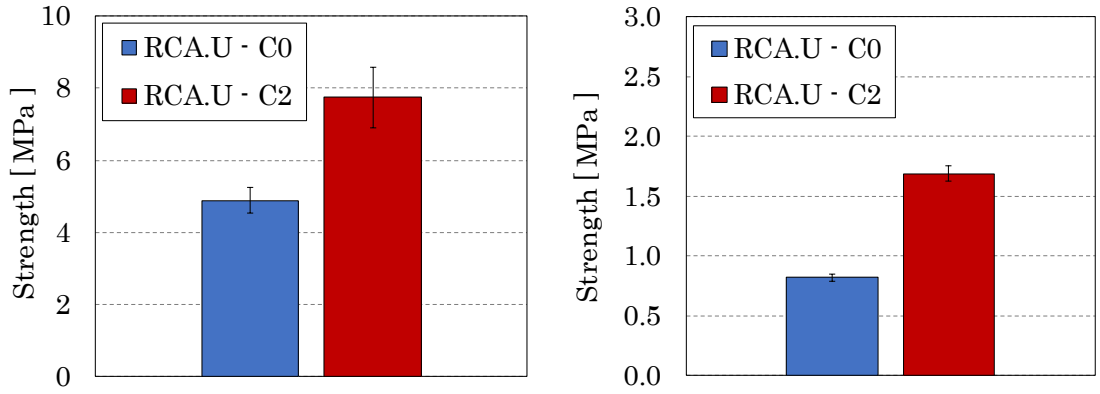

Figure 5-8: UCS (left) and ITS (right) results of unexposed RCA

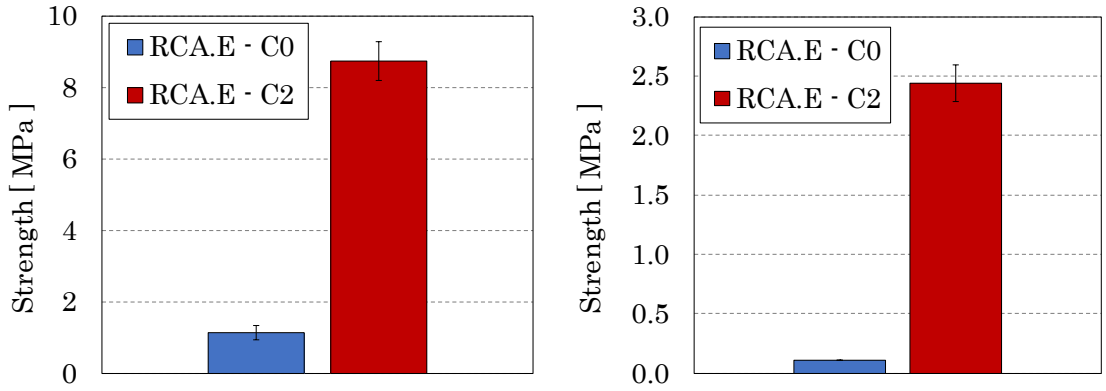

Figure 5-9: UCS (left) and ITS (right) results of exposed RCA

5.1.4.3 CTM vs RCA

UCS

The 0% unexposed RCA (orange) is showing slightly higher strength than CTMs, which could be due to the active latent cement content, giving high strength from increased hydration, see Figure 5-10. As mentioned in with the ICC test, the RCA.U can be seen as equivalent to at least a 2% equivalent granular. However, based on the increased UCS results it seems it can be assumed a 3% equivalent granular.

The 0% exposed RCA (green) has the lowest strength. Due to the exposure there is little active cement content. It can be concluded that the exposed RCA behaves as a 0% equivalent granular material and needs to be stabilised in order to reach the classification requirements of a C3. This is confirmed through the ICC results, where the exposed RCA had comparable pH levels when compared with the Andesite.

The large increase in strength of the exposed RCA is in part due to the increase in cement content. The RCA.E 0% shows slightly lower density and higher moisture content than the RCA.E 2%, which also substantiates the increase in strength. However, it does not seem logical for the small change in moisture and bulk density to cause such a large increase in strength alone. It is therefore not possible to differentiate between the proportional contribution each variable.

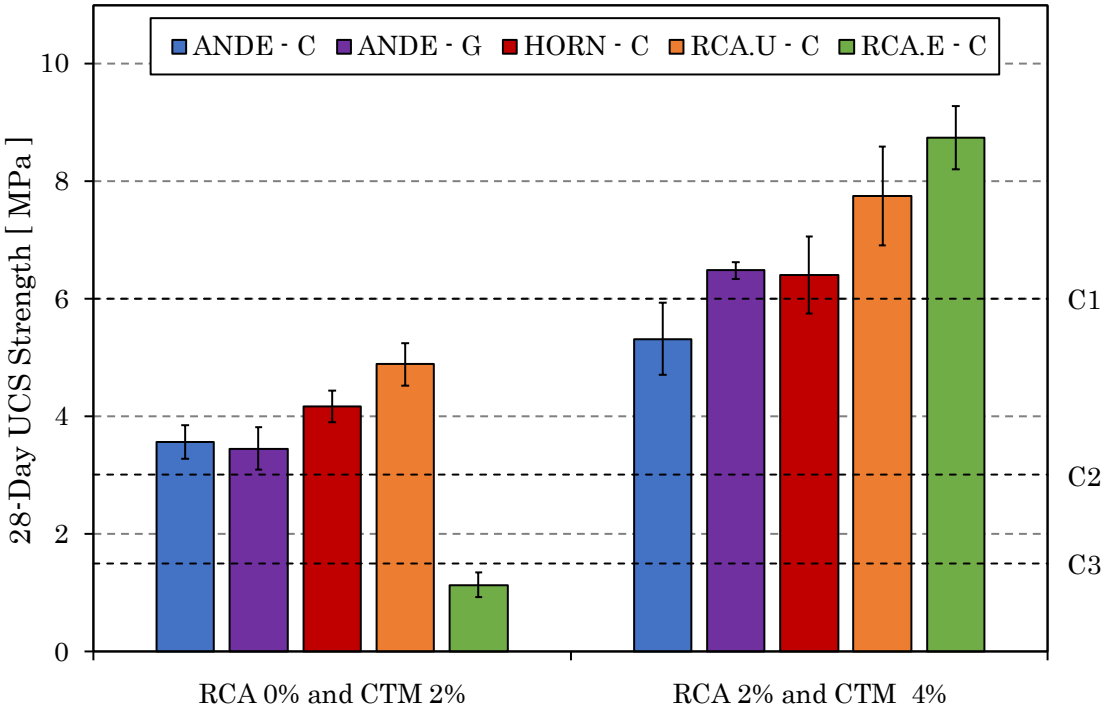

Figure 5-10: Day UCS results of RCA and CTM

ITS

As with the UCS, the material with the higher percentages cement perform consistently better than the lower stabilised materials. All material barring the 0% exposed RCA pass the min ITS required strength for a C3 material. According to the SAPEM manual (2014c), there is no maximum requirement for ITS strength, see Figure 5-11. All 2% CTMs and 0% RCA.U have comparable ITS strengths.

When assessing the 4% CTMs and 2% RCA, the 2% unexposed RCA performs the worst out of all materials. This is in contrast with the 2% UCS strength. This suggests that the unexposed RCA has better compressive strength but is lacking in the tensile strength when compared to other CTM material. The 2% RCA.E shows a higher bulk density than the 2% RCA.U. This is a possible reason why the 2% exposed RCA is performing better than the 2% unexposed RCA. The more contact surface area available through increased bulk density, the more cement bonds can form which can improve the tensile strength.

The 0% exposed RCA underperforms again due to the lack of adequate stabilising agent. Then when the additional 2% cement is added, the ITS strength improves drastically as with the UCS strength.

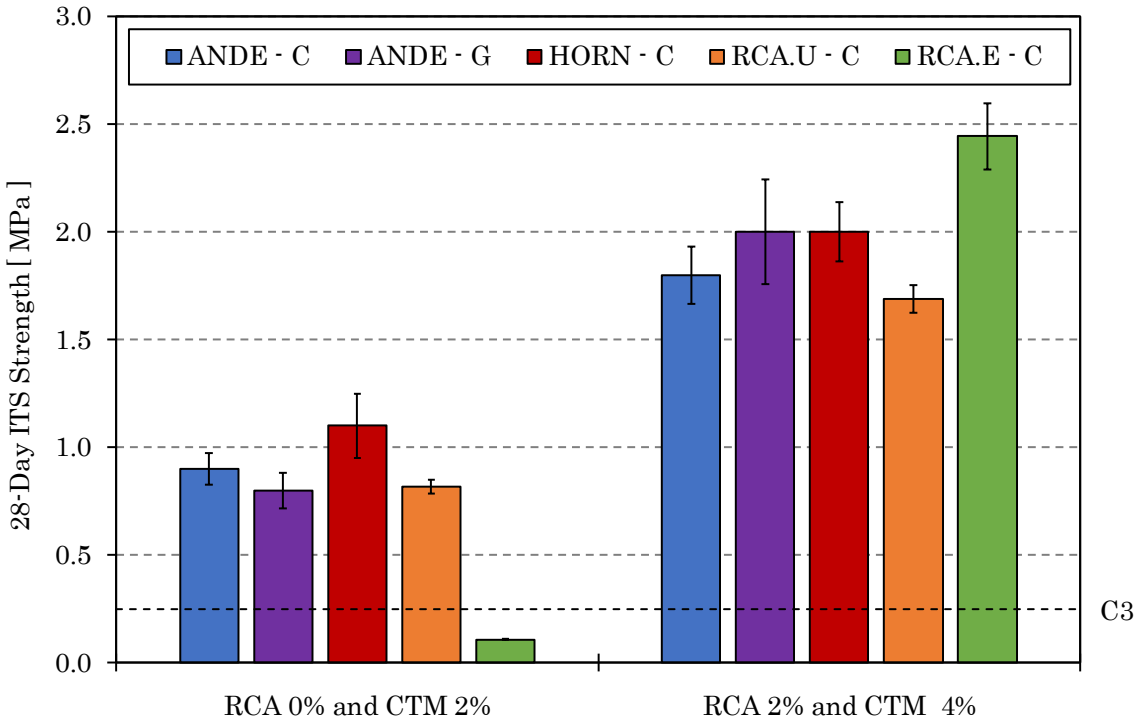

Figure 5-11: 28-Day ITS results of RCA and CTM

5.1.4.4 Synthesis of Findings

In this section the 28-day UCS and ITS findings of Semugaza (2016) are compared to that of this study. The materials of Semugaza include: Hornfels (HORN.S); RCA (RCA.S) and New Concrete RCA (NC.S). Refer to Table 5-10 for the corresponding 28-day UCS and ITS results.

Table 5-10: Semugaza (2016) results for 28-day UCS and ITS strength (MPa)

Material	28-Day UCS Strength [MPa]			28-Day ITS Strength [MPa]		
	0%	2.5%	4%	0%	2.5%	4%
HORN.S	1.20	8.20	12.20	0.09	0.74	1.20
RCA.S	1.40	7.60	11.20	0.11	0.71	1.20
NC.S	1.80	7.00	10.30	0.12	0.50	0.95

The Andesite and Hornfels of this study are summarised as a range of CTM. This was possible as the strength of CTM materials were similar enough to group for the purpose of this comparison. The Unexposed and Exposed RCA 28-day UCS and ITS results of this

study are also used for comparison. Refer to Table 5-11 for the corresponding 28-day UCS and ITS results.

Table 5-11: CTM and RCA 28-Day UCS and ITS results for comparison

Material	UCS Strength [MPa]		ITS Strength [MPa]	
	2%	4%	2%	4%
CTM Range	3.5 - 4.2	5.3 - 6.4	0.8 -1.1	1.8 – 2

Material	UCS Strength [MPa]		ITS Strength [MPa]	
	0%	2%	0%	2%
RCA.U	4.9	7.7	0.8	1.7
RCA.E	1.1	8.7	0.1	2.4

5.1.4.4.1 CTM

In comparing the UCS strength of HORN.S with the range of CTM, it must be noted that the 2.5% and 4% HORN.S were double that of the CTM 2% and 4% strengths respectively. This could be due to differences in host material, compaction method, compaction density and moisture content despite that they are all classified as granular materials.

The difference in ITS results show that the 2% CTM falls in between the HORN.S 2.5 – 4% range and the 4% CTM is stronger than the 4% HORN.S. This suggest that Semugaza's Hornfels would perform better in compression than CTM however CTM would perform better in tension than HORN.S. In terms of resistance to shrinkage cracking, it alludes to the CTM possibly performing better than the HORN.S due to the higher tensile strength.

5.1.4.4.2 RCA

Each RCA has a different degree of active latent cement present. In order to simplify the effects thereof, it is equated to an equivalent granular material with a percentage cement for stabilisation. This simplification helps to model the behaviour of RCA.

Unexposed RCA

The 0% unexposed RCA UCS strength (4.9 MPa) of this study is about 2-3 times higher than 0% RCA.S and NC (1.4 - 1.8 MPa). This again suggests that there are material differences and this reflects in the UCS strengths.

The 2% RCA.U UCS is comparable to the 2.5% RCA.S. This suggests that the RCA of Semugaza is more susceptible to additional cement as there is a large difference between the 0% and 2.5% when compared to RCA.U.

When comparing the 0% RCA.U with 2% CTM UCS strengths in Table 5-11, it could be concluded that RCA.U is an equivalent 3% CTM, and the 2% RCA.U is equivalent to 5% CTM based on the UCS strength alone.

As with the UCS, the ITS strengths of 0% RCA.U are much higher than the 0% RCA.S. The RCA.U 0% and 2% are comparable with RCA.S 2.5% and 4% respectively. When comparing the RCA.U to CTM, the 0% and 2% RCA.U fall into the 2% and 4% CTM ranges respectively. Therefore in terms of ITS strength, it can be assumed that the 0% unexposed RCA can be an equivalent 2% CTM and the 2% RCA.U can be an equivalent 4% CTM.

Exposed RCA

The 0% and 2% RCA.E UCS and ITS strengths are comparable with RCA.S 0% and 2.5% respectively. This suggests that RCA.S has undergone some natural exposure. The fact that HORN.S and RCA.E are very comparable could suggest that RCA.E could be considered a poor quality granular. However, when an additional 2% cement is added to RCA.E, there is a significant increase in both UCS and ITS and equates to a 4% equivalent granular for both. There is an increase in bulk density from the 0% RCA.E to the 2% RCA.E, which could lead to the large increase in strength for both UCS and ITS. However, it is not possible to accurately differentiate between the variable contibution.

5.1.5 Conclusion

In conclusion, the unexposed RCA can be considered a good quality granular material with 2% cement. When exposing this material, it reduces to a poor quality granular material with 0% cement, see Table 5-12. This is due to the nature of the exposure, where the active latent cement particles undergo hydration, leaving fewer active latent cement particles to make new bonds.

Table 5-12: RCA as equivalent granular

Material		Equivalent Granular		
		UCS	ITS	Final
Unexposed RCA	0%	3%	2%	2%
	2%	5%	4%	4%
Exposed RCA	0%	0%	0%	0%
	2%	3%	4%	4%

It is important to realise that all RCA materials have different material properties and will therefore behave differently. The characterisation tests mentioned are crucial as has been shown in determining the individual material characteristics and to understand how a specific RCA will perform.

5.2 Trends of Cylindrical Shrinkage Test

The shrinkage-time curves of the various mixes will be discussed in this section. The large and small cylindrical shrinkage tests are analysed and compared. General trends are determined and illustrated in schematic diagrams. The maximum axial shrinkage will be addressed and compared. The influence of cement, host material and aggregate size on shrinkage is discussed and compared to literature.

5.2.1 Influence of Cement and Host Material on Large Shrinkage Tests

The large shrinkage test results are displayed from Figure 5-12 - Figure 5-16. In all the figures the darker line represents the average of 2 or 3 repeats. The repeats are displayed in the background of the graph. The lower percentage cement is always in blue and the higher percentage is in red. CTM only have 28 days of shrinkage data, whereas RCA has 100 days. But also accepting that a significant proportion of the hydration would have occurred before 21 days.

5.2.1.1 CTM

Figure 5-12 and Figure 5-13 illustrate the shrinkage of continuous and gap graded Andesite and Figure 5-14 shows the shrinkage of continuous graded Hornfels. It is clear

that the shrinkage of the 4% cement continuous and gap Andesite is consistently more than that of the 2% for both. As previously noted, drying shrinkage governs the shrinkage strain of CTM and is the leading cause of cracking, (Mbaraga, 2015). However, it is evident from Figure 5-12 and Figure 5-13 that the increase in cement content by 2% has led to an increased hydration and therefore autogenous shrinkage is the cause for the additional shrinkage. The amount of autogenous shrinkage depends on the extent of hydration process, (Mbaraga, 2015). The amount of autogenous shrinkage can also be dependent of the reaction with the host material, moisture content and mixing procedure.

In the first 7 days of 100% RH, both Andesite materials indicate reduction in slope indicating shrinkage. The Hornfels shows a reduction in slope, as well as some swelling. It is evident in all 3 materials that after 7 days, the drying shrinkage begins to dominate. The further increase in downward slope of the shrinkage suggests the rate of shrinkage is influenced by the drying effect. In terms of comparison between host materials, both Andesite gradings and Hornfels show similar order size of shrinkage as well as similar trends.

When comparing the 2% continuous with the 2% gap grading in Figure 5-12 and Figure 5-13 the continuous shows less initial shrinkage for the first 14 days which could be due to better packing and aggregate interlock. This is an important feature as the most vulnerable time for shrinkage cracking to occur is in this time period. However overall shrinkage both materials are similar for both percentages of cement.

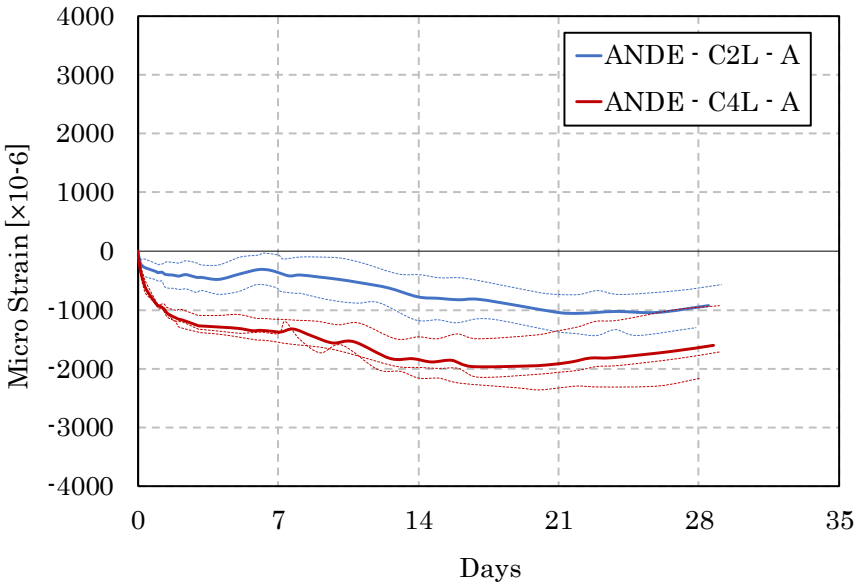

Figure 5-12: Shrinkage of 2% and 4% large continuous Andesite

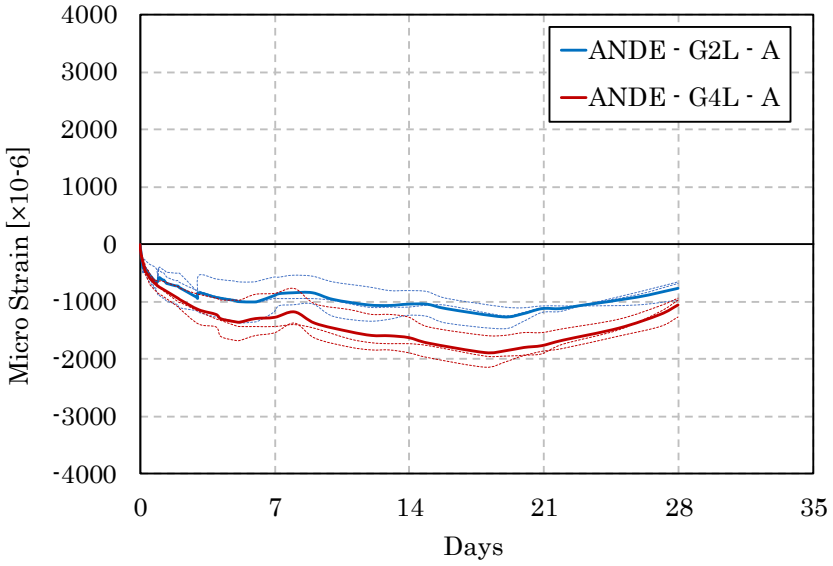

Figure 5-13: Shrinkage of 2% and 4% large gap graded Andesite

The variation of the repeat tests concludes that this material is not fully homogenous. The outlier in Figure 5-14 shows variation of a 4% repeat, which was due to a faulty dial gauge. This was excluded from the average calculation as it would have been a misrepresentation of the actual shrinkage measured. The Hornfels follows similar trends as the Andesite where the 4% shrinks more than the 2%. However, the difference in shrinkage between the two percentages is not nearly as large as both Andesites.

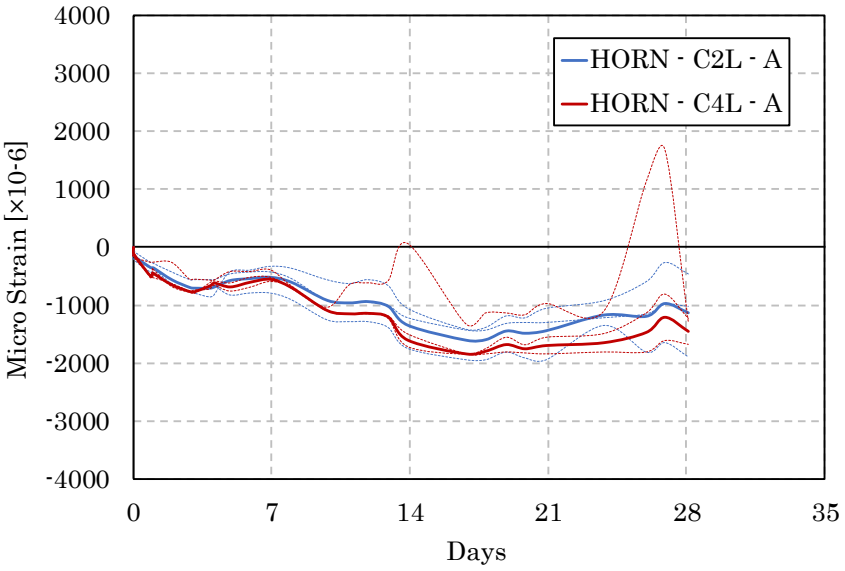

Figure 5-14: Shrinkage of 2% and 4% large continuous Hornfels

5.2.1.2 RCA

Unexposed RCA behaves entirely different to CTM, see Figure 5-15. The 2% RCA.U samples show a significant amount of swelling within the first 7 days. This corresponds to the 7 day curing at 100% RH, where there was assumed to be high levels of hydration swelling and no drying shrinkage. The material experienced hydration due to the large portion of active latent cement in the original material plus the additional 2% cement added during mixing. After 7 days, drying shrinkage becomes the dominating factor. The shrinkage seems to stabilise after 63 days. The fluctuations seen are mainly due to the variable humidity in the curing room, which is further explained in Section 5.2.4.

The 0% RCA.U average excluded the outlier due to a faulty dial gauge. It appears the 0% RCA.U experiences some hydration, however not nearly to the same extent as the 2%. The shrinkage seems to stabilise after 21 days.

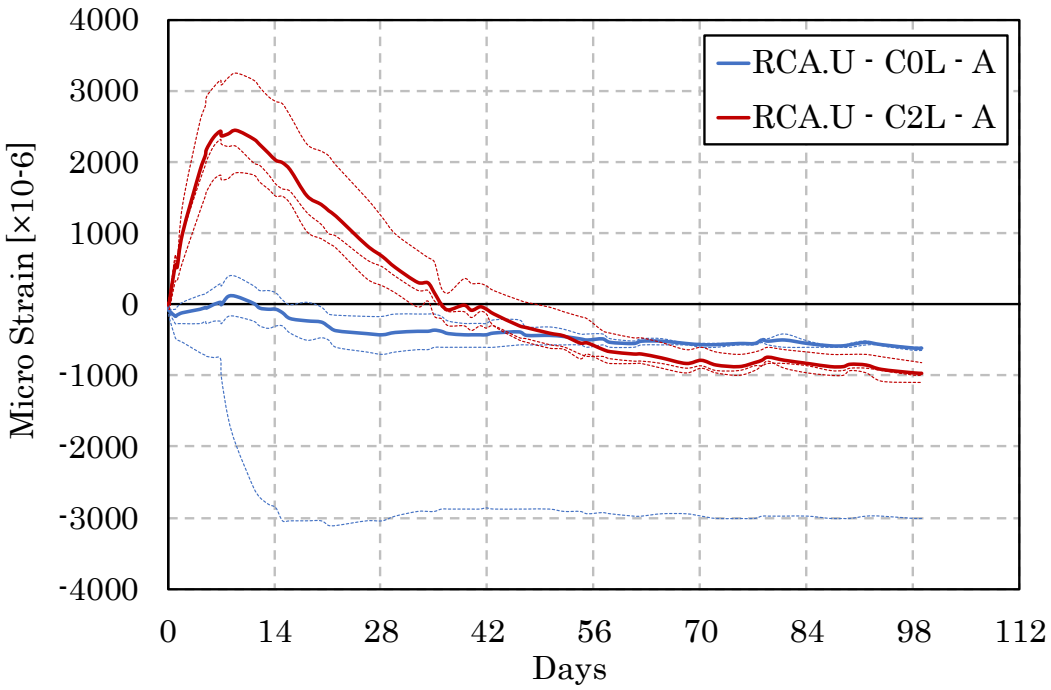

Figure 5-15: Unexposed RCA 0% and 2% shrinkage results

Both percentages of exposed RCA follow similar trends of CTM, see Figure 5-16. There is no initial swelling as with the unexposed RCA. This is due to the wetting and drying process of the exposure which reduced the active latent cement content. As with the CTM, the material with the higher percentage cement shrinks more than the lower percentage.

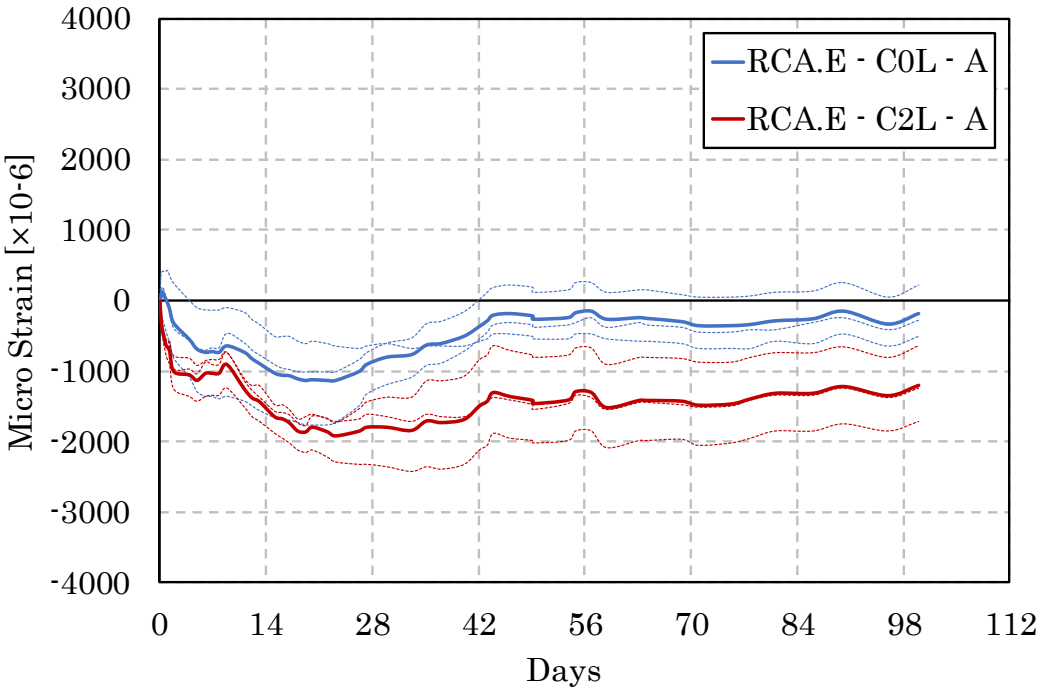

Figure 5-16: Exposed RCA 0% and 2% shrinkage results

5.2.1.3 Maximum Axial Shrinkage

The RCA.E, Hornfels and both Andesites have not shown any swelling, therefore the maximum axial shrinkage was determined as the lowest point of the shrinkage curve, see the schematic diagram in Figure 5-17.

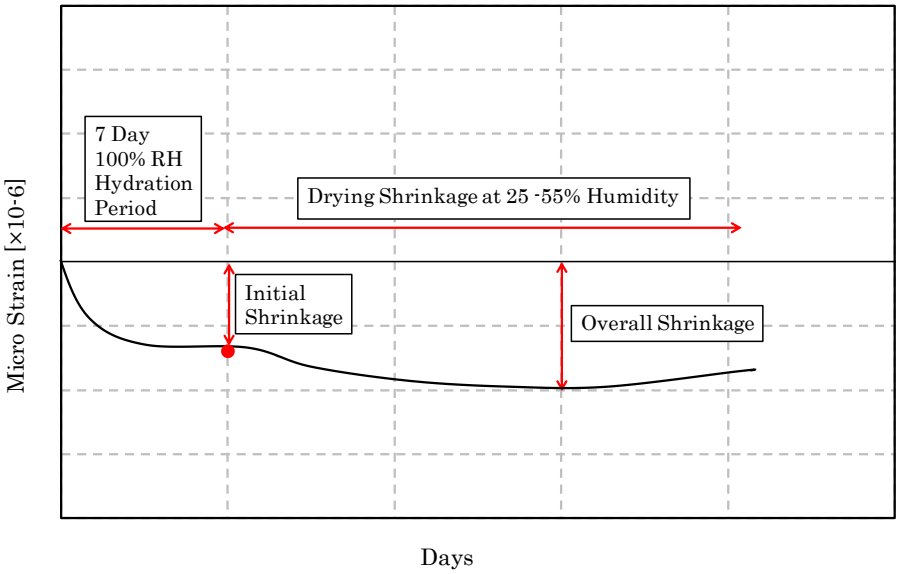

Figure 5-17: Schematic of CTM shrinkage curve trends

The shrinkage of the CTM and RCA.E can be categorised into three phases. Firstly, there is the hydration phase from 0 – 7 days where the cement reacts with the water molecules. There is some initial shrinkage, however it reaches equilibrium and does not indicate any drying shrinkage due to the 100% RH curing room. Thereafter the plastic wrapping is removed and drying shrinkage begins. This stage occurs immediately after 7 days and continues for 14 days. After 14 days, the material begins to recover. This is noted by the slight upward curve of shrinkage, suggesting mild swelling. This is clearly seen with the exposed material from 21 days until the end of the test. In the case of the CTM, the slight upwards curve increase is seen after 14 days, however the test was cut short. Therefore, the extent of the increase is unknown.

The unexposed RCA however follows its own trend, see Figure 5-18. This is substantiated as it is essentially a material with different characteristics due to the large amount of active latent cement present. The maximum shrinkage is calculated from the peak of hydration to the lowest point. In terms of stages, there is the 0-7-day hydration period, and thereafter is the drying shrinkage. The RCA.U does not display any increase in shrinkage curve once the drying shrinkage phase has begun.

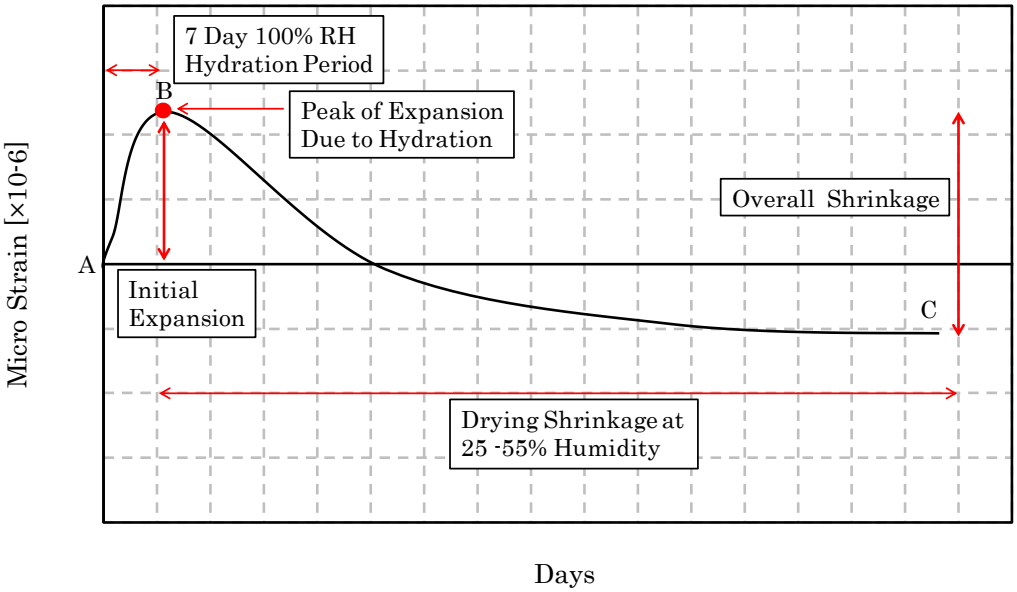

Figure 5-18: Schematic of shrinkage curve for RCA.U 2%

The maximum shrinkage for each CTM and corresponding cement percentage can be seen in Figure 5-19 and Table 5-13. The Hornfels results would suggest that autogenous shrinkage played less of a role than in both Andesite materials as the difference between the 2% and 4% curves is small (15%) in comparison, see Table 5-13.

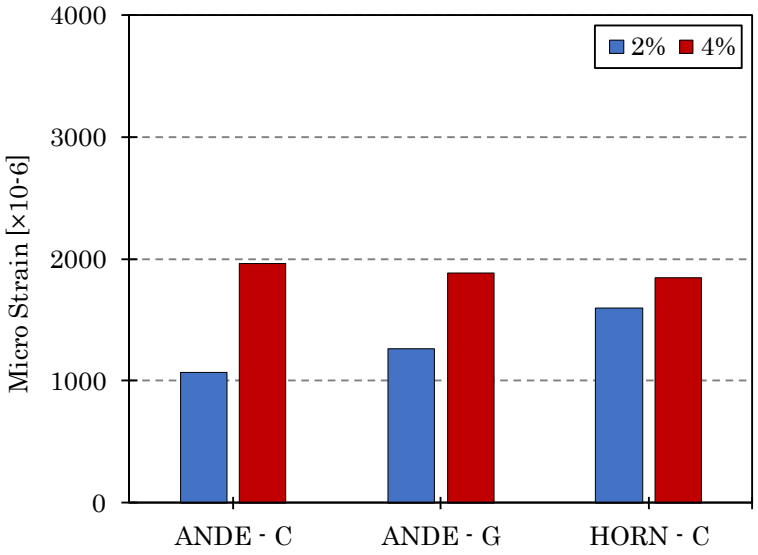

Figure 5-19: Maximum shrinkage strain of large CTM

The cement content has the biggest influence on the continuous Andesite where the shrinkage increase due to cement was 84%. Based on this increase, the ranking of factors affecting shrinkage is firstly material dependent, where the continuous Andesite increase was 84%, and the continuous Hornfels increase was only 15%. The influence of grading is therefore not as critical.

Table 5-13: Maximum shrinkage strain of large CTM samples

Maximum Shrinkage in Micro Strain [×10-6]			
Material	2%	4%	Increase
ANDE - C	1067	1967	84%
ANDE - G	1267	1889	49%
HORN - C	1601	1846	15%

As mentioned the RCA.E follows the same schematic shrinkage curve that was applied for the CTM. The maximum axial shrinkage is also very comparable with that of the CTM, which suggests that the exposed RCA, behaves in a similar way as the granular materials, see Table 5-14.

In term of shrinkage alone, the 0% RCA.E yields similar behaviour to a 2% CTM, and the 2% RCA.E is similar to the 4%. The 0% RCA.E does have some active latent cement particles. This is seen with the ICC test, where the 0% RCA.E showed higher pH readings

than the 0% CTMs. This is in contrast to the UCS strength, where the 0% RCA.E was comparable to a 0% CTM. These are however different mechanisms. The mechanisms have overlapping contributing variables; however this would be a comparison between two incongruent mechanisms.

Table 5-14: Maximum shrinkage strain of large RCA samples

Maximum Shrinkage in Micro Strain [×10-6]			
Material	0%	2%	increase
RCA.U - C	806	3536	339%
RCA.E - C	1246	1911	53%

When comparing trends and maximum shrinkage strain, the 0% RCA.U performs as a 2% CTM, see Table 5-13 and Table 5-14. The large jump of 339% in shrinkage, see Figure 5-20, with the additional 2% cement is seen for RCA.U. This is largely due to the initial hydration that occurs within the first 7 days. The RCA.U 0% shows less shrinkage than the RCA.E despite that it has more active latent cement. It also has the least shrinkage out of all the materials, and has slightly better UCS and ITS results than the CTM 2%.

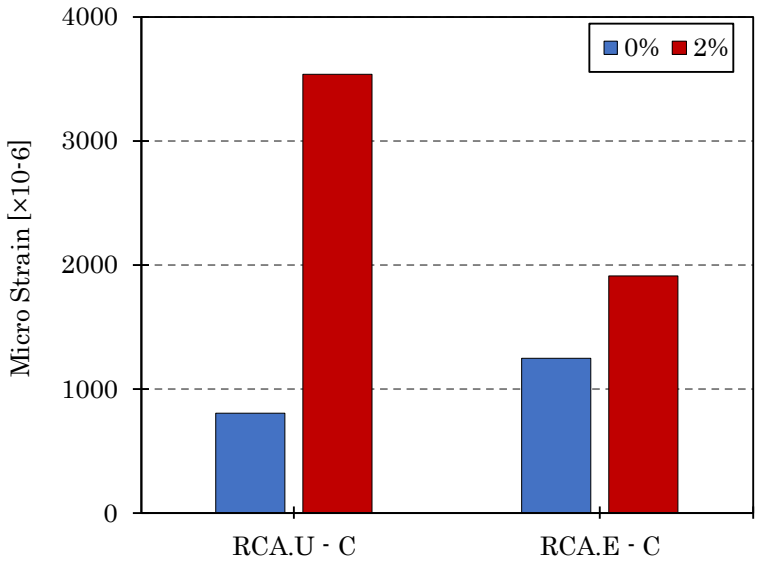

Figure 5-20: Maximum Shrinkage of RCA

5.2.2 Influence of Cement and Host Material on Small Shrinkage Tests

The small shrinkage test results are displayed from Figure 5-22 - Figure 5-26. In all the figures the darker line represents the average of 2 or 3 repeats. The repeats are displayed in the background of the graph to illustrate variability. The lower percentage cement is always in blue and the higher percentage is represented by red. Only 50 days of results are reported for the Andesite and Hornfels verses the RCA which has 100 days due to time and apparatus constraints.

The shrinkage trend of the small samples are all similar in terms of an initial swelling in the first 7 days, due to the 100% RH curing. Thereafter immediate drying shrinkage occurs once the plastic wrapping was removed. Similar shrinkage curve trends are seen, as with the 2% RCA.U, see schematic sketch Figure 5-18. The shrinkage behaviour appears to reach equilibrium after 21 days with some fluctuations. These fluctuations are due to the change in humidity (30 – 60% RH) of the curing room.

Humidity can influence drying shrinkage. A decrease in humidity causes the air to be dry and consequential evaporation increases. This induces tensile stresses in the pore structures and ultimately volume reduction. The increase of humidity ensures there is sufficient moisture in the air, and gives the material time to undergo hydration. However the influence is discussed in greater detail in Section 5.2.4. Temperature change has a large influence on shrinkage during construction and during the initial setting phase. However, this is only when there is a large temperature change. The range in the curing room was too small (19 – 24 ˚C) to make a significant difference.

The maximum axial shrinkage strain was calculated differently than for the large samples. Due to the initial swelling and the fluctuations in the shrinkage curve during the drying shrinkage stage, an average reading was taken at a point when the drying shrinkage seemed to reach its maximum. This was usually at 14 days. RCA.U took a bit longer and levelled out at 21 days. Hornfels was used as an example to illustrate the calculation, see Figure 5-21.

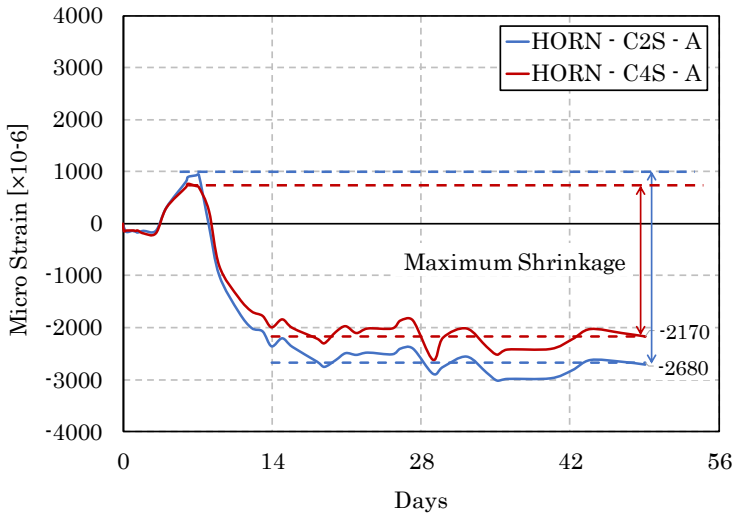

Figure 5-21: Maximum shrinkage of small Hornfels samples

5.2.2.1 CTM

In terms of cement content and host materials, it appears the ANDE – C4 material undergoes a higher state of hydration in the first 7 days than the 2%, due to the additional cement content. Despite the initial swelling, after 21 days both materials level out and follow almost identical final shrinkage. The Hornfels experiences similar swelling for both percentages cement in the first 7 days. Thereafter it appears that the mix with 2% cement undergoes more shrinkage than the mix with 4% cement. This is counterintuitive as the more cement content the more shrinkage is expected.

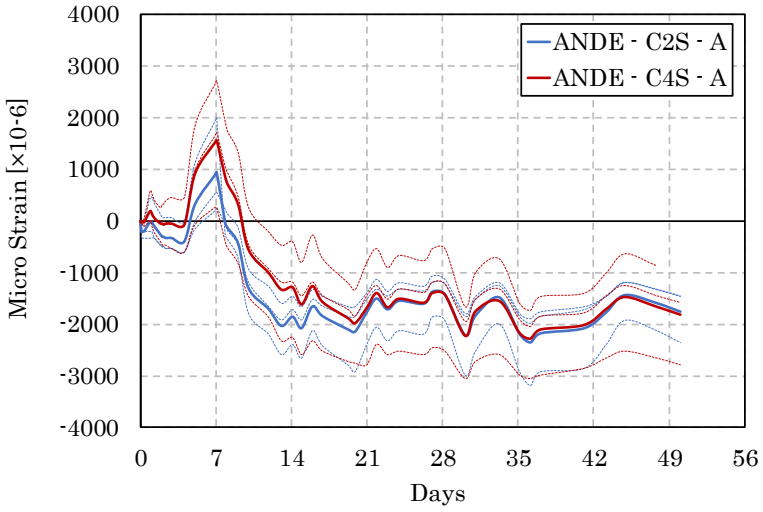

Figure 5-22: Small Andesite shrinkage results

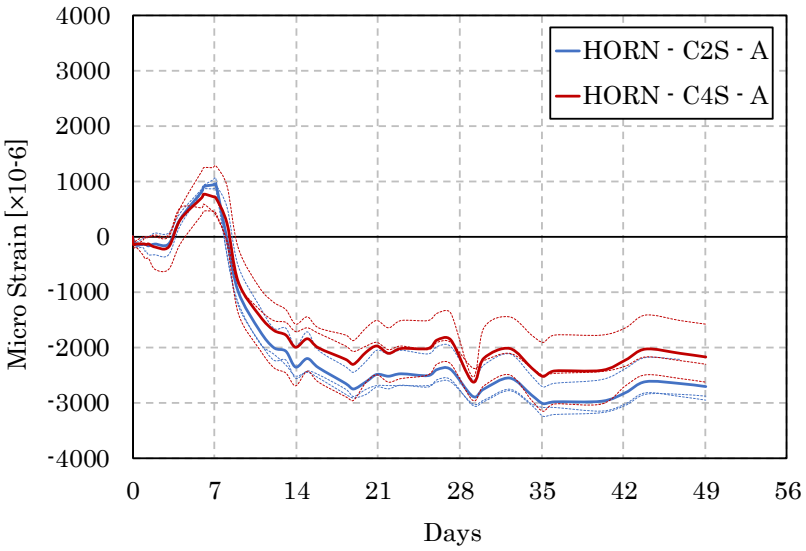

Figure 5-23: Small Hornfels shrinkage results

However, when looking at the percentage increase in shrinkage, Table 5-15 shows a percentage decrease of 19% for Hornfels. This suggests that the 2% Hornfels shrinks more than the 4% Hornfels. However, the variability of the repeats must be noted, as seen in the repeats in Figure 5-23. This indicates that this material cannot be considered 100% homogenous. This is evident due to the variability of up to 20% between repeats.

Table 5-15: Maximum shrinkage strain for small CTM samples

Maximum Shrinkage in Micro Strain [×10-6]			
Material	2%	4%	Increase
ANDE	2699	3300	22%
HORN	3632	2940	-19%

When comparing Andesite with Hornfels, it appears that Hornfels is more susceptible to shrinkage, as the 2% strain results show an increase in axial shrinkage. This finding is also consistent with the large shrinkage test for the same material. However, this is not consistent with the 4% Andesite and Hornfels, this is where random variability must be taken into account.

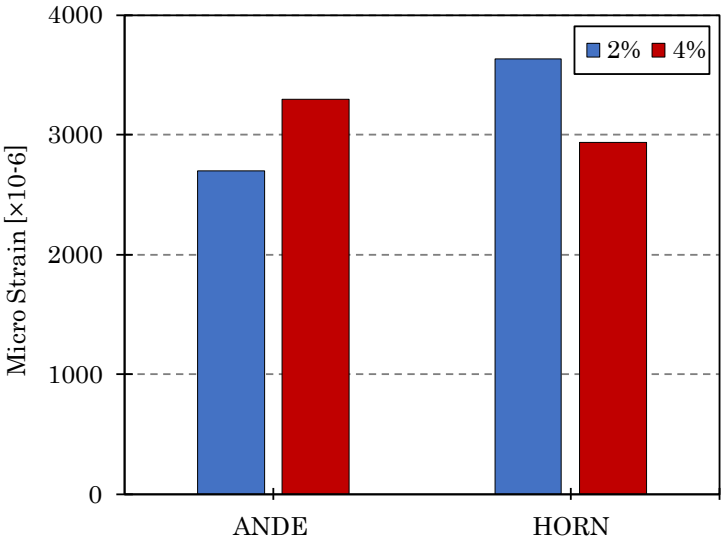

Figure 5-24: Maximum shrinkage of small Andesite and Hornfels

5.2.2.2 RCA

During the initial 7-day curing period, both percentages RCA.U show swelling. The 0% however shows more swelling than the 2%, which is counter intuitive. The 0% is less stable and is more susceptible to humidity changes than the 2%, as the fluctuations during the drying shrinkage period is 30% more than with the 2%, Figure 5-25.

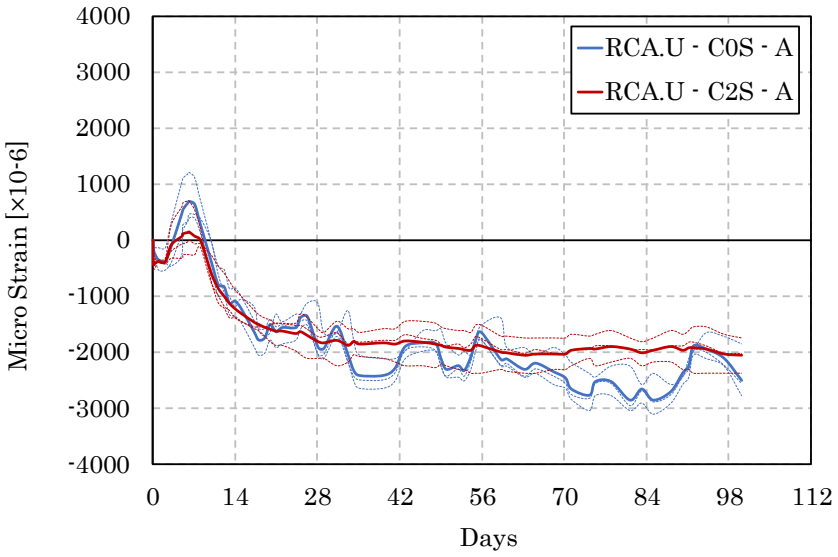

Figure 5-25: Shrinkage of small unexposed RCA

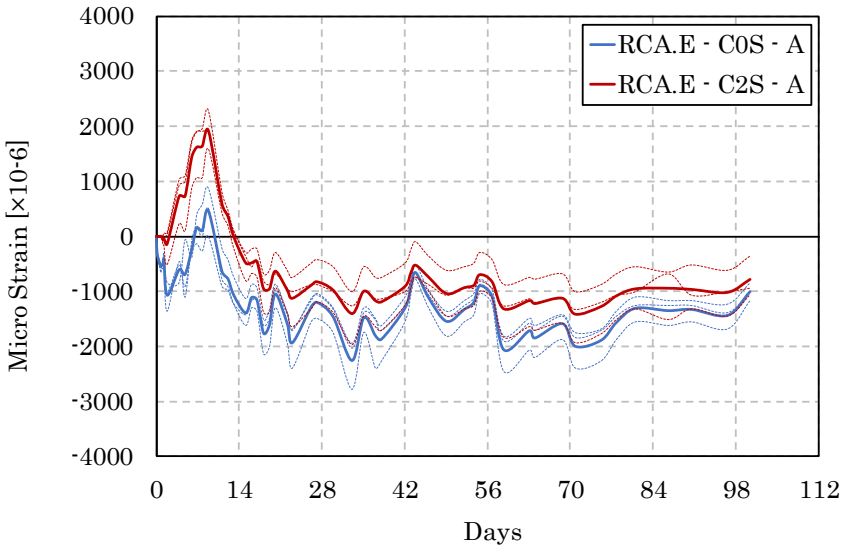

Figure 5-26: Shrinkage of small exposed RCA

The exposed RCA also experiences an increase during the first 7 days, due to the hydration reactions that take place. The 2% RCA.E again shrinks more than the 0%, due to the increase in cement percentage, see Figure 5-26. As with the large shrinkage results, the exposed RCA acts similarly to CTM.

Table 5-16: Maximum axial shrinkage of RCA

Maximum Shrinkage in Micro Strain [×10-6]			
Material	0%	2%	increase
RCA.U	2954	2060	-30%
RCA.E	1948	2942	51%

The unexposed RCA resulted in a 30% decrease. This shows that the rate of self-cementing is not linear, nor is it uniformly distributed. Due to the large and uneven percentage of active latent cement in the fine grading, the material is considered non- homogenous.

The 0% RCA.U yields more shrinkage than the 0% RCA.E in the finer grading, see Figure 5-27. The pH tests of the fine material of RCA.U contains a higher percentage of active latent cement than the exposed material. According to Poon et al. (2006) the active latent cement sits in the finer fractions and is where majority of the shrinkage occurs. The results of the shrinkage at 0% RCA seems to substantiate with that of the pH test. The unexposed material has a larger hydration peak and ultimately more shrinkage than the exposed material due to this fact.

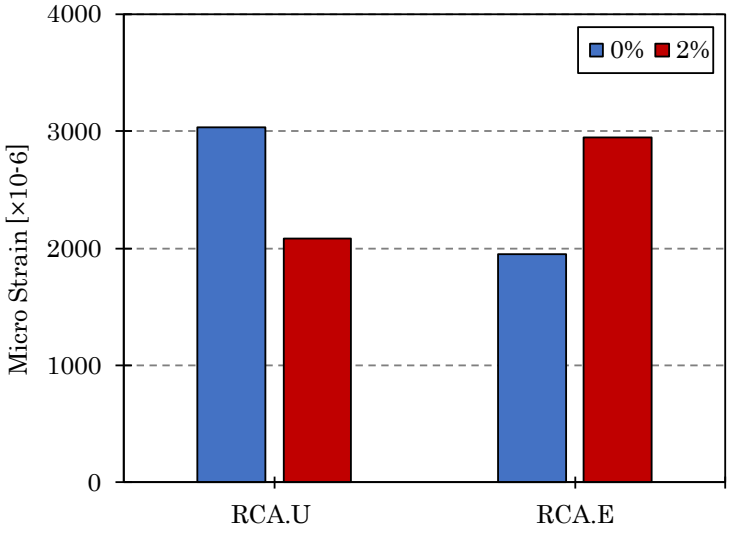

Figure 5-27: Maximum axial shrinkage of small RCA

5.2.3 Influence of Aggregate Size on Shrinkage Tests

As discussed, the RCA.E shrinkage curve increases after 21 days. Unfortunately, due to time and equipment restraints, the large samples of the CTM have a maximum shrinkage data of only 30 days, however the curve of the large CTM also increases after 21 days. The shrinkage data was therefore extended based on the last reading of 28 days, as it can be assumed that it would follow the same increasing trend as the RCA.E.

The graphs and bar charts in Figure 5-28 - Figure 5-31, compare the lower percentage cement in blue and the high percentage cement in red. The shrinkage curves in solid lines represent the large shrinkage and the dotted curves represent the small shrinkage samples.

It can be seen from the graphs that the fine graded (small) samples all show much higher magnitudes of shrinkage than the full graded or large samples due to the initial swelling of the materials. This confirms that most of the shrinkage occurs in the fine fractions as well as a high rate of hydration occurring within the first 7 days due to the large amount of active cement. This suggests that the larger aggregates restrain the shrinkage, as there is improved aggregate interlock and improved quality of aggregate. The smaller fractions also have larger surface areas which requires more moulding moisture for the same maximum dry density. The more moisture, the more shrinkage occurs. The voids in the small samples due to packing are also smaller and cause higher suction/ drying pressures.

This coincides with Mbaraga's findings. Mbaraga tested the potential shrinkage of mixes with various maximum aggregate sizes, 19mm, 4.75mm and 2.36mm. The testing geometry of the mould was a linear beam instead of a cylinder, however his findings were the same as presented in this study. The mix with the 2.36mm exhibited the most shrinkage and the 19mm resulted the least, (Mbaraga, 2015).

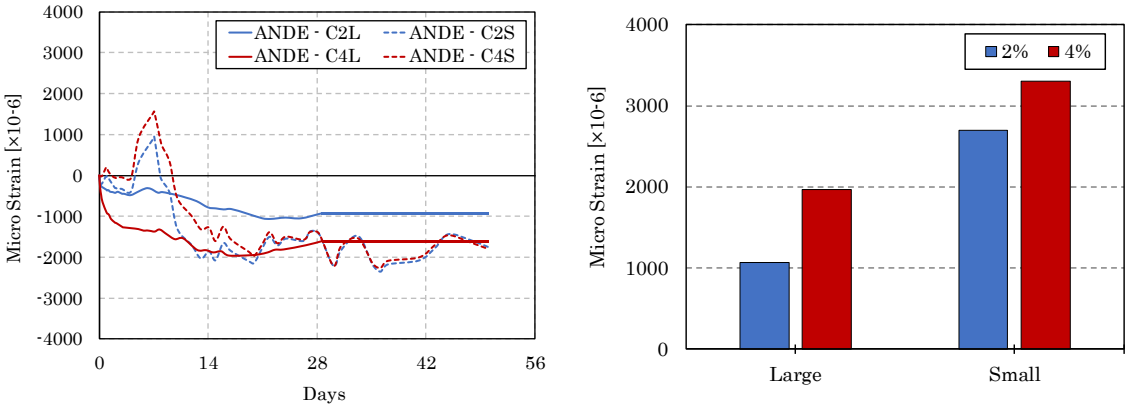

Figure 5-28: Large vs small shrinkage results of Andesite

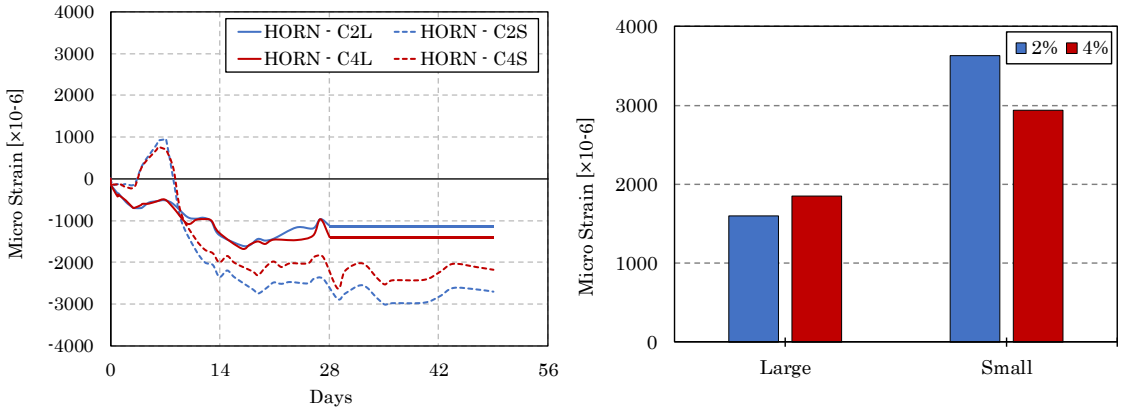

Figure 5-29: Large vs small shrinkage results of Hornfels

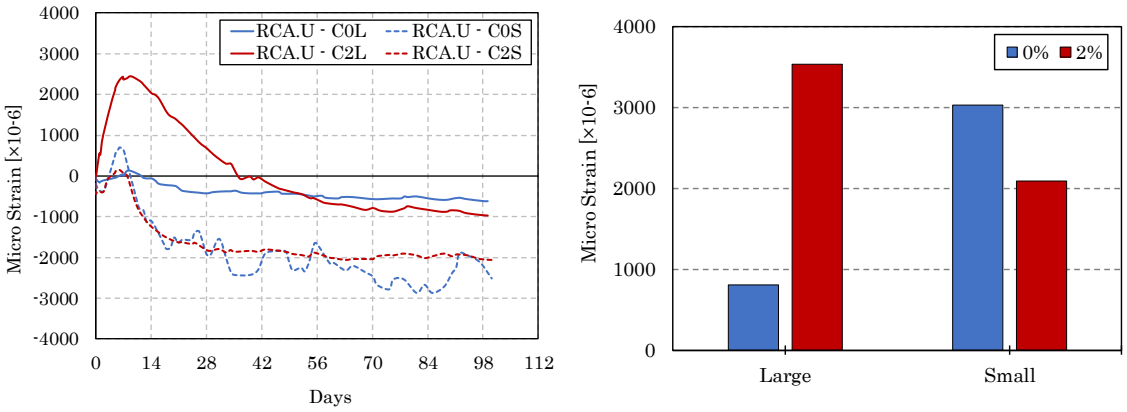

Figure 5-30: Large vs small Unexposed RCA

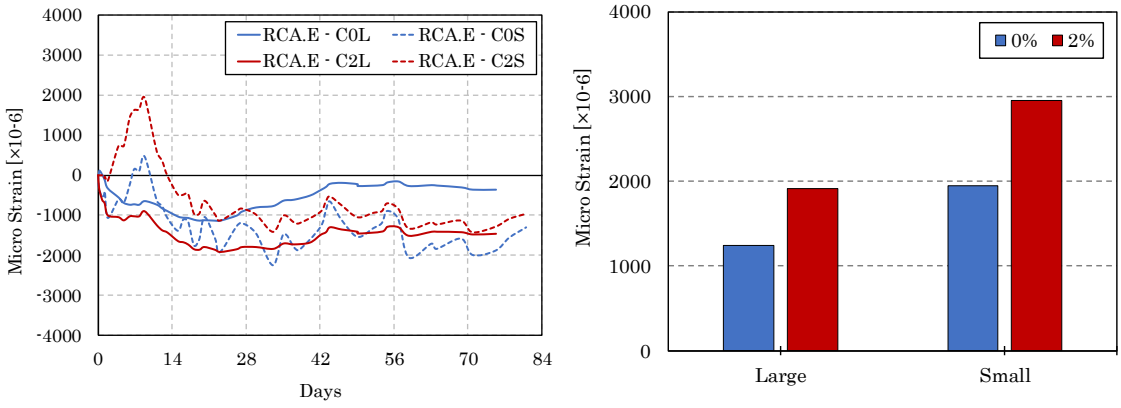

Figure 5-31: Large vs small Exposed RCA

5.2.4 Influence of Humidity on Shrinkage Tests

Humidity has a direct influence on the level of shrinkage. The lower the humidity, the less moisture in the air. An equilibrium is reached between the environment and the material. Therefore, moisture is lost through evaporation at low humidities. Evaporation causes suction pressures to be built up in the material and causes the particles to pack more tightly, resulting in volume decrease.

The finer the grading, the smaller the voids within the material matrix and therefore increased suction pressures are a result, leading to an increase in shrinkage behaviour. This also depends on the moisture content. The more moisture present, the less suction forces, as seen in Ululuza (2011). However, in terms of shrinkage, the more moisture

available the more there is to evaporate, which will again cause increased suction pressures. Due to the increase in surface area the water requirements are higher which also contributes to more shrinkage in comparison to the large shrinkage test results.

In this study the humidity ranged between 28 – 52 % RH. The RH was only analysed after 28 days so that the peaks from hydration did not come into play. After 28 days the materials seem to stabilise.

The change in peaks are displayed with their corresponding humidities. This change showed a larger influence with the small tests when compared to the large tests, as the results are more disparate, Figure 5-32 and Figure 5-33. The disparity observed is due to the increased sensitivity to humidity of the small grading. Whereas with the full grading, the larger aggregates restrain the shrinkage behaviour. It can be concluded that with an increase in humidity there is some swelling and with decrease in humidity, shrinkage occurs. Due to the small range in humidity, the fluctuations are not that significant. However, in practise there are large daily fluctuations from night time to day time where this could pose a problem for construction in the forms of premature cracking.

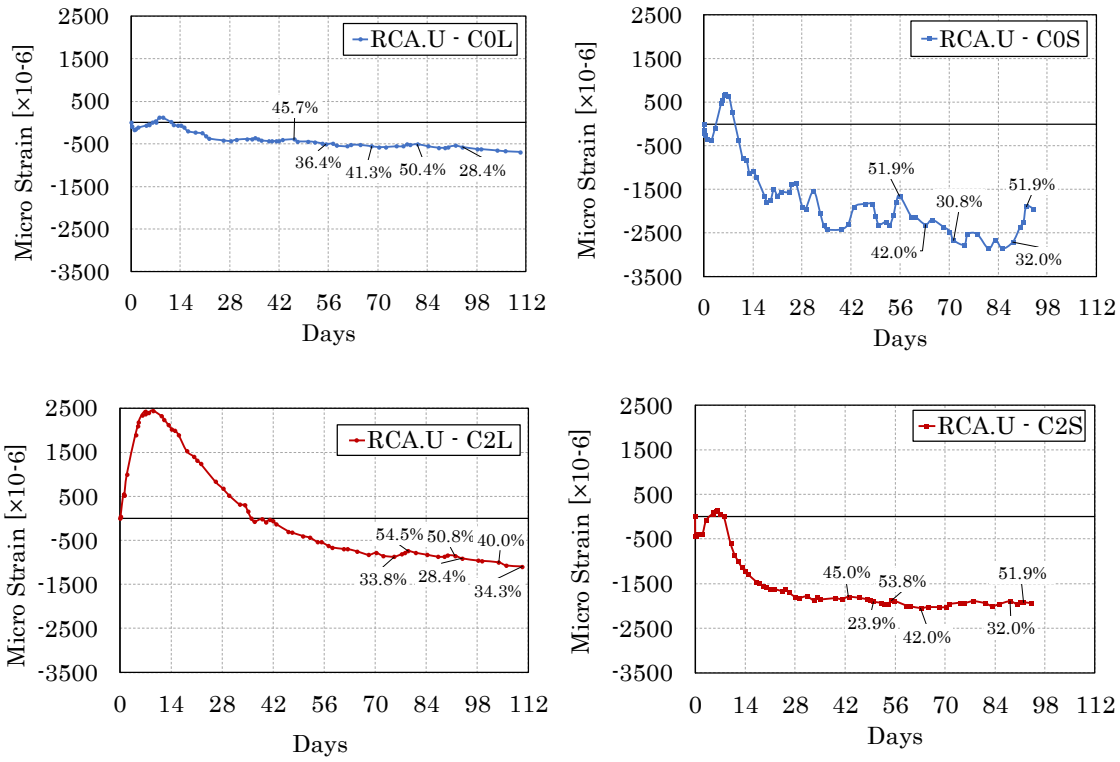

Figure 5-32: Influence of humidity on Unexposed RCA

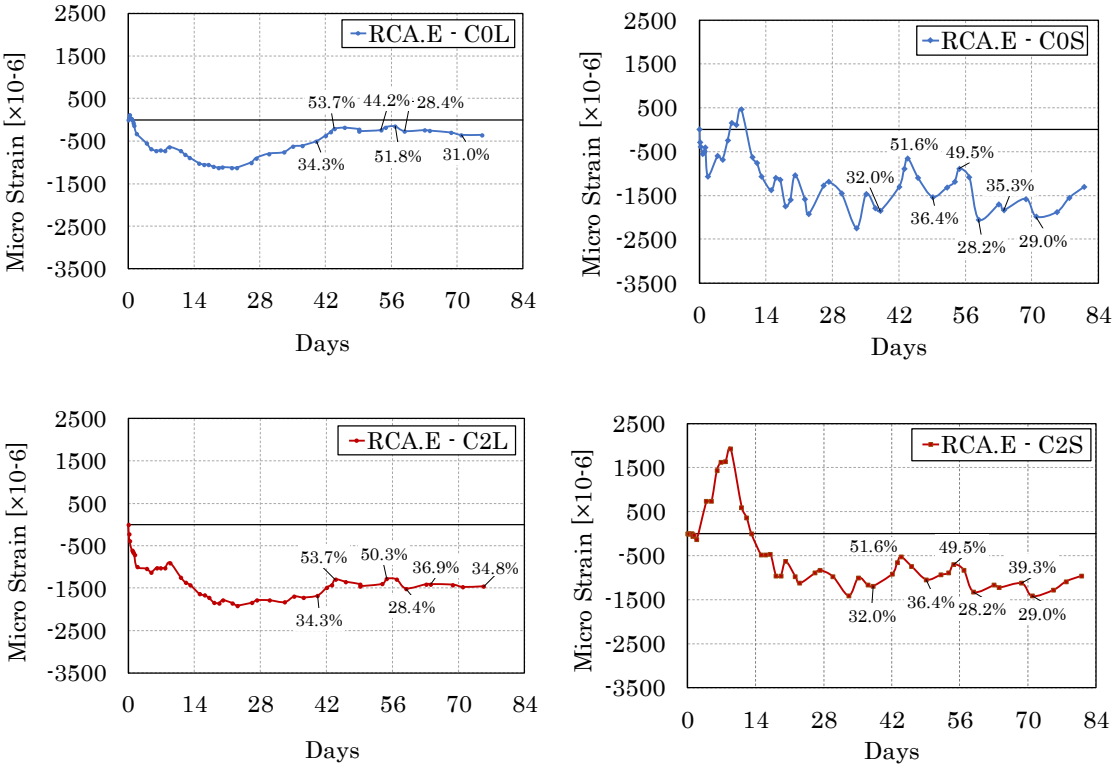

Figure 5-33: Influence of humidity on Exposed RCA

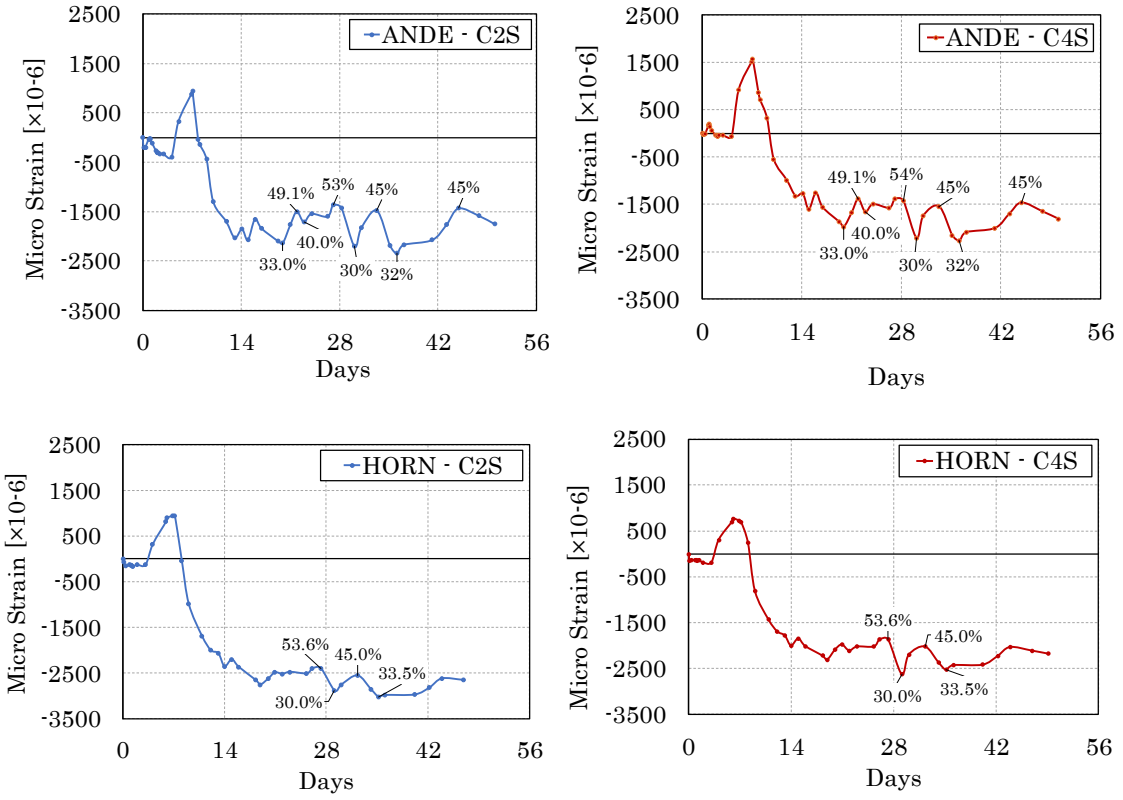

Figure 5-34: Influence of humidity on Andesite and Hornfels

5.2.5 Summary of trend variation

In order to summarise the variations in trends, all the materials with lower and higher cement percentages were plotted on the same axis, see Figure 5-35 and Figure 5-36 respectively.

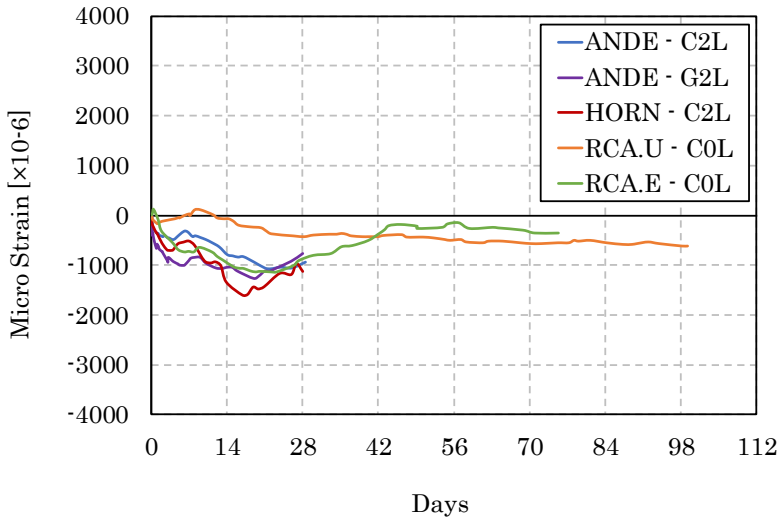

Figure 5-35: Lower percentages cement CTM and RCA

From Figure 5-35 it is clear that Andesite, Hornfels and RCA.E experience similar trends and have comparable magnitudes of shrinkage. The unexposed RCA.U is the most stable and shows the least shrinkage. The unexposed RCA show more initial swelling, but is not so heavily affected by drying shrinkage in the drying shrinkage phase (7 - 21 days).

Figure 5-36 shows the materials with higher percentages of cement. Again the Andesite, Hornfels and RCA.E show comparable trends and magnitudes of shrinkage. The unexposed RCA again shows more initial swelling; however this is a substantial increase when comparing to the 0%RCA.U. Again this is due to the high percentage of active latent cement as well as the additional cement percentage.

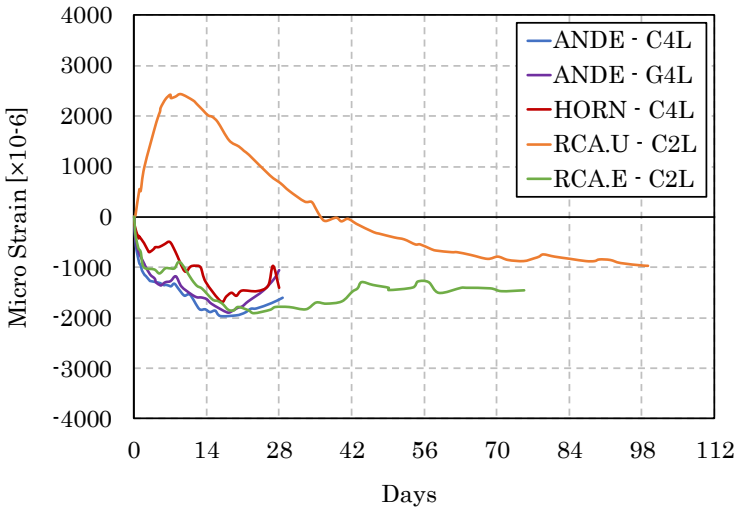

Figure 5-36: Higher percentages cement of CTM and RCA

In conclusion, the factors addressed namely material source, cement content, grading and humidity have different degrees of influence on shrinkage. Material source is the most influential factor, refer to Table 5-17 .

Table 5-17: Degree of influence of factors on shrinkage

Factor	Degree of Influence
Material Type	↑↑↑
Cement Content	↑↑
Grading	↑
Humidity	↑

5.2.6 Synthesis of Findings

Other researchers such as Xuan, Mbaraga and Semugaza have performed similar shrinkage tests and achieved similar results. These results are compared and synthesized with the results obtained from this study.

5.2.6.1 Stabilised Granular Material

Mbaraga (2015) performed large cylindrical shrinkage tests on Hornfels and Ferricrete with a maximum aggregate size of 19mm. The test was executed under accelerated curing,

which involved curing the specimens for 3 days in a 70 ºC oven. This simulated 3 months in the field. In Figure 5-37 and Figure 5-38, swelling is defined as positive and shrinkage is negative.

It can be seen from Figure 5-37 and Figure 5-38, that all material experienced initial swelling from A -B. This was due to the high curing temperature which caused expansion of the hydrated product, CSH gel and the aggregates. With an increase in cement content, came an increase in initial swelling. Mbaraga confirms that swelling is not only related to cement content and hydration, it is material specific. Factors such as aggregate type and expansion due to temperature change and internal distribution of moisture greatly influence the behaviour (Mbaraga, 2015). Mbaraga's figures never go in the negative y axis, however the material does shrink from point B to C.

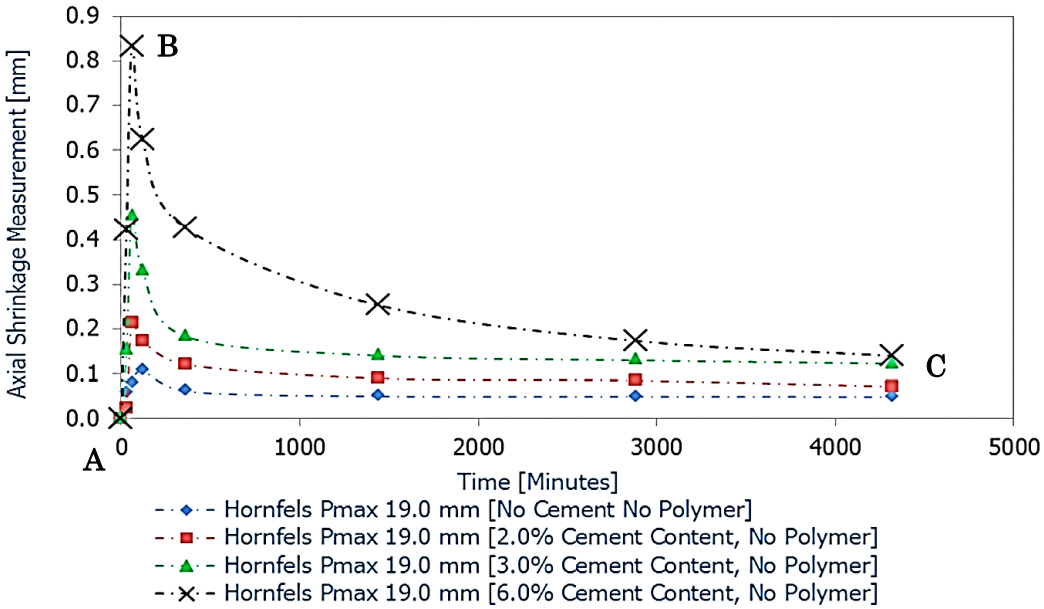

Figure 5-37: Typical Hornfels axial shrinkage curve at varying cement content,(Mbaraga, 2015)

In both Figure 5-37 and Figure 5-38, the 0% cement shrinkage curves also show limited swelling which is due to the above mentioned aggregate expansion from the elevated temperature. The Ferricrete however shows much higher magnitude of axial swelling/shrinkage than the Hornfels. The Ferricrete had a higher PI than the Hornfels and could be the reason for the increase. Materials with higher PIs hold more moisture due to the clayey characteristics and therefore experience more shrinkage.

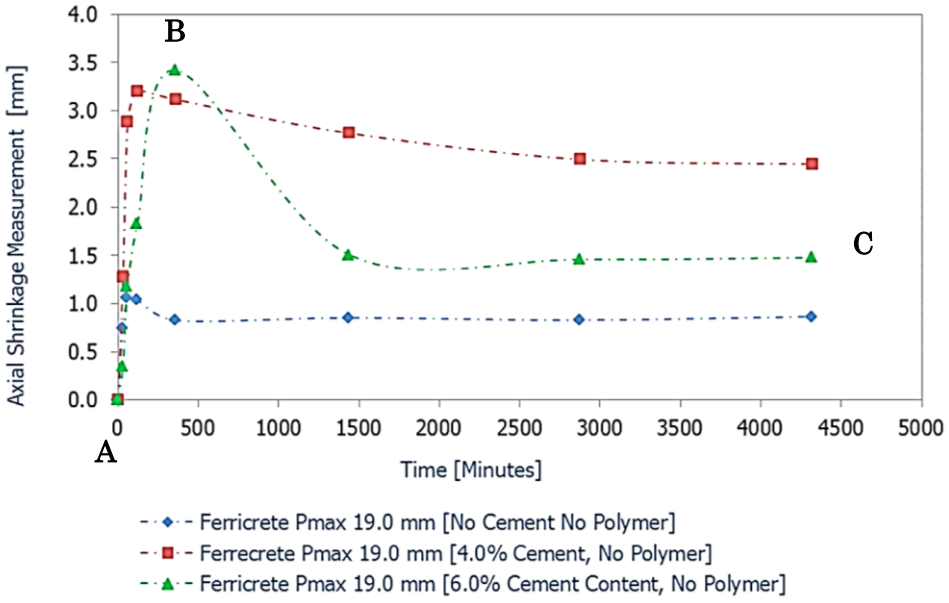

Figure 5-38: Typical Ferricrete axial shrinkage curve at varying cement content, (Mbaraga, 2015)

The curing temperature of Semugaza (2016) was between 22ºC - 25 ºC. Therefore, the shrinkage trend yielded is similar to that of the Hornfels of this study in comparison with that of Mbaraga's study, see Figure 5-39. An increase in shrinkage with an increase in cement is also found with the Hornfels of both Semugaza and Mbaraga.

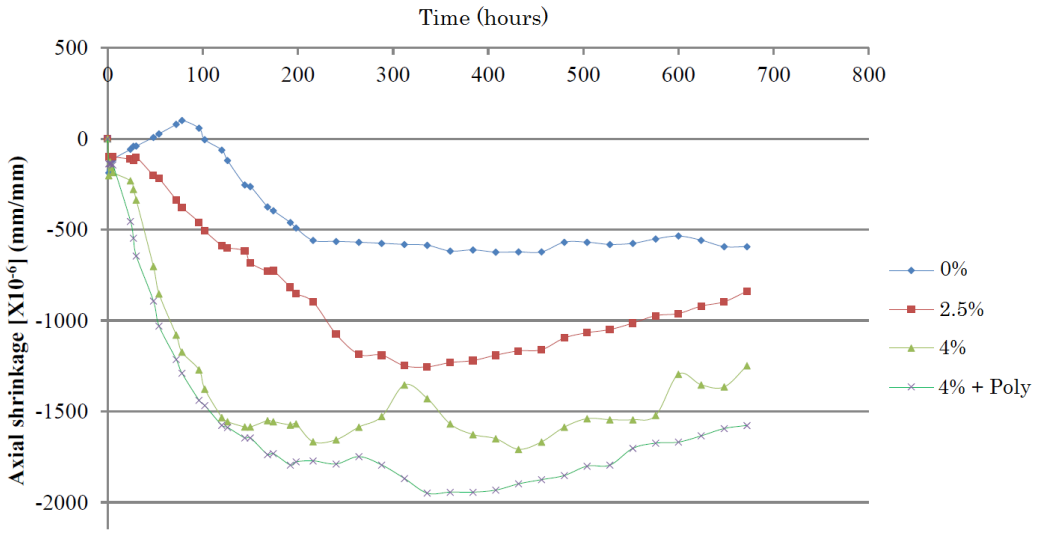

Figure 5-39: Average Hornfels shrinkage results for various cement contents

The maximum axial shrinkage results of the above mentioned authors are compared to that of the CTM in the current study in Table 5-18. The results are compared in reference to each other with a colour scale, where green indicates the lowest maximum shrinkage

and red shows the highest. Through this analysis it is determined that the Hornfels used in Mbaraga's study is the best quality material and exhibits the least shrinkage. The Hornfels of Semugaza and the Hornfels used in the current study are of a much lower quality, due to their higher shrinkage values.

The 4% Ferricrete of Mbaraga shows comparable shrinkage order size as that of the materials from the current study and the Hornfels from Semugaza. From the crack pattern of Mbaraga, which will be discussed in further detail in Chapter 7, it suggests that a material with this magnitude of shrinkage will result in severe cracking.

Table 5-18: Maximum axial shrinkage comparison of CTM, (Mbaraga, 2015; Semugaza, 2016)

Study	Material	Cement	PI	Max Axial Shrinkage (×10-6)
Mbaraga (2015)	Ferricrete	4%	3	1549
		6%	3	3956
	Hornfels	2%	Non Plastic	250
		3%	Non Plastic	499
		6%	Non Plastic	970
Semugaza (2016)	Hornfels	2.5%	Non Plastic	1330
		4%	Non Plastic	1782
Author	Andesite	2%	4	1067
		4%	4	1967
	Hornfels	2%	5	1601
		4%	5	1846

5.2.6.2 RCA

Semugaza's average shrinkage results for Hornfels, RCA and NC at 0%, 2.5% and 4% are displayed in Figure 5-40 - Figure 5-42. It can be observed that with increasing cement percentages there is an increase in drying shrinkage for all materials considered. The shrinkage trends and magnitudes of the RCA and NC are similar to that of the exposed RCA, as previously seen. This is also supported by the UCS and ITS results that were previously discussed.

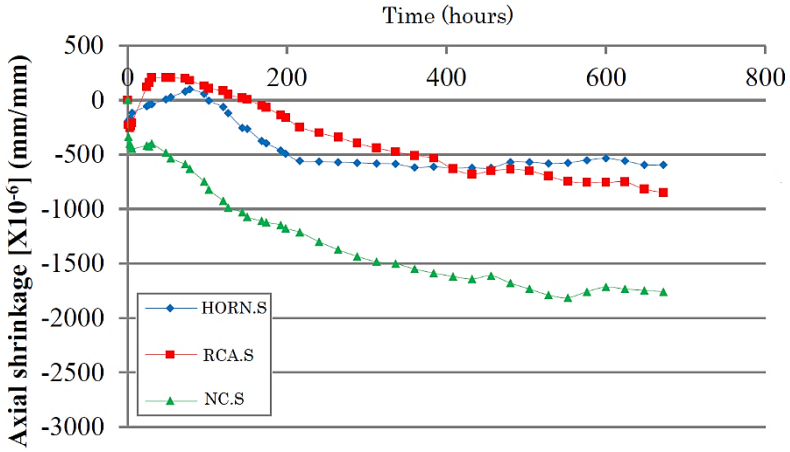

Figure 5-40: Average shrinkage of Hornfels, RCA and NC at 0% cement Semugaza (2016)

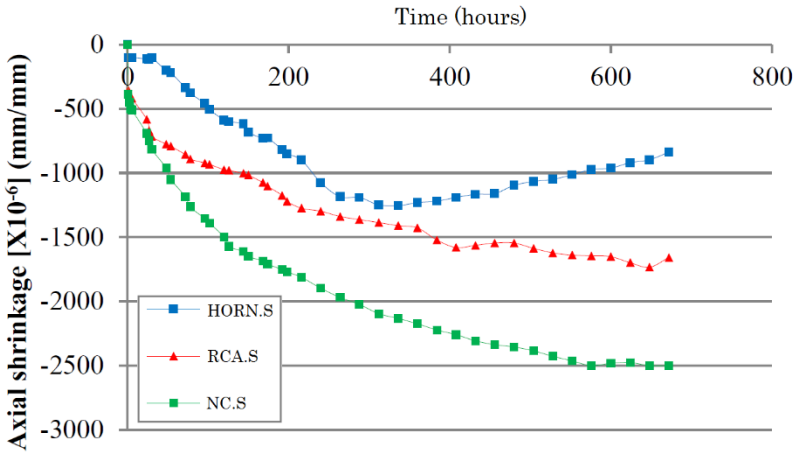

Figure 5-41: Average shrinkage of Hornfels, RCA and NC at 2.5% cement Semugaza (2016)

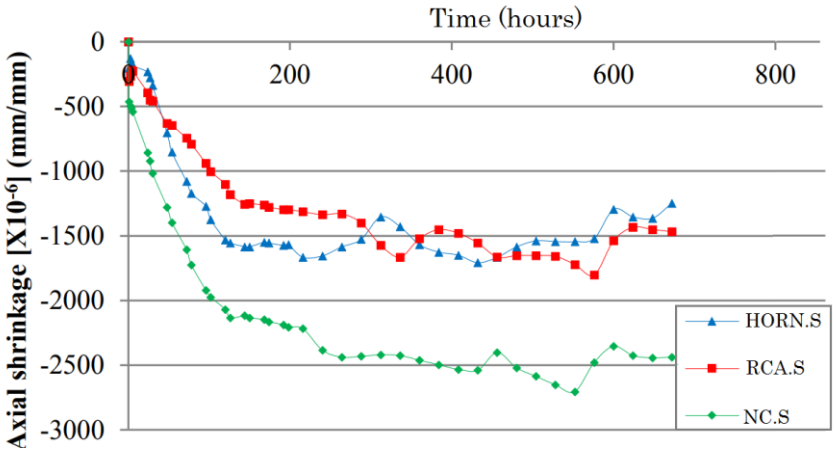

Figure 5-42:Average shrinkage of Hornfels, RCA and NC at 4% cement Semugaza (2016)

The same colour scale is used to compare the RCAs of Semugaza with the RCA of the current study, see Table 5-19. The maximum shrinkage of the 0% RCA of Semugaza is in

the same order size as the 0% Unexposed RCA. These shrinkage results are much lower than in comparison to that of the other results. According to Semugaza's shrinkage crack pattern predictions, the RCA 0% was the only material that showed a "medium" degree of cracking. All other materials displayed severe cracking. This correlation between maximum shrinkage magnitudes and degree of cracking would suggest that the 2% Unexposed RCA, and both Exposed RCAs of this study will display severe cracking.

Table 5-19: Maximum axial shrinkage comparison of RCA, (Semugaza, 2016)

Study	Material	Cement	PI	Max Axial Shrinkage (×10-6)
Semugaza (2016)	New Concrete RCA	0%	Non Plastic	1814
		2.5%	Non Plastic	2525
	RCA	0%	Non Plastic	848
		2.5%	Non Plastic	1740
Author	Unexposed RCA	0%	Non Plastic	806
		2%	Non Plastic	3536
	Exposed RCA	0%	Non Plastic	1246
		2%	Non Plastic	1911

Xuan defines shrinkage as positive and swelling as negative, see Figure 5-43. The mixes used contained various percentages of masonry and recycled concrete aggregate. It is assumed that the 0% masonry is the equivalent of 100% RCA and the 100% masonry is equivalent to a stabilised granular material. With this in mind, all shrinkage curves with RCA show initial swelling in the first 7 days. This corresponds to Xuan's curing procedure, where the specimens are wrapped up to ensure no moisture loss. This agrees with the findings of the unexposed RCA of this study. The equivalent stabilised granular material shows no swelling, which is what occurs with the shrinkage of CTM and exposed RCA from this study.

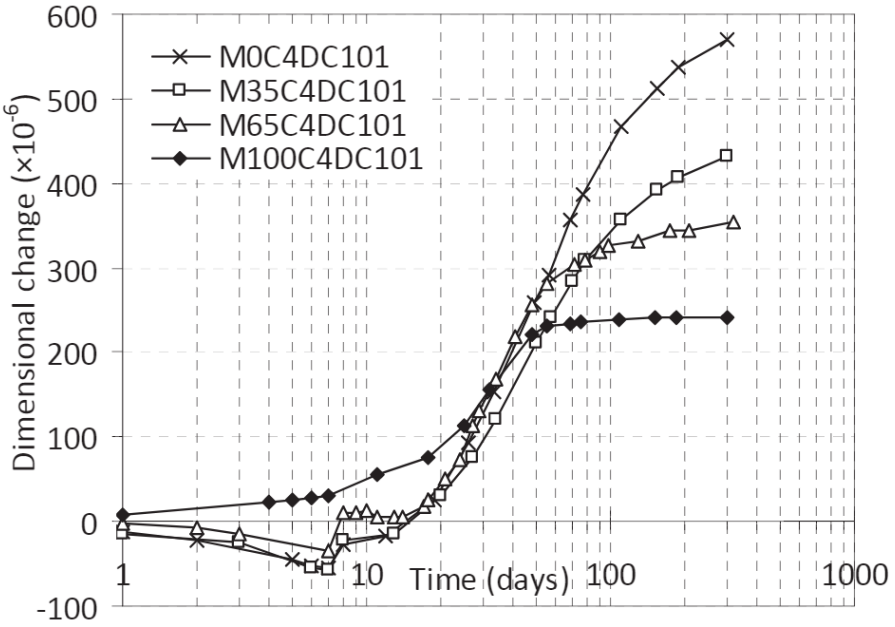

Figure 5-43: Deformation changes of CTMG, (Xuan, 2012)

5.3 Conclusion

Shrinkage of CTM and RCA is a complex process. There are many factors that occur in various phases that influence shrinkage. Drying shrinkage is however dominant over autogenous shrinkage.

The most influential factor of shrinkage is the source material. This is evident when comparing CTM and RCA. When looking at RCA specifically, the differences in shrinkage, UCS and ITS between exposed and unexposed RCA are significant.

The second most prominent factor is the cement content. This is true for all tests performed. The increase in cement for every material has improved strength and increased shrinkage. The extent of this influence is dependent again on the original material characteristics. The majority of RCA's constituents are unknown. There is no way of knowing exactly how much unreacted cement there is, and how it reacts, especially if fresh cement is added to the mix. It is unknown which cement will react first, or whether there are parallel reactions happening simultaneously. This effects the hydration reaction which could cause expansion or shrinkage.

The timing of these reactions are also unpredictable. This can be seen from the shrinkage results of the small exposed RCA, where the material behaviour is disparate. It could be

that various spots in the material undergo hydration at various times, which is also related to the humidity. At a higher humidity there is more moisture available to contribute to hydration whereas at lower humidity there is more drying shrinkage. Further studies are suggested where humidity is eliminated as a variable to understand the absolute influence of the other variables.

To conclude, RCA is not a homogenous material and must be designed for with caution. It is imperative to perform all necessary characterisation tests to understand the specific properties of an individual RCA and the extent of the variability.

Chapter 6

Overview of Shrinkage Crack Model

6.1 Introduction

Shrinkage cracking is a common problem in concrete and cement stabilised pavements. RCA can be considered somewhere in between CTM and a granular material. Due to its self-cementing properties, it could show similar shrinkage problems to CTM, especially with additional cement added.

A shrinkage cracking model for concrete pavements was established by Houben (2008). The model estimates shrinkage crack widths and spacing. It includes variables such as time and temperature variations, tensile and compressive strengths of materials and stress relaxation. This model however, was specifically designed for concrete pavements.

Xuan (2012), used the basic principle of Houben's model, but manipulated them to suit Cement Treated Mix Granulates with Recycled Masonry and Concrete (CTMG). He established functions for shrinkage, thermal expansions etc. based on his shrinkage experiments that provided 1 year of shrinkage data. These were used to update the Houben model to better suit CTMG properties and behaviour.

Mbaraga (2015), used a combination of the Houben model and Xuan's model to more accurately estimate shrinkage behaviour for Cemented Treated Materials (CTM), by adjusting the input values. Mbaraga made use of accelerated curing for 3 days in a 70°C draught oven which was equated to 3 months in the field

Due to an initial expansion with Mbaraga's cylindrical axial shrinkage results, it is deferred to long term tests that spanned 28 to 100 days at ambient temperature range (19°C to 24°C). This provides a more realistic approach to what happens in industry. No curing will have detrimental effects on the material, no matter the constitutes. As some of the model adaptions follow Xuan's process, as will be discussed, it was decided to follow his mixing and curing procedures which included 7 days of curing at 100% humidity. The

model will investigate 3 materials namely Andesite 2% continuous, Unexposed RCA 0% and Exposed RCA 0%. These three materials were selected as they are the more realistic materials that would be implemented on site. In Chapter 5 the 0% Unexposed RCA has also been compared to an equivalent granular (Andesite) with 2% cement stabilisation, and therefore seemed fitting for comparison. Details on the input parameters and shrinkage calculations based on Houben's approach are discussed and evaluated in this chapter. The results of the model are discussed in Chapter 7.

6.1.1 Brief Overview of Houben Model Shrinkage Crack Pattern

The Houben model works on the basis that cracks form when there is a build-up of tensile stresses from the fluctuations in temperature and humidity. Cracks will manifest when the tensile strength of the material is less than that of the tensile stresses developed (Houben, 2008).

The first or primary cracks will occur to release the stress. This discontinuity is then assumed to decrease the slab length i.e. the length between the two primary cracks. It is assumed that the secondary cracks will occur in the middle of the reduced length. This again halves the length due to the discontinuity. This process is then repeated until the induced stresses are smaller than the yielding stress of the material, see Figure 6-1, (Mbaraga, 2015).

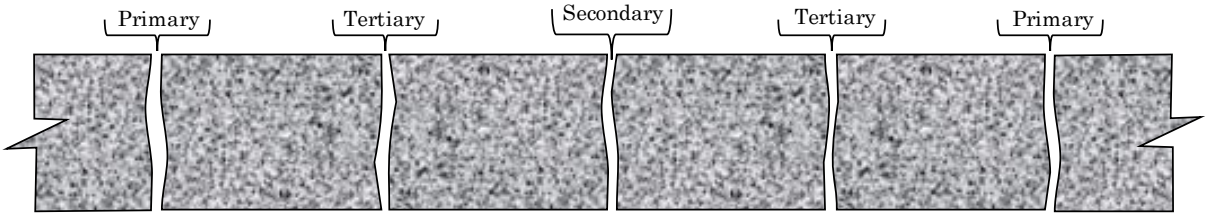

Figure 6-1: Houben Crack Pattern (Mbaraga, 2015)

6.2 Crack Width and Crack Spacing Calculations

Cracks negatively affect pavements in terms of bearing capacity of the pavement structure as well as accelerated deterioration should these cracks propagate through to the surface. It is important to be able to estimate the frequency, spacing and widths of these cracks to predict the life of a pavement. The goal is to develop a simplified method

to estimate shrinkage crack spacing's and widths of CTM and RCA. The method is based on Hookes Law and the structural properties, while also incorporating drying shrinkage and thermal shrinkage. Two main stages of crack formation is a) crack initiation and b) crack growth. Both are time dependent and are influenced by material properties and climatic conditions, (Xuan, 2012).

6.2.1 Mechanical Analysis of Shrinkage Cracking

The Houben Model is designed specifically to evaluate the crack behaviour in concrete pavements. The basis of the model is that as soon as the induced occurring tensile stress in the material exceeds the tensile strength of the material, transverse cracks will form, see Equation 6-1. These cracks act as stress relief for the pavement, and are referred to as primary cracks.

$$\boldsymbol{\sigma(t) > f_{ctm}(t)} \tag{6-1}$$

Where:

$\sigma(t)$ is the induced tensile stress due to shrinkage at time t in hours

$f_{ctm}(t)$ is the direct tensile strength of the base material at time t in hours

The tensile stresses that build up, are due to the surrounding layers that cause resistance in the form of frictional forces onto the layer that is undergoing drying shrinkage, see Figure 6-2. Environmental and chemical transformations of the material itself are what cause the layer to undergo drying shrinkage, (Xuan, 2012).

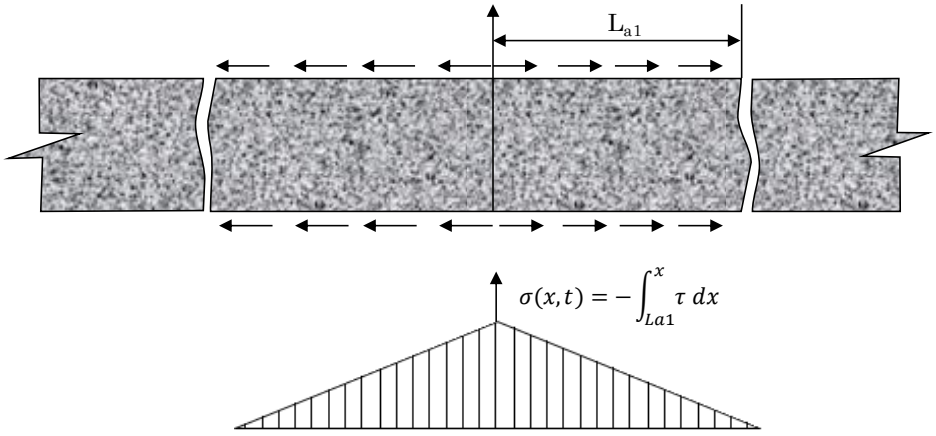

Figure 6-2: Tensile stress of the layer that is acting against shrinkage (Xuan, 2012)

As the material experiences temperature variations and undergoes further chemical transformations, tensile stresses will again build up in the material until it exceeds the tensile strength of the material. It is assumed that the secondary cracks will form half way between two primary cracks. This procedure will repeat itself until the tensile stress in the material does not exceed the tensile strength of the material, see Figure 6-3. Houben defines a breathing length L_{a1} at the primary crack as half of the crack spacing length L_{w1}.

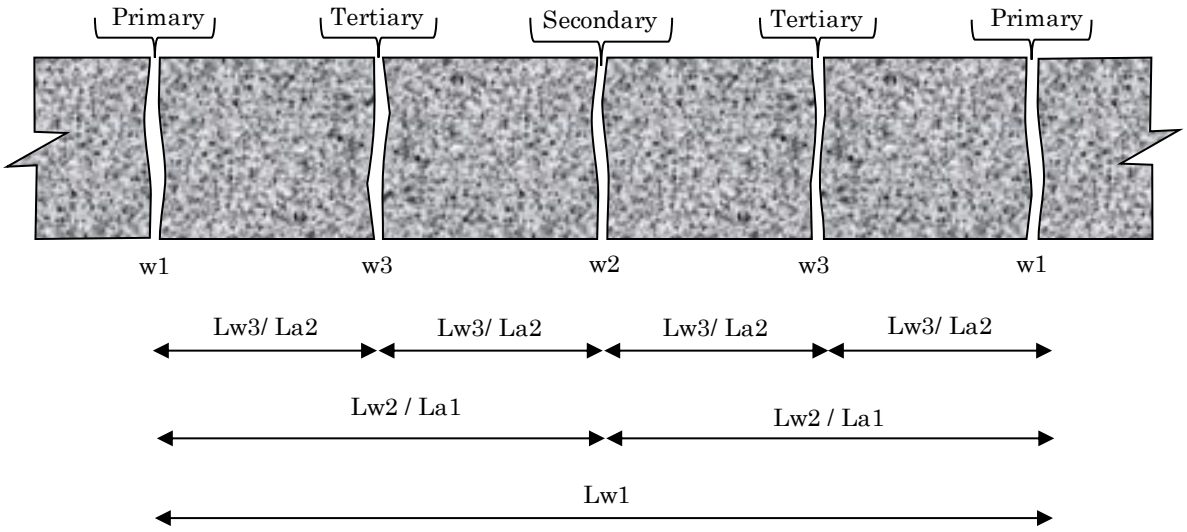

Figure 6-3: Crack Formation and Spacing

As mentioned, the occurring tensile stress is resistance of the surrounding layer against the layer in question that is undergoing drying shrinkage, see Equation 6-2.

$$\boldsymbol{\sigma(t_1) = -\int_{La1}^{0} \tau\, dx = \gamma \rho g \cdot L_{a1}} \qquad 6\text{-}2$$

Where:

γ = Coefficient of sliding friction 3.8 (Mbaraga, 2015)

ρ = Material density $[kg/m^3]$

g = 9.8m / sec^2

L_{a1} =Breathing length [m]

The breathing length is calculated by Equation 6-3, and is defined as fined as half of the crack spacing length, see Figure 6-3. At this time t_1 the tensile stresses have exceeded the tensile strength of the material and the primary crack has formed.

$$\boldsymbol{L_{a1} = \frac{\sigma(t_1)}{\gamma\rho g} = \frac{E(t_1) \cdot \varepsilon(t_1)}{\gamma\rho g}} \qquad 6\text{-}3$$

Where:

$E(t_1)$ = Elastic Modulus [MPa]

$\varepsilon(t_1)$ = Maximum tensile strain

The crack width at the time of the primary crack is determined by two factors: the shrinkage of the layer and the opposing friction action from the surrounding layers.

$$\boldsymbol{w_{shrinkage} = \frac{\sigma(t_1)}{E(t_1)} \cdot 2L_{a1} = \varepsilon(t_1) \cdot 2L_{a1}} \qquad 6\text{-}4$$

$$\boldsymbol{w_{friction} = 2\int_0^{L_{a1}} \frac{\gamma\rho g}{E(t_1)} \cdot x \cdot dx = \frac{\gamma\rho g {L_{a1}}^2}{E(t_1)}} \qquad 6\text{-}5$$

Equation 6-6 calculates the total initial crack width of the primary crack. It is simplified by substituting L_{a1} with the Equation 6-3.

.

$$\boldsymbol{w_i = w_{shrinkage} - w_{friction} = \frac{\sigma(t_1)^2}{\gamma\rho g \cdot E(t_1)} = \frac{E(t_1) \cdot \varepsilon(t_1)^2}{\gamma\rho g}} \qquad 6\text{-}6$$

Note: Equations 6-2 - 6-6 are according to Xuan, where stress σ is calculated in kPa and crack width w in m.

At this point, a reduction in tensile stress would be calculated due to the relief in stress that the primary cracks provide. Thereafter the tensile stresses will continue to develop

due to ongoing chemical and temperature reactions. This will also influence the development of the crack width before the secondary cracks occur. This process is repeated for the tertiary cracks, see Figure 6-4 for the crack hierarchy process. Under the right circumstances the primary and secondary cracks can occur immediately after each other that it can be assumed they occur at the same time.

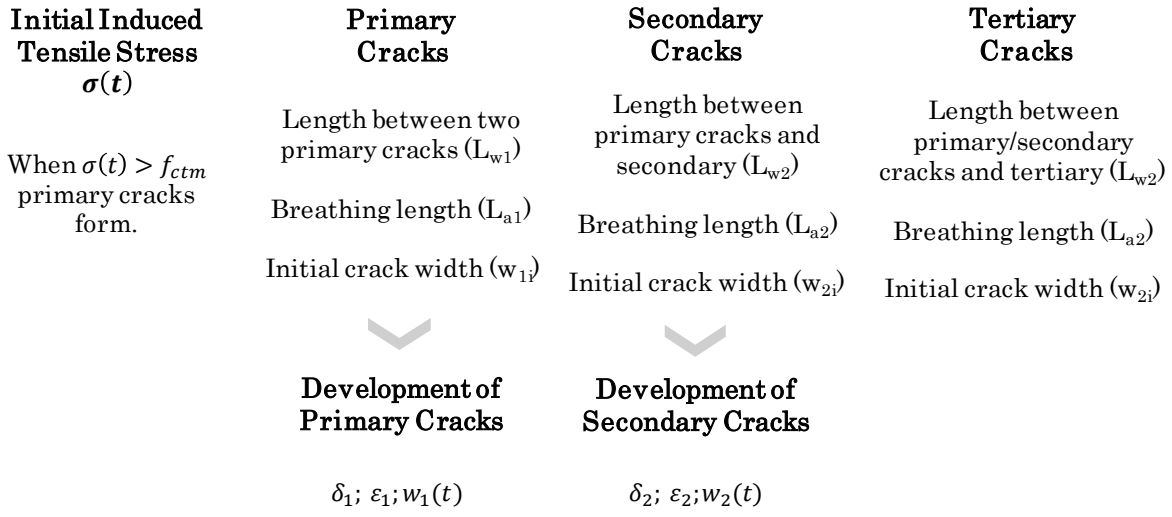

Figure 6-4: Shrinkage crack hierarchy

6.2.1.1 Primary and Secondary Cracks

Because of a small primary crack width, the stress reduction is very small. This leads to the secondary cracks occurring very soon after, and can be assumed that they occur at the same time. This assumption is carried out by Houben and Xuan.

For this case the following equations according to Houben were used for:

L_{a12} Breathing length [m]

L_{w12} Distance between the primary and adjacent secondary cracks [m]

w_{12i} Initial crack width of the primary and secondary cracks [mm]

$\Delta\sigma_{12}$ Reduction of tensile stress [MPa]

$\Delta\varepsilon_{12}$ Reduction in tensile strain midway between a primary and secondary crack

$$L_{a12} = \frac{\sigma(t_1)}{\gamma\rho g} = \frac{1000 \cdot E(t_1) \cdot \varepsilon(t_1)}{\gamma\rho g} \quad 6\text{-}7$$

As the primary and secondary cracks occur simultaneously, the breathing length and distance between the cracks will be equal.

$$L_{a12} = L_{w12} \quad 6\text{-}8$$

$$w_{12i} = \frac{1\,000\,000 \cdot E(t_1) \cdot \varepsilon(t_1)^2}{2\,\gamma\rho g} \quad 6\text{-}9$$

$$\Delta\sigma_{12} = 0.5\sigma(t_1) \cdot \left[1 + \frac{w_{12i}}{1000 \cdot L_{a12}}\right] \quad 6\text{-}10$$

After the initial crack, there is a reduction in maximum tensile stress. To clarify, t_1 refers to the time of occurrence of the primary/secondary cracks.

6.2.1.2 Development of Primary/Secondary Cracks and Stresses

According to Houben, the friction coefficient should increase after the primary/secondary cracks, as the model will yield unrealistically large crack widths. Houben arbitrarily assumed an increase in friction by a factor of 10. This factor was included in the crack width equations. After the primary/secondary cracks have occurred, the material experiences further chemical and thermal processes which further develops the maximum tensile stress $\sigma_2(t)$. This in turn also effects the strain.

$$\sigma_2(t) = \sigma(t_1) - \Delta\sigma_{12} \quad 6\text{-}11$$

$$\varepsilon_2(t) = \frac{\sigma_2(t)}{E(t)} \quad 6\text{-}12$$

A change in width of the crack occurs, due to developed stresses. The change in width is calculated as the difference in widths at a time t and t_1 (time of primary/secondary crack). The total crack width at time t is therefore the initial crack plus the growth of the crack,

see Equations 6-13 and 6-14. The friction factor is multiplied by a factor of 10, according to Houben, as unrealistically large crack widths are obtained.

$$\Delta w_{12}(t) = \frac{1\,000\,000 \cdot E(t) \cdot \varepsilon_2(t)^2}{10\gamma\rho g} - \frac{1\,000\,000 \cdot E(t_1) \cdot \varepsilon(t_1)^2}{10\gamma\rho g} \quad 6\text{-}13$$

$$w_{12}(t) = w_{12i} + \Delta w_{12}(t) \quad 6\text{-}14$$

6.2.1.3 Tertiary Cracks

At the moment that the tensile stress σ_2 exceeds the tensile strength of the material, a tertiary crack will form midway between the present primary/secondary cracks, see 6-15. The time of the tertiary crack is denoted as t_2. The initial tertiary crack width is calculated with the developed ε_2, see Equation 6-16.

$$w_{3i} = \frac{1\,000\,000 \cdot E(t_2) \cdot \varepsilon_2(t_2)^2}{10\gamma\rho g} \quad 6\text{-}15$$

$$w_{3i} = \frac{1\,000\,000 \cdot E(t_2) \cdot \varepsilon_2(t_2)^2}{10\gamma\rho g} \quad 6\text{-}16$$

The breathing length of the tertiary crack is calculated as a quarter of the L_{a12}, while taking into account the widths of the cracks.

$$L_{a3} = 0.25L_{a12} - \frac{0.5w_{12}(t_2)}{1000} - \frac{0.5w_{3i}}{1000} \quad 6\text{-}17$$

After the occurrence of the tertiary cracks, the length between them is equal to half of $L_{w12} = L_{a12}$.

$$L_{w3} = 0.5\,L_{w12} \quad 6\text{-}18$$

The decrease in tensile stress due to the tertiary cracks can be seen in Equation 6-19.

$$\Delta\sigma_3 = 0.5\sigma_2(t_2) \cdot \left[1 + \frac{w_{3i}}{1000 \cdot L_{a3}}\right] \quad 6\text{-}19$$

Here after the same process if followed where the tertiary cracks develop due to the developing stresses, until the tensile stress exceed the tensile strength of the material and a quarterly cracks occur and so on, see Figure 6-5.

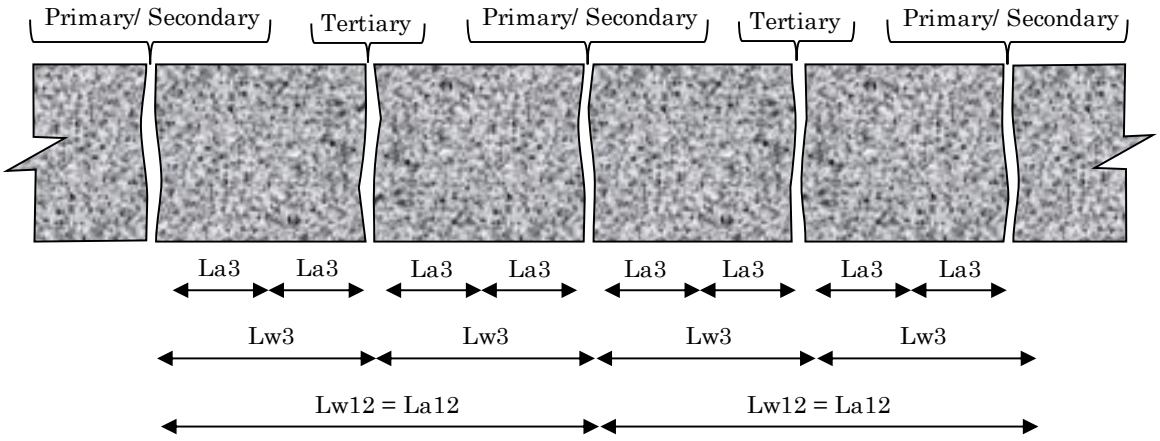

Figure 6-5: Schematic of tertiary cracking

6.3 Input Parameters

The drying shrinkage and therefore stress build up are dependent on the environmental and physical characteristics of the material. This section explains how these factors are modelled and serve as input parameters to the model explained above.

The input parameters can be broken down into 4 sections to make it easier to follow which factors were adjusted and where assumptions were made. The following sections will branch off into more detail: climate, temperature and time factors; drying shrinkage deformations; thermal deformations; and material properties.

6.3.1 Climate, Temperature and Time Factors

Climatic influences at construction and during the course of the pavement life can greatly influence the shrinkage behaviour of a pavement. It is important to take note of these variabilities and ensure the typical values are used for the area undergoing investigation. The variables include daily, seasonal and annual temperatures of the stabilised layer at the time of construction and during the course of the analysis period (Mbaraga, 2015).

The analysis was performed for Cape Town specifically. The average annual maximum, average annual minimum and average annual temperatures were provided by the South African Weather Services. These annual averages are calculated from 5 years of data (2010-2015). It was assumed that the temperature of the cement stabilised layer was the same as the air temperature, due to a lack of field temperature data. All climate, temperature and time variables were based from the original Houben Model, (Houben, 2008).

6.3.1.1 Seasonal Temperature Variations

As mentioned, the model analysis period is approximately 1 year, and therefore the temperatures of the varying seasons needed to be taken into account. The average annual temperature in Cape Town was taken as 17°C, the average annual maximum and average annual minimum were 22°C and 12°C respectively, see Table 6-1.

Table 6-1: Monthly average temperatures over 5 years

MONTH	January	February	March	April	May	June
Ave. Max. Temp. [°C]	26	26.4	25	22	20	17.6
Ave. Temp. [°C]	21	21.8	19.5	17	15	12.8
Ave. Min. Temp. [°C]	16	17.2	14	12	10	8

July	August	September	October	November	December	**Annual**
17	18	19	21	23	25	**22**
12.8	13	14	16	18	19.5	**17**
8.5	8	9	11	13	14	**12**

The average seasonal temperature on the day of construction,$T_{seasonal}$ can be calculated with Equation 6-20. Where $T_{aveyear}$ is the average annual temperature of 17°C; $T_{ampyear}$ is the annual average air temperature amplitude of 5°C and t_1 is the time of construction measured in number of days, (Houben, 2008).

$$\boldsymbol{T_{seasonal} = T_{aveyear} + T_{ampyear} \cdot \sin(t_1)} \qquad \text{6-20}$$

Construction began on 1st of November at 10am with an average of 17°C, thereafter the February obtained a higher average temperature of 22°C as it is typically the hottest month in Cape Town. The May obtained an average of 17°C and lastly August a low average of 12°C as it is typically the coldest month in Cape Town, (Mbaraga, 2015). These average temperatures form a sinus graph with an annual average air temperature amplitude of 5°C, see Figure 6-6, (Mbaraga, 2015).

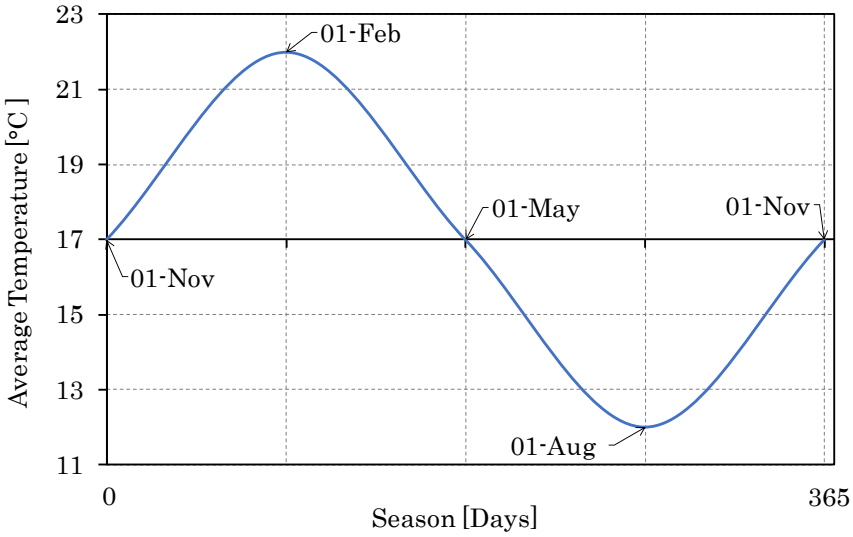

Figure 6-6: Sinus graph of seasonal temperatures in Cape Town

6.3.1.2 Daily Temperature Variation

The daily temperature variations are important to include in the calculations as it is typically warmer during the day than at night. The daily average temperature of 17°C would be at 10:00AM and 10:00PM. The daily average maximum temperature at 4:00PM

and the daily average minimum temperature at 4:00AM. Similarly to the seasonal changes, a sinus Equation 6-21 was derived by Houben to estimate the daily temperature fluctuations by including the daily air temperature amplitude of 4.5°C. The variable t_2 is the clock hour of construction, i.e. 0 to 24 hours, see Figure 6-7.

$$\boldsymbol{T_{daily} = T_{seasonal} + T_{ampday} \cdot \sin(15(t_2 - 10))} \quad \text{6-21}$$

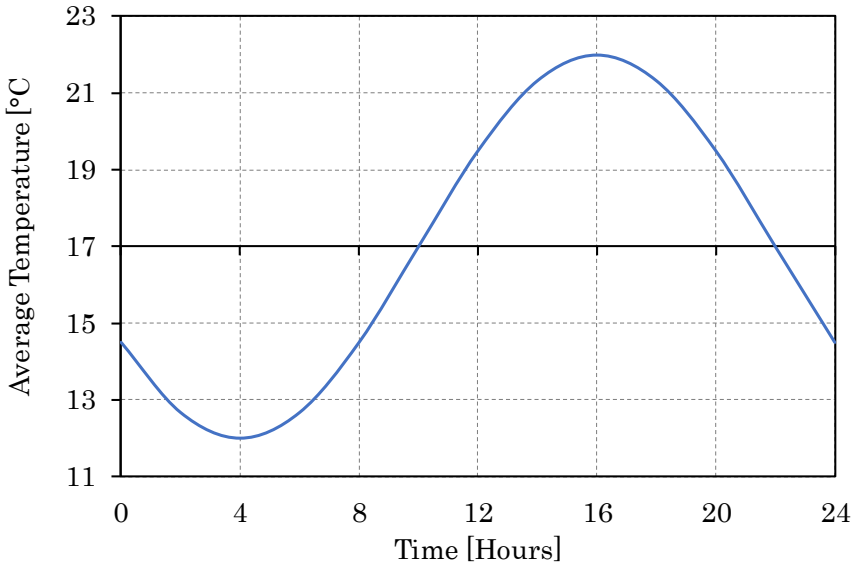

Figure 6-7: Daily variation of temperature in the road layer

6.3.1.3 Climate Dependent Temperature

The climate dependant temperature, $T_{climate}$ incorporates both the seasonal and daily temperature variations, see Equation 6-22, where t is the number of hours after construction.

$$\boldsymbol{T_{climate} = T_{daily} + T_{ampyear} \cdot \sin\left(\frac{t}{24} + t_1\right) - T_{ampyear} \cdot \sin(t_1) + T_{ampday} \cdot \sin(15t)} \quad \text{6-22}$$

6.3.1.4 Hydration Temperature

The hydration process takes place after the construction and increases the temperature of the layer. The Houben Model makes use of Equation 6-23.

$$T_{hydration} = c_1 \cdot f_1 \cdot f_2 \tag{6-23}$$

Where:

$c_1 = 1$

$f_1 = t^{c2}$ $\quad c_2 = 2$

$f_2 = e^{-c3 \cdot t}$ $\quad c_3 = 0.27$

The hydration coefficient is dependent on the percentage cement content. In concrete it is typically 15% to 17% whereas cement stabilised materials rarely go above 4%. Houben calculated $c_1 = 1$ and assumed 375kg cement per cubic meter in his mix. The hydration of concrete is far less than that of cement stabilised material, therefore Mbaraga altered the hydration coefficient as follows with Equation 6-24. Note that c_1 is mix dependent.

$$c_1 = \frac{\%\ cement\ used \times MDD}{375} \tag{6-24}$$

Mbaraga and Houben performed sensitivity analyses together for c_2 and c_3 and found that the coefficients remained similar enough to the concrete values, and could therefore be used for RCA and CTM analysis. The coefficient used in this study was calculated in the same way as Mbaraga, and changed with each mix, see Table 6-2. Based on the UCS and ITS tests from the previous chapter it was assumed that the active latent cement percentage contribution was 2% for the unexposed RCA and 1% for the exposed RCA.

Table 6-2: Hydration coefficient inputs

Material	Cement (%)	MDD [kg/m3]	c1
Andesite	2	2380	0.127
Unexposed RCA	2	2100	0.122
Exposed RCA	1	2136	0.057

6.3.1.5 Temperature of Stabilised Layer

The temperature of the stabilised layer, T_{road}, is the sum of the climatic dependant temperature, $T_{climate}$ and the hydration temperature, $T_{hydration}$ see Equation 6-25.

$$\boldsymbol{T_{road} = T_{climate} + T_{hydration}} \quad \text{6-25}$$

6.3.2 Drying Shrinkage Deformation

As mentioned in the Houben model, total deformation is described as the sum of drying shrinkage, thermal deformation and autogenous shrinkage. Both Xuan and Mbaraga based their models on only drying shrinkage and thermal deformation. This could be due to drying shrinkage being the most dominating factor in CTM. Autogenous shrinkage plays a large role in the shrinkage of concrete as the water cement ratio can be as low as 0.42, where all the water is used for hydration. This leads to surface tension in the capillaries and causes cracks, and is the reason why proper curing is a crucial step in concrete design. CTMs however have much higher water cement ratios and therefore the assumption to exclude autogenous shrinkage was substantiated. As per Mbaraga and Xuan, the total deformation is the sum of drying shrinkage and thermal expansion, see Equation 6-26.

$$\boldsymbol{\varepsilon(t) = \varepsilon_S + \varepsilon_T} \quad \text{6-26}$$

6.3.2.1 Drying Shrinkage (Houben)

Houben makes use of drying shrinkage Equation 6-27, where $\varepsilon_{cd,0}$ is a concrete coefficient and is grade dependent. Values can be found in Eurocode 2. The time dependency factor is calculated with Equation 6-28, which forms part of the shrinkage formula, where t is time, t_s is the start of drying time after construction, both are measured in hours. It is known that concrete tends to warp due to shrinkage and therefore Houben included shape factors k_h and h_0.

$$\varepsilon(t) = \beta_{ds}(t) \cdot k_h \cdot \varepsilon_{cd,0} \quad \text{6-27}$$

$$\beta_{ds}(t) = \left(t/24 - t_s/24\right) / \left\{\left(t/24 - t_s/24\right) + 0.04 \cdot {h_0}^{1.5}\right\} \quad \text{6-28}$$

6.3.2.2 Drying shrinkage (Xuan)

Xuan uses equations for shrinkage based on his own results. His shrinkage experiments are separated into two sections, 0 - 7 days and >7 days. For the first 7 days Xuan cures his samples in 100% humidity and there after monitors shrinkage at 50% humidity. Two formulas were developed for these two phases see Equation 6-29 and 6-30 respectively.

$$S(t) = a \cdot \ln(t+1) \quad \text{6-29}$$

$$S(t) = S_{min} + (S_{max} - S_{min}) \left[1 + \left(\frac{t}{t_r}\right)^k\right]^{\frac{-m}{k}} \quad \text{6-30}$$

Xuan provides a formula for the constant a. It depends on the degree of compaction, cement content, moisture content and recycled masonry content. As mentioned Equation 6-29 is specifically for the curing phase which is less than 7 days. The Equation 6-30 makes use of initial deformation at 7 days, S_{min} and the maximum deformation at 360 days, S_{max}. The t depicts time in days in both formulas.

In Equation 6-29 t represents time at 100% relative humidity and in Equation 6-30 t shows number of days at relative humidity of 50%. The parameter t_r is a ref parameter, while k and m are both shape factors. All three are calculated by formulas based on recycled masonry content.

6.3.2.3 Drying Shrinkage (Mbaraga)

Mbaraga used Xuan's 0 - 7 day Equation for drying shrinkage. This equation best suited his data. As already mentioned his test duration was 3 days, which simulated 3 months

of field data. The *a* value was determined by optimising this data with Excel's solver function.

6.3.2.4 Conclusion

The shrinkage model that best represented all the data was Equation 6-30. The equation was implemented from 0-365 days, and the coefficients were optimised with Excel's solver function, see Table 6-3.

Table 6-3: Drying shrinkage input parameters

Material	S_{min}	S_{max}	t_r	k	m	r^2
Andesite	0	-1067	26	-25	-0.63	0.8
Unexposed RCA	0	-680	1.49	-0.84	-7.03	0.81
Exposed RCA	0	-1127	3.82	-1.24	-1.89	0.96

In Figure 6-8 - Figure 6-10 drying shrinkage from the cylindrical shrinkage tests are modelled. Due to the time constraints 365 days of data was not achievable. The graphs are plotted on a log scale in order to see the shrinkage within the first 21 days more clearly.

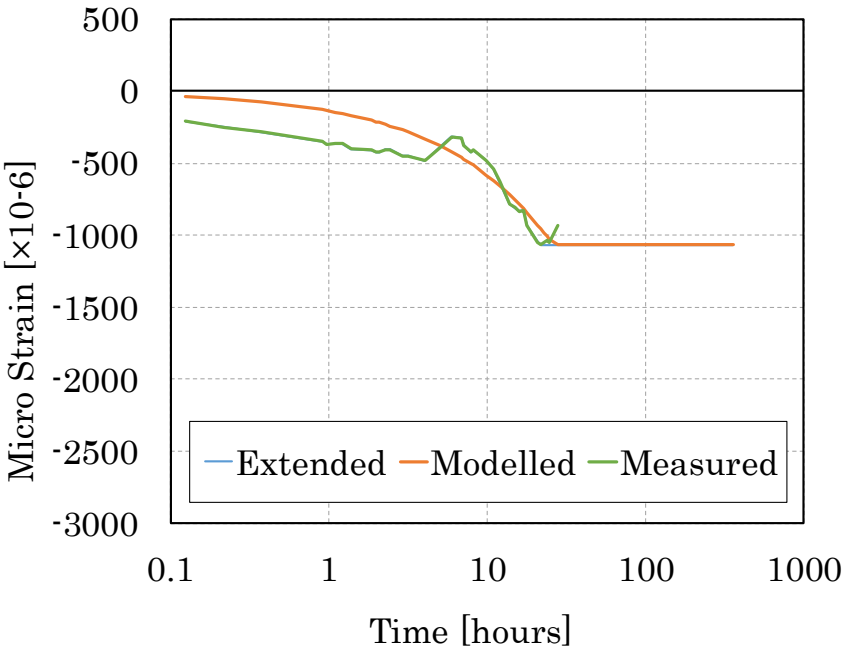

Figure 6-8: Drying shrinkage modelling of Andesite 2%

As previously discussed this is the most critical time for drying shrinkage. The material seems to recover after 21 days. Therefore the models are based on the extended shrinkage plotted. Once these have been implemented into the model, cracking after 21 days will be defined as unrealistic as material begins to recover after 21 days.

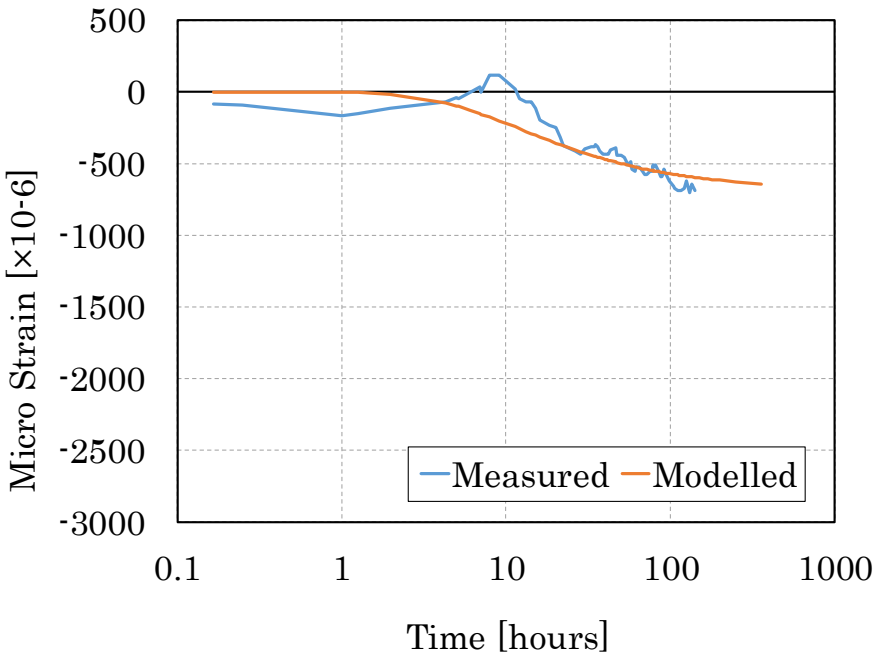

Figure 6-9: Drying Shrinkage modelling of Unexposed RCA 0%

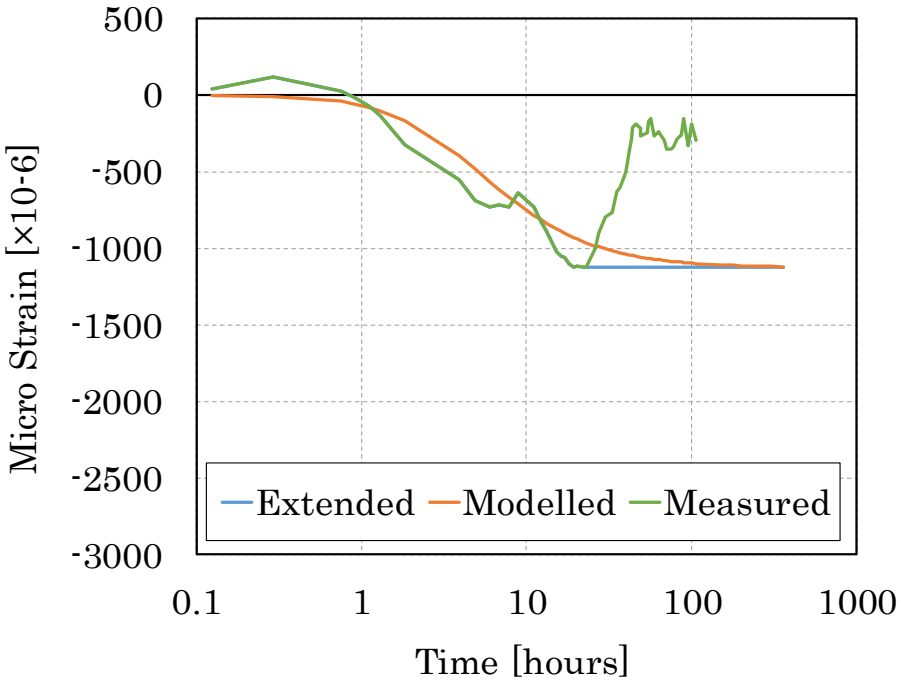

Figure 6-10: Drying shrinkage modelling of Exposed RCA 0%

6.3.3 Thermal Deformation

As mentioned before the hydration process takes place after construction and increases the temperature of the layer. This in turn causes the concrete or cement stabilised layer to expand and contact. The magnitude of deformation depends on the cement content and material type.

6.3.3.1 Thermal Deformation (Houben)

According to Houben, the Eurocode 2 (2005) advises a coefficient of thermal expansion of $\alpha = 1 \times 10^{-5}$ for concrete. Houben explains that the problem with this is when the time of construction is taken into account the calculation results in pavement failure within the first few days which is not the case. He therefore makes use of Equation 6-31 which is dependent on the Elastic Modulus $E_{cm}(t)$.

$$\boldsymbol{\alpha = 3.095 \cdot 10^{-10} \cdot E_{cm}(t)} \qquad \text{6-31}$$

The total thermal expansion can be calculated with Equation 6-32.

$$\boldsymbol{\varepsilon_T(t) = -\alpha \cdot \Delta T} \qquad \text{6-32}$$

Where:

$\Delta T = T_{road} - T_{daily}$

I.e. the difference in in temperature at t and time of construction

6.3.3.2 Thermal Deformation (Xuan)

Xuan makes use of Houben's total thermal expansion Equation 6-32, however the coefficient of thermal expansion (CTE) was based on his own 1 year shrinkage data. The CTE as seen in Equation 6-33, from observations taking into account RMA content (M), degree of compaction (DC) and cement content (C).

$$CTE = \frac{2.65}{1 + e^{(0.13 \cdot M - 6.04)}} + 0.51 \cdot \ln(C) + 0.37 \cdot \ln\left(\frac{DC}{100}\right) + 6.87 \quad 6\text{-}33$$

This 1 year CTE is then used to calculate $\alpha(t)$, see Equation 6-34.

.

$$\alpha(t) = CTE \cdot \left(0.72 \cdot \left[1 + \left(\frac{t}{0.04}\right)^{-0.38}\right]^{-0.95} + 0.30\right) \quad 6\text{-}34$$

6.3.3.3 Thermal Deformation (Mbaraga)

Mbaraga makes use of 8×10^{-6} for α based on Xuan's above mentioned recommendations for CTMG which is similar to RCA. This α and 28 day Elastic Modulus is used to calculate an unknown constant C_8, see Equation 6-35.

$$C_8 = \frac{E_{cm28\,day}}{\alpha} \quad 6\text{-}35$$

Once C_8 is calculated, it is used similarly as in Houben's Equation 6-31, which re-calculates α with the time dependent Elastic Modulus, see Equation 6-36.

$$\alpha(t) = C_8 \cdot E_{cm}(t) \quad 6\text{-}36$$

6.3.3.4 Conclusion

Xuan's adaptions for thermal deformation was selected for implementation in this study. This choice was substantiated as Xuan's adaptions were based on physical test results. Equations 6-33 and 6-34 were used to determine the CTE for each case investigated namely Andesite 2% continuous, Unexposed RCA 0% and Exposed RCA 0%, see Table 6-4.

Table 6-4: CTE inputs

Material	M [%]	DC	C [%]	CTE
ANDE	100	105	2	7.23
RCA.U	0	105	0.1	8.35
RCA.E	0	105	0.1	8.35

A sensitivity analysis was performed where the influence of cement content, masonry content and degree of compaction on the thermal expansion were compared, see Table 6-5. Figure 6-11 and Figure 6-12 are at 105% and 97% compaction respectively. In each figure the different colours represent material with different percentages of RCA as well as 1% and 4% cement percentages are compared.

Table 6-5: Legend of Figure 6-11 and Figure 6-12

Material	Cement Percentages	
RCA 100%	1%	4%
RCA 65%	1%	4%
RCA 35%	1%	4%
RCA 0%	1%	4%

From both graphs, it can be concluded that degree of compaction has the least effect on thermal expansion. Cement percentage is the second biggest influencing factor, when comparing the 1% and 4%, it can be seen that the 4% always achieves a higher CTE. Lastly the biggest influencing factor is material type. The 100% RCA gives the highest CTE and the 0% RCA i.e. 100% masonry gives the smallest CTE. This suggests that RCA has a bigger influence on CTE than masonry.

It was assumed that the Andesite would be equivalent to Xuan's 100% masonry (0% RCA). This was decided based on Xuan's shrinkage results. The 100% Masonry exhibited the same shrinkage trend as a stabilised granular material and showed no swelling.

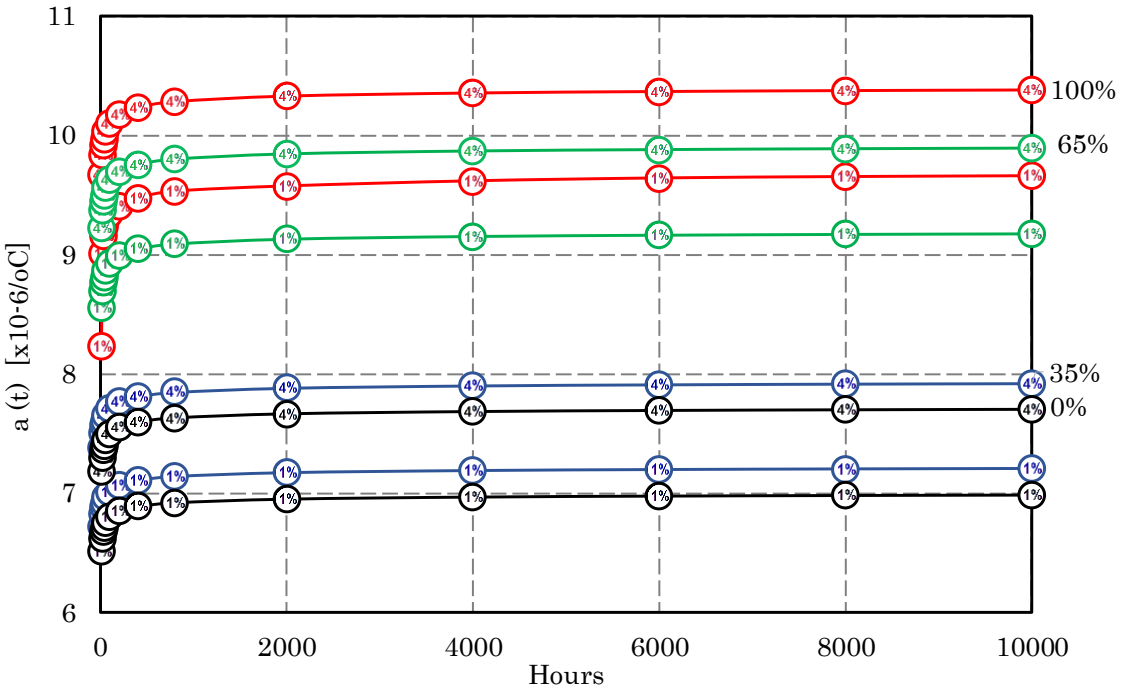

Figure 6-11: Thermal expansion of various percentages of RCA at 1% and 4% and 105 DC

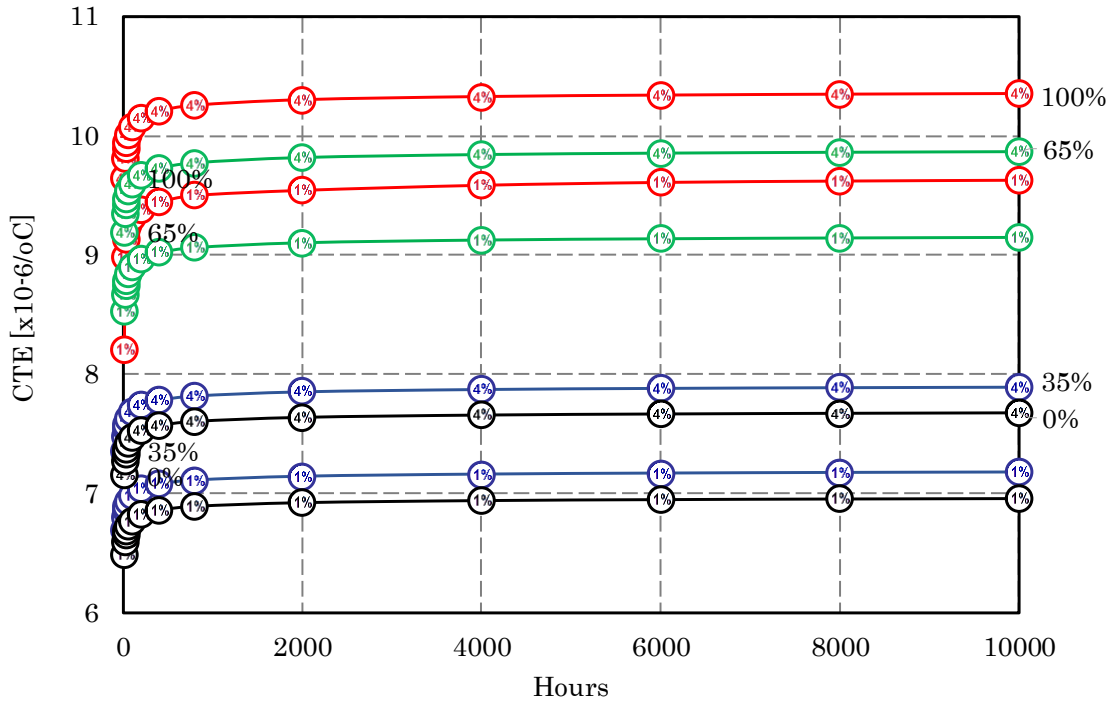

Figure 6-12: Thermal expansion of various percentages of RCA at 1% and 4% and 97 DC

6.3.4 Material Properties

The material properties include compressive strength, tensile strengths and modulus of elasticity. Each sub section explains the process of achieving the actual values based on lab testing as well as the process of using those values in the model to predict the outcomes at the end of the analysis period. Houben and Mbaraga determine time dependent material properties, however Xuan calculates constant values for all material properties. Xuan explains that the induced tensile stress in a CTMG layer acts for an extended period and the response on cracking can be considered under a static level. The time dependent behaviour is included in the shrinkage and thermal deformation factors.

6.3.4.1 Average Compressive Strength

6.3.4.1.1 Average Compressive Strength (Houben)

Houben used the standard Eurocode 2 for the average 28 day compressive strength values, $f_{cm28day}$ for concrete. The average compressive strength changes over time and is expressed in Equation 6-37. The strength coefficient of cement, s is dependent on the type of cement. This time dependent compressive strength is used to calculate a time dependent Elastic Modulus. To clarify all the compressive strengths are cylindrical compressive strengths, not cube strength.

$$\boldsymbol{f_{cm}(t) = \beta_{cc}(t) \cdot f_{cm28\ day} = e^{s\cdot\left(1-\sqrt{672/t}\right)} \cdot f_{cm28\ day}} \qquad 6\text{-}37$$

6.3.4.1.2 Average Compressive Strength (Mbaraga)

Mbaraga makes use of UCS test results as the average compressive strength. The conversion Equation 6-38 was used to convert the 28-day average compressive strength to a 28-day characteristic compressive strength.

$$\boldsymbol{f_{ck28day} = 0.8355\, f_{cm28day}} \qquad 6\text{-}38$$

Mbaraga calculates Elastic Modulus based on flexural beam tests, and therefore does not need to calculate a time dependent compressive strength as with Houben. The characteristic 28 day compressive strength is later used to calculate a 28 day tensile strength with a conversion factor. There are other methods of approaching this, but all approaches have some limitations and one should take cognisance of this. as all results are based on assumptions.

6.3.4.1.3 Average Compressive Strength (Xuan)

Xuan does not specifically calculate a compressive strength. However, the UCS results are utilised to determine the static Elastic Modulus through conversions.

6.3.4.1.4 Conclusion

The average 28-day UCS strength was used as the average compressive strength $f_{cm28day}$. To be conservative, a characteristic value $f_{ck28day}$ was determined by assuming a 95% confidence factor of 1.645, see Equation 6-39, (NIST/SEMATECH, 2013).

$$\boldsymbol{f_{ck28day} = f_{cm28day} - (1.645 \cdot Std\ Dev.)} \quad \text{6-39}$$

As with Mbaraga, the characteristic 28-day compressive strength is used to further calculate a time dependent tensile strength and Elastic Modulus.

6.3.4.2 Average Tensile Strength

6.3.4.2.1 Average Tensile Strength (Houben)

Houben makes use of the average characteristic compressive strength $f_{ck28day}$ when calculating the average tensile strength after 28 days, $f_{ctm28day}$ see Equation 6-40. This conversion is a standard compression to tensile strength conversion for concrete.

$$f_{ctm28day} = 0.3 \cdot f_{ck28day}^{\frac{2}{3}} \quad \text{6-40}$$

As with the average compressive strength, the average tensile strength varies with time and is described with Equation 6-41 which is similar to Equation 6-37.

$$f_{ctm}(t) = \{\beta_{cc}(t)\}^{\partial} \cdot f_{ctm28\ day} = \left\{e^{s\cdot\left(1-\sqrt{672/t}\right)}\right\}^{\partial} \cdot f_{ctm28\ day} \quad \text{6-41}$$

Where:

$\partial = 1$ for $t < 672$ hours (28 days)

$\partial = \frac{2}{3}$ for $t \geq 672$ hours (28 days)

6.3.4.2.2 Average Tensile Strength (Mbaraga)

Mbaraga uses the same relationship for 28-day average compressive strength to 28-day average tensile strength, as in Equation 6-40. He considers a tensile strength that varies with time as mentioned in Equation 6-41. Mbaraga makes use of $\partial = 1$ as a constant for all days tested. This simplification is assumed to be based on the low sensitivity between the two trends for $\partial = 1$ vs $\partial = \frac{2}{3}$.

6.3.4.2.3 Average Tensile Strength (Xuan)

Xuan explores various direct tensile strength models that include the UCS strength see (Xuan, 2012). However, he defines the tensile strength of the material as 80% of the ITS strength, see Equation 6-42.

$$f_{ctm\ 28day} = 0.8 \times ITS \quad \text{6-42}$$

6.3.4.2.4 Conclusion

It was decided to calculate the 28-day direct tensile strength in the same way as Xuan with Equation 6-42 using the 28-day ITS results. This was chosen instead of converting a UCS strength, as ITS results are more realistic. This was taken further and the time dependent tensile strength was calculated with Equation 6-41, in the same way as Mbaraga.

6.3.4.3 Modulus of Elasticity

6.3.4.3.1 Modulus of Elasticity (Houben)

Houben relates the cylindrical 28-day average compressive strength $f_{cm28day}$ to the average modulus of elasticity $E_{cm28day}$ with Equation 6-43.

$$\boldsymbol{E_{cm28day} = 22000 \cdot (0.1 \cdot f_{cm28day})^{0.3}} \qquad 6\text{-}43$$

The Elastic Modulus is time dependent and is calculated with Equation 6-44.

$$\boldsymbol{E_{cm}(t) = \left(\frac{f_{cm28day}(t)}{f_{cm28day}}\right)^{0.3} \cdot E_{cm28day}} \qquad 6\text{-}44$$

6.3.4.3.2 Modulus of Elasticity (Mbaraga)

Mbaraga calculated $E_{cm28day}$ from the flexural beam test. This value was used in combination with a similar equation used with the average tensile strength to achieve the time dependant Elastic Modulus, see Equation 6-45.

$$\boldsymbol{E_{cm}(t) = \{\beta_{cc}(t)\}^{\partial} \cdot E_{cm28\ day} = \left\{e^{s\cdot\left(1-\sqrt{672/t}\right)}\right\}^{\partial} \cdot E_{cm28\ day}} \qquad 6\text{-}45$$

6.3.4.3.3 Modulus of Elasticity (Xuan)

A monotonic or static Elastic Modulus was determined from a monotonic compression test. This E_{static} was calculated per material analysed and was used as a constant in the model. Xuan investigated many different relationships between UCS, density (D) and E_{static} and resulted in Equation 6-46.

$$\boldsymbol{E_{static} = \frac{366.8 \cdot UCS^{0.56} \cdot D}{1000^{3.8}}} \qquad 6\text{-}46$$

6.3.4.3.4 Conclusion

The 28-day Elastic Modulus was calculated with Equation 6-47 from Molenaar (2007) as it gave the most realistic results. The time dependent Elastic Modulus was thereafter calculated with Mbaraga's Equation 6-45. This was done for each mix.

$$\boldsymbol{E_f = 1435 \cdot UCS^{0.885}} \qquad 6\text{-}47$$

6.3.5 Relaxation Factor Occurring Tensile Stresses

According to Xuan (2012), tensile stresses build up in CTM when shrinkage is restrained. As the material gains in strength, all the cement particles react with the water present, long term drying shrinkage will occur due to the absence of water.

As cement treated material is partially elastic, it follows Hooke's Law. However, due to the semi-static loading, relaxation of the material must be taken into account. This in turn means the reduction of tensile stresses over time (Houben, 2008). There has been little research done on stress relaxation for CTM. However, research of creep and stress relaxation in concrete has been explored (Xuan, 2012).

Jansen van Rensberg (2015), explains that initially concrete experiences elastic deformation that seems to be independent of time, when a stress, that is less than the yield stress, is applied. When this stress is maintained for a long period of time, an additional time dependent deformation occurs known as creep. A creep test requires

constant stress, and measures long term deformation. If the deformation/ length of specimen is kept constant while the specimen is loaded, the stresses in the material will slowly reduce over time. This is referred to as relaxation of the material.

6.3.5.1 Concrete Relaxation Factor (Houben)

Concrete also follows Hooke's law, and as mentioned before because of semi-static loading, relaxation of the material needs to be included (Houben, 2008). Houben makes use of Equation 6-48, which includes the relaxation factor into Hooke's law.

$$\boldsymbol{\sigma(t) = e^{-0.0003 \cdot t} \cdot E_{cm}(t) \cdot \varepsilon(t)} \tag{6-48}$$

Without the relaxation factor, the calculation results would lead to total pavement destruction within the analysis period of 360 days, which is unrealistic (Houben, 2008).

6.3.5.2 CTMG Relaxation Factor (Xuan)

Xuan (2012), follows the same principle as Houben with regards to the relaxation factor included into Hooke's law, see Equation 6-49, however he altered the relaxation factor to better suit CTMG.

$$\boldsymbol{\sigma(t) = R(t) \cdot E(t) \cdot \varepsilon(t)} \tag{6-49}$$

He explored 4 different concrete stress relaxation models, and decided on the following Equation 6-50 as his basis to adapt which would best suit his data.

$$\boldsymbol{R(t) = a \cdot t^{-b}} \tag{6-50}$$

Xuan produced 3 stress relaxation Equations 6-51, 6-52 and 6-53 which are high, average and low relaxation.

$$R(t) = 2.59 \cdot t^{-0.3} \quad 6\text{-}51$$

$$R(t) = 2.22 \cdot t^{-0.25} \quad 6\text{-}52$$

$$R(t) = 1.89 \cdot t^{-0.2} \quad 6\text{-}53$$

The reason for producing 3 equations was to perform a relative analysis, as there was not enough data available to properly calibrate the results. A relative analysis would better analyse the influence of various simulation conditions (Xuan, 2012).

Xuan (2012), concluded that stress relaxation has a large influence on the build-up of induced tensile stresses as well as crack patterns in a CTMG layer in the road. A lower stress relaxation factor, will give more cracks and smaller final crack spacing.

6.3.5.3 CTM Relaxation Factor (Mbaraga)

Mbaraga (2015), performed a sensitivity analysis with Houben's concrete formula and Xuan's 3 CTMG formulas. He discovered that Xuan's average best suited his data.

6.3.5.4 Conclusion

This study makes use of Xuan's average relaxation factor based on Mbaraga's observations. However, this forms part of the limitations, as all these models are empirical data as there is no standard relaxation test that can be used to calibrate these results.

6.3.6 Sliding Friction Factor

As the layer undergoes shrinkage, sliding friction is generated between the layer and the surrounding layers. Jung et al (Jung et al., 2010) refers to a Frictional Stiffness which is the measured slope of frictional resistance (MPa) against the horizontal movement of the layer (m). High friction conditions generate more cracks due to the friction induced

restraint between the layers. This substantiates the increase in friction coefficient as more cracking occurs, (Jung et al., 2010).

6.3.6.1 Sliding Friction Factor (Houben)

Houben makes use of a friction factor of 1 initially, and after the first crack he arbitrarily increases it by 10 (f = 10 ·1). His reasoning is that if it is not increased, unrealistically large crack widths occur.

6.3.6.2 Sliding Friction Factor (Xuan)

Xuan assumes a friction factor of 3 according to Penev & Kawamura (1993).

6.3.6.3 Sliding Friction Factor (Mbaraga)

Mbaraga makes use of a friction factor of 3.8 based on field pavement studies.

6.3.6.4 Conclusion

According to Jung et al. (2010), the frictional coefficient of a CTM ranges for low – medium and high are between 3.5 – 8.9 -13 respectively, see Table 6-6. Therefore a beginning frictional factor was assumed as 3.8 as with Mbaraga.

Table 6-6: Value range of frictional coefficient, (Jung et al., 2010)

Subbase Type	Frictional Coefficient (Low - Mean -High)
Fine-grained soil	0.5 - 1.1 - 2.0
Aggregate	0.5 - 2.5 -4.0
Lime-stabilized clay	3.0 - 4.1 -5.3
ATB	2.5 -7.5 - 15.0
CTM	3.5 - 8.9 - 13.0
Soil cement	6.0 - 7.9 - 23.0
LCB	1.0 - 6.6 - 20.0

Chapter 7

Modelling of Shrinkage Results

This chapter utilises the inputs and various equations presented in Chapter 6 in the model. The three materials that are modelled in this chapter are Andesite 2% continuous, Unexposed RCA 0% and Exposed RCA 0%. The Andesite 2% was selected as a benchmark for the 0% Unexposed RCA, as in Chapter 5 it was compared to an equivalent granular (Andesite) with 2% cement stabilisation. The 0% Exposed RCA was selected to analyse the sensitivity of the exposure in comparison to the 0% unexposed RCA.

7.1 Seasonal and Temperature Variations

The seasonal and temperature variations throughout the year have a direct influence on the thermal strain. Daily, seasonal and hydration temperature fluctuations are included in the final road temperature assumption. The hydration temperature has the maximum influence at hour 7 and then reduces rapidly, see Figure 7-1 and Figure 7-2 of the model. These parameters remained constant for each material investigated.

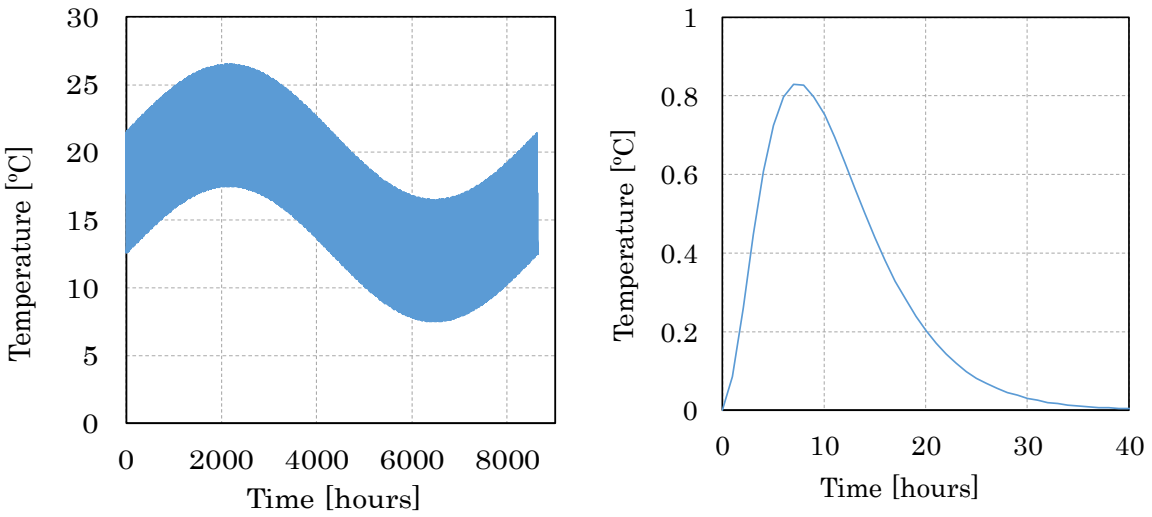

Figure 7-1: Climate temperature (left) hydration temperature (right)

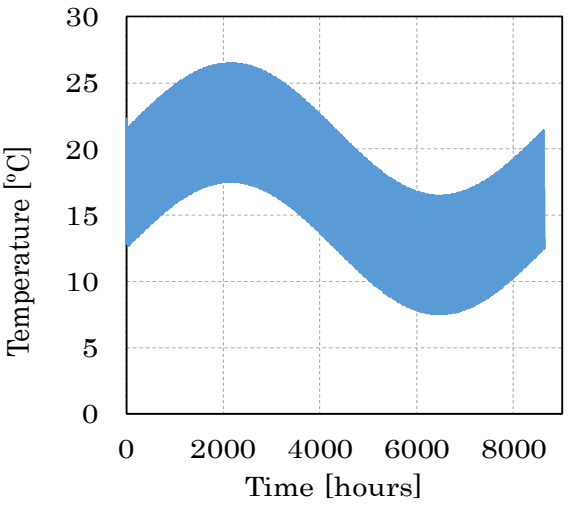

Figure 7-2: Road temperature

7.2 Deformation

The total deformation consists of a thermal deformation and drying shrinkage, see Figure 7-3 and Figure 7-4. For the thermal deformation calculation, see Section 6.3.3 . There is not a substantial difference in magnitude between thermal deformations of the various materials and their corresponding cement percentages.

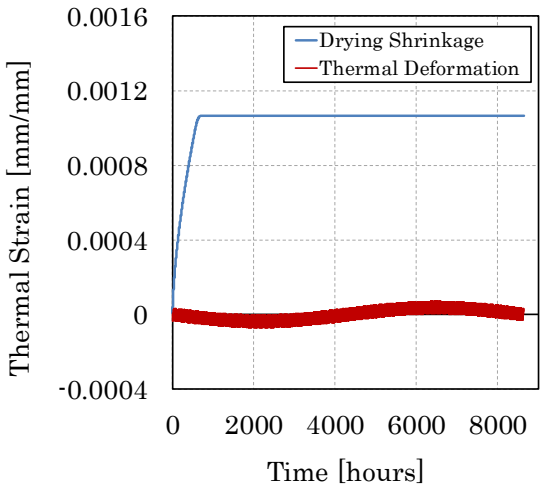

Figure 7-3: Andesite 2% drying shrinkage and thermal strain

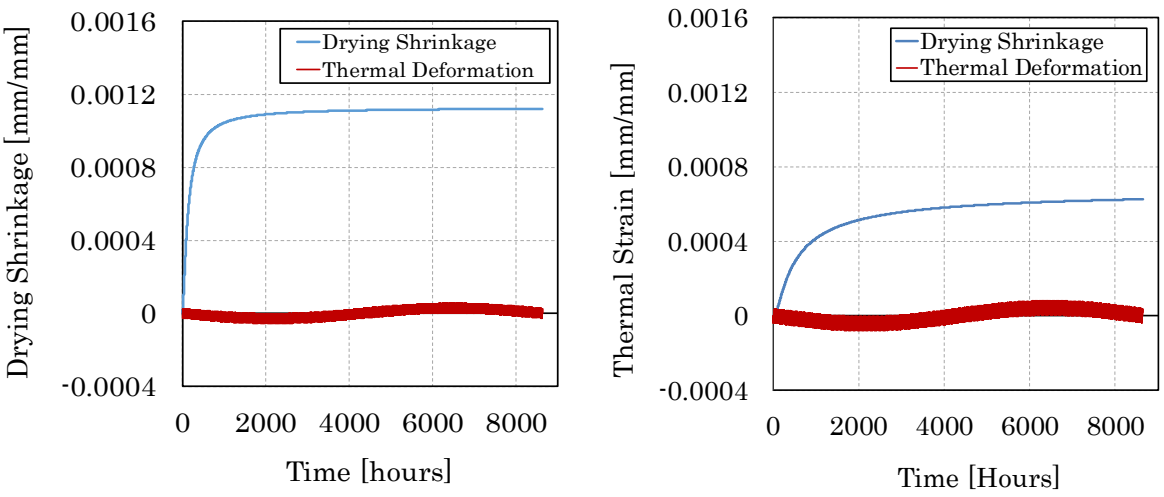

Figure 7-4: Exposed and Unexposed RCA 0% drying shrinkage and thermal strain

The drying shrinkage was modelled based on Xuan's shrinkage Equation 6-30. This equation was used to model axial shrinkage from 0 – 365 days, as it was the best fit for the shrinkage data from the lab testing in Section 5.2. It is clear that drying shrinkage has the biggest influence on total deformation. The drying shrinkage of Exposed RCA and Andesite have same order size while the Unexposed RCA is about 60% of that, see Figure 7-5 and Figure 7-6.

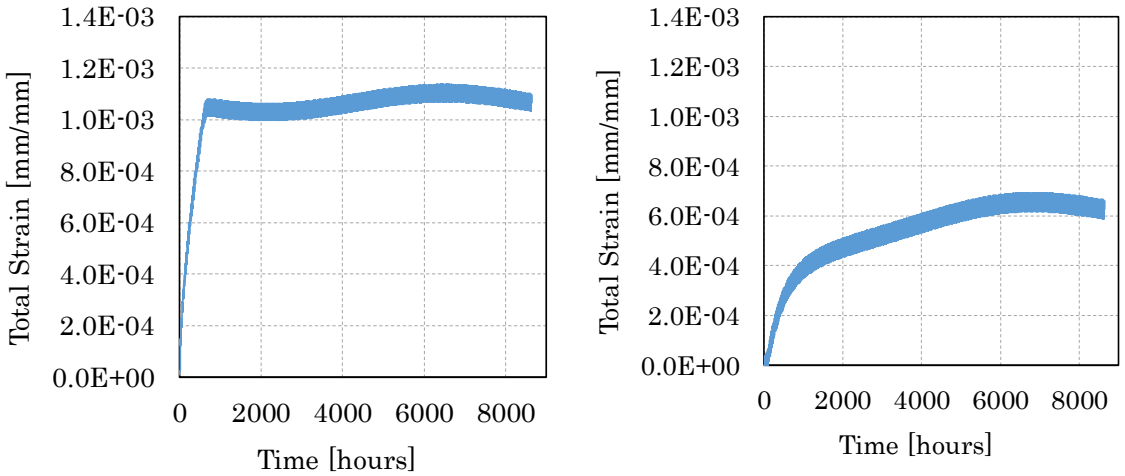

Figure 7-5: Total deformation of Andesite 2% (right) and Unexposed RCA 0% (left)

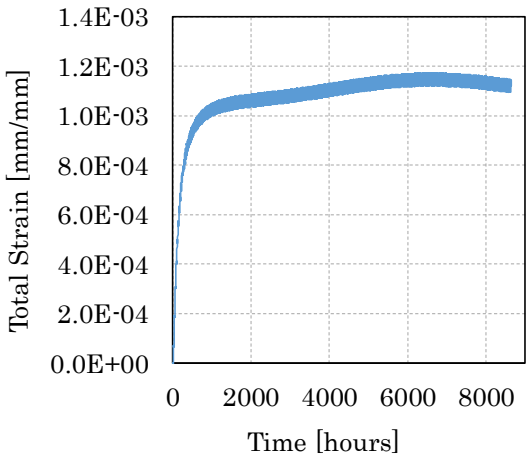

Figure 7-6: Total deformation of Exposed RCA 0%

7.3 Tensile Strength vs Tensile Stress

The average relaxation factor by Xuan was used as it was designed to be used for RCAs. While Andesite is a stabilised granular material, the relaxation factor was used to be consistent.

From Figure 7-7 - Figure 7-9 it can be seen that the Andesite and the Exposed RCA display tensile stresses that exceed the tensile strength even after the stress reduction. The arrows on the magnified figures illustrate where the tensile stress (orange) has exceeded the tensile strength (blue). There is always a reduction in strength at first. Furthermore, as the induced tensile stresses increase, as previously mentioned, the tensile stress again exceeds the tensile strength. This point is illustrated with the second arrow and so forth.

It is considered problematic that quarterly cracks occur within the first 140 hours. The Unexposed RCA however, performs better than the other two materials. After the tertiary crack, the tensile stresses do not further exceed the tensile strength of the material

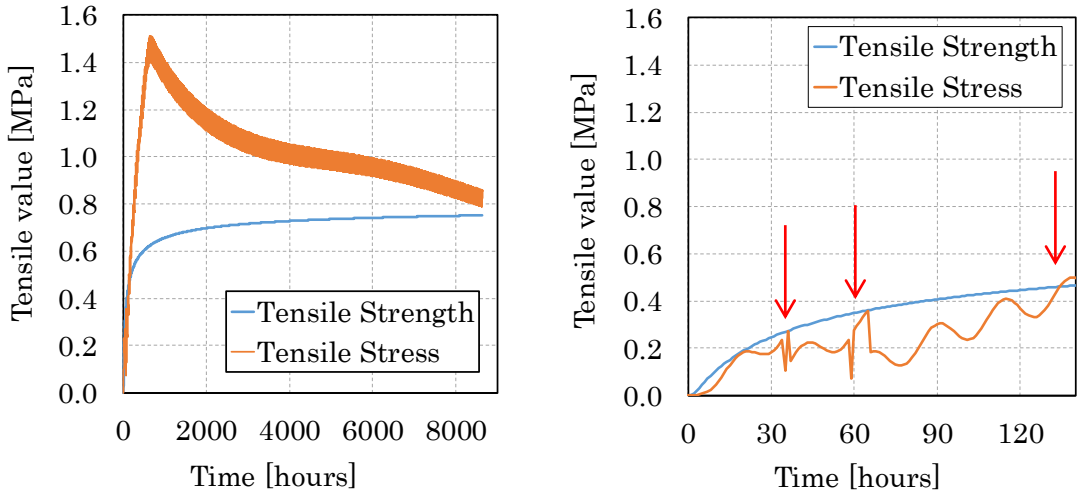

Figure 7-7: Tensile stress vs tensile strength of Andesite 2% (left) and magnified (right)

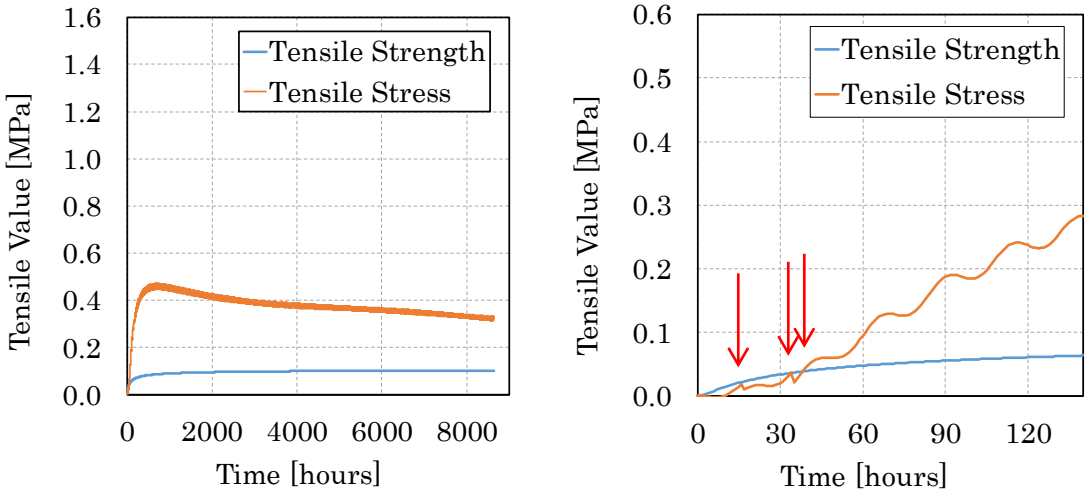

Figure 7-8: Tensile stress vs tensile strength of Exposed RCA 0% (left) and magnified (right)

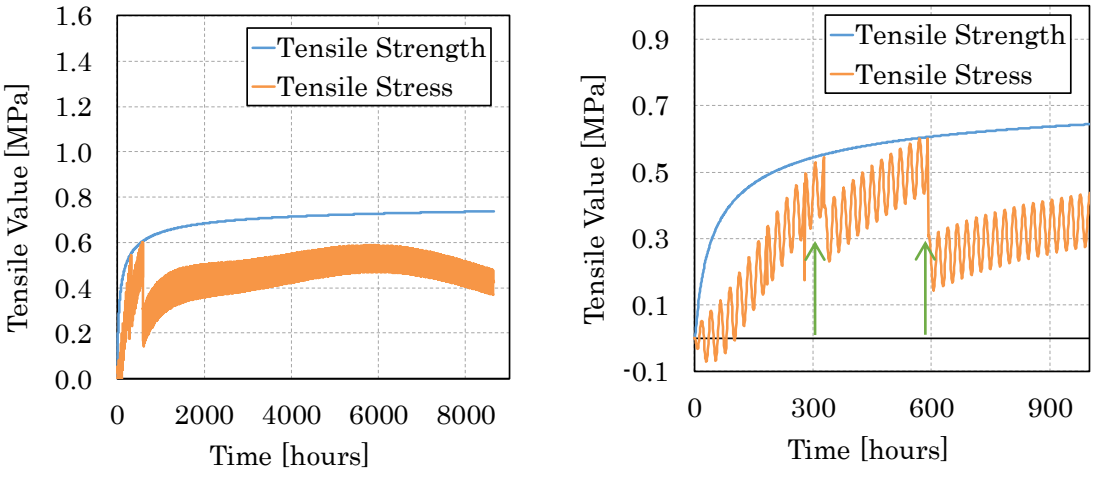

Figure 7-9: Tensile stress vs tensile strength of Unexposed RCA 0% (left) and magnified (right)

7.3.1 Shrinkage Crack Pattern Results

Table 7-1 summarises the crack pattern results for the material in this study and results from Mbaraga's study. See Figure 7-10 - Figure 7-12 for a schematic comparison between the crack patterns of the different materials.

Andesite continuous stabilised at 2% exhibited the following crack pattern:

→ Experiences its primary/secondary crack after 37h (1.5 days) at a close spacing of 3.65m and a width of 0.34mm.

→ The tertiary cracks occur at 66h after construction (2.75 days) at 1.82m spacing and 0.2mm crack width.

→ Quarterly cracks occurred at 135h (5.6 days). Subsequent cracking was not analysed as the layer typifies severe cracking after the occurrence quarterly cracks.

Unexposed RCA stabilised at 0% exhibited the following crack pattern:

→ Experiences its primary/secondary crack after 329h (13.7 days) at a spacing of 13.6m and a width of 1.56mm.

→ The tertiary cracks occur at 593 h after construction (24 days) at 6.79 m spacing and 0.74mm crack width.

→ At this stage, the reduction in stress was adequate and further cracking was not observed.

Exposed RCA stabilised at 0% exhibited the following crack pattern:

→ Experiences its primary/secondary crack after 17h at a very close spacing of 0.27m and a width of 0.009mm.

→ The tertiary cracks occur at 35h after construction (1.5 days) at 0.137m spacing and 0.0076mm crack width.

→ Quarterly cracks occurred at 38h (1.6 days). Subsequent cracking was not analysed as the layer typifies severe cracking after the occurrence quarterly cracks.

Table 7-1: Summary of crack patterns results

Material	C [%]	Crack type	Time of initial crack after construction [h]	Crack spacing [m]	Initial crack width [mm]	Tertiary crack widths [mm]
ANDE	2	Primary/ Secondary	37	3.65	0.34	6.50
		Tertiary	66	1.82	0.20	
		>Quarterly	135	Severe Cracking		
RCA.U	0	Primary/ Secondary	329	13.58	1.56	4.90
		Tertiary	593	6.79	0.74	
RCA.E	0	Primary/ Secondary	17	0.27	0.009	2.32
		Tertiary	35	0.137	0.0076	
		>Quarterly	38	Severe Cracking		

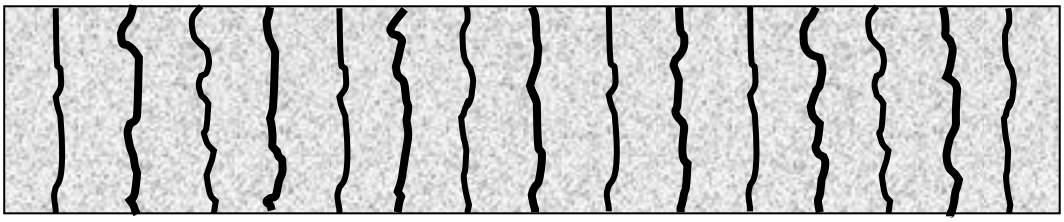

Figure 7-10: Schematic Andesite 2% crack pattern

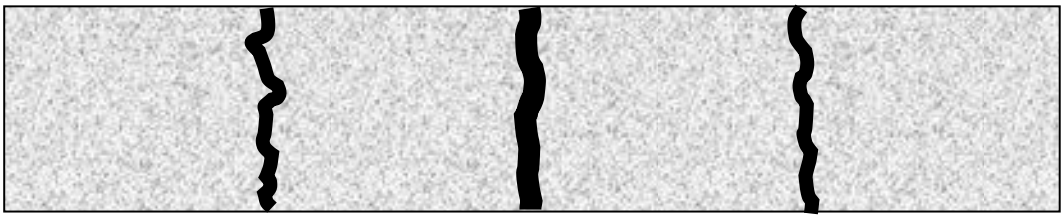

Figure 7-11: Schematic Unexposed 0% crack pattern

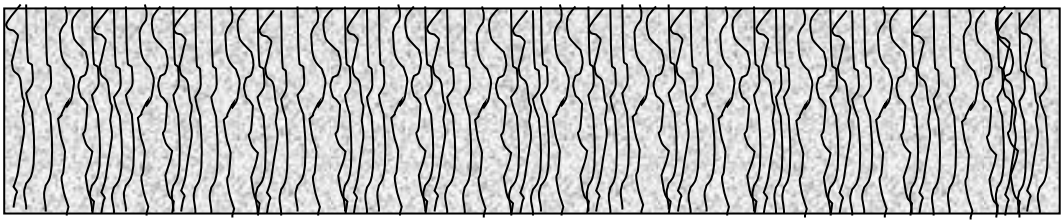

Figure 7-12: Schematic Exposed 0% crack pattern

These results indicate that the Exposed RCA experiences very narrow cracks almost immediately after construction. This is an expected outcome as the Exposed RCA obtained very low ITS values which contributed to a low tensile strength. This behaviour is confirmed, as mentioned by the TRH13 (1986) in Chapter 2, where the stress exceeds the tensile strength at relatively low tensile strength. The cracks shown are hair line cracks that are very closely spaced, see Figure 7-12.

The Andesite results show bigger initial crack widths and larger spacings, however these all occur in the first 5.6 days. The Andesite showed expected ITS values, however due to stabilisation, the UCS strengths also increased. This causes a stiffer pavement and increases the potential tensile stress build up in the layer.

Due to the stress reduction of the Unexposed RCA, the stresses built up in the pavement will not exceed the strength of the material after tertiary cracking. This has largely to do with the low drying shrinkage of the material. A possible reason is its self-cementing property. It therefore undergoes a different drying shrinkage mechanism due to the additional active latent cement content present. Unexposed RCA results in bigger yet manageable initial cracks (1.56mm) at 13.6m spacings and further 0.74mm cracks at 6.79m spacings. The TRH13 again verifies these findings as the tensile stress exceeds the tensile strength at a relatively high tensile strength which leads to wider cracks that spaced further apart.

7.3.1.1 Influence of Self - Cementation and Axial Shrinkage on Shrinkage Cracking

Semugaza categorises the crack patterns of Mbaraga's modelled results in terms of the maximum axial shrinkage. He defines three categories that form the crack pattern envelope:

→ Acceptable axial shrinkage: 0 – 475 [$\times 10^{-6}$]

→ Medium axial shrinkage: 475 – 800 [$\times 10^{-6}$]

→ Unacceptable axial shrinkage: 800 – 4000 [$\times 10^{-6}$]

From Mbaraga's results, the "acceptable" typically shows no cracking. The "medium" range includes cracks up to tertiary cracks. The "unacceptable" range include cracks past quarterly cracks and is defined as severe cracking, see Table 7-2.

Table 7-2: Mbaraga's Ferricrete and Hornfels cracking vs Andesite

Material	C [%]	Crack type	Average Max Axial Shrinkage [$\times 10^{-6}$ mm]
Hornfels, (Mbaraga, 2015)	2	No Cracks/ *Acceptable*	250
	3	No Cracks/ *Acceptable*	499
	6	Severe Cracking/ *Unacceptable*	970
Ferricrete, (Mbaraga, 2015)	4	Severe Cracking/ *Unacceptable*	1549
	6	Severe Cracking/ *Unacceptable*	3956
Andesite	2	Severe Cracking/ *Unacceptable*	1067
Unexposed RCA	0	Tertiary Cracks/ *Medium*	680
Exposed RCA	0	Severe Cracking/ *Unacceptable*	1127

The Exposed RCA exhibit many initial, narrow hair line cracks. Tertiary crack widths were the last crack widths recorded due to limitations of the analysis. It was clear from the tensile stress vs strength graphs, that there would be many more cracks. The crack widths at tertiary cracks are 2.32mm, with the potential to increase. These fine cracks are unlikely to propagate through to the surfacing. However, the layer will turn into an equivalent granular layer within 1 year, as seen from the analysis. This will decrease the Elastic Modulus, which could leave the subgrade in a vulnerable state. It can be assumed that the behaviour is similar to a granular material with little self-cementation.

The Andesite exhibit wider initial cracks than that of the Exposed RCA, but narrower initial cracks than the Unexposed RCA. However, after 1 year the crack width will increase to 6.5mm. A crack wider than 6mm is considered severe according to Adaska & Luhr, (2004). Again from the tensile stress vs tensile strength graphs, it is likely that there will be cracking past tertiary cracks. These 6.5mm cracks are more likely to propagate through to the asphalt surfacing causing poor load transfer and negatively effecting riding quality. The pavement is therefore vulnerable to water ingress. The layer will eventually reach equivalent granular status, but will have a higher Elastic Modulus than the Exposed RCA due larger intact sections.

The Unexposed material has the widest initial cracks of 1.56mm. After 1 year the cracks widths will increase to 4.9mm, this is not as severe compared to Andesite. It will have the highest Elastic Modulus as it obtained the widest spacing, leaving larger intact sections. The material displays high levels of self-cementation as expected. This material can be assumed to be the equivalent of a lightly stabilised layer.

Chapter 8

Conclusions and Recommendations

This chapter aims to conclude this study by meeting all the objectives and recommending further insights that can benefit other research studies.

Objectives and conclusions:

→ *To gain an understanding on the variables that influence the durability behaviour of stabilised materials such as cement content, moisture content, curing period, material density, plasticity and host material in order to understand how this manifests into shrinkage cracking.*

All the above mentioned factors influence the potential shrinkage magnitude, which in turn influences the shrinkage cracking. From the Literature Study it is concluded that host material has the largest influence on shrinkage, then cement content. Host material is a broad term as it includes plasticity, water absorption and porosity, grading and aggregate mineralogy. These in effect have direct influences on the potential density and moisture content of a material which also directly influence drying shrinkage. Drying shrinkage is a complex phenomenon and requires much more research.

→ *To evaluate the active latent cement content of RCA and equate that to an equivalent stabilised granular material.*

As Unexposed RCA contains a significant percentage of active latent cement which influences the properties of the material. It is difficult to accurately quantify the amount of active latent cement present. However it was possible to get a good indication of how RCA compares with a stabilised granular material where the exact cement percentage was known. This was discovered though various tests such as ICC, pH of suspended soils, Atterberg Limits, UCS and ITS testing. It was found that unexposed RCA could be seen as an equivalent 2% cement stabilised granular

material. Although this is not necessarily the case for all RCA, and therefore the preliminary testing specified in this study are crucial.

→ *To predict the shrinkage crack pattern i.e. the width and spacing of cracks within a RCA and CTM pavement layer.*

Three materials were modelled with an adapted Houben Shrinkage Crack Model, namely Andesite (2%), Unexposed RCA (0%) and Exposed RCA (0%). The shrinkage crack pattern of the Unexposed RCA exhibited the best results due to its self-cementing property. It yielded slightly larger yet manageable cracks at larger spacings, while still maintaining a stiff Elastic Modulus. Whereas the Andesite revealed smaller initial cracks and at smaller spacings, however resulted in 6.5mm tertiary cracks after 1 year. This suggests that an Andesite pavement demonstrate crack propagation which leaves the pavement vulnerable to water ingress, poor load transfer and therefore poor riding quality. The Exposed RCA revealed the smallest tertiary cracks of 2.32mm after 1 year, however there is still crack growing potential. It is unlikely that these cracks will propagate through to the asphalt surfacing, however may lead to material degradation once trafficked

Further research should include the following:

→ *Relaxation*

There has not been much research done on the relaxation of stabilised materials. Relaxation of CTM and RCA is an essential component in modelling of shrinkage cracking as it reduces the stress build up in the material.

→ *Friction*

The reduction of friction with cracking and how it would affect the shrinkage crack pattern is a worthwhile study.

→ *Humidity*

Humidity had a bigger shrinkage effect on the specimens with the fine grading than that with the fuller grading. However more research is needed in controlled relative humidity environments. Relative humidities that are suggested are 50%

and 100%. Both environments will give an idea of the sensitivity of the material to humidity.

→ *Grading*

A possible investigation could be on the potential for micro cracking of the fine fractions within the larger grading. The influence of a gap grading on RCA would provide more insight into durability issues such as shrinkage, but also the characterisation requirements such as ICC, UCS and ITS.

References

Adaska, W.S. & Luhr, D.R. 2004. Control of reflective cracking in cement stabilized pavements. In *Proceedings of 5th International RILEM Conference on Cracking in Pavements*. 309–316.

Barisanga, F. 2014. Material Characterisation and Response Modelling of Recycled Concrete and Masonry in Pavements. Stellenbosch University.

Bhandari, R.K.M. 1975. Factors Influencing the Drying Shrinkage of Cement Stabilised Mixtures. In Vol. 5 *Australian Road Research Board Conference Proc*. 9–23.

Brooks, J.J. 2015. *Concrete and masonry movements*. Oxford: Elsevier.

Campher, L. 2015. Shrinkage and Flexibility Behaviour of Bitumen Stabilised Materials. Stellenbosch University.

Chai, L., Monismith, C.L. & Harvey, J. 2009. *Re - Cementation of Crushed Material in Pavement Bases*. California.

Chakrabarti, S. & Kodikara, J. 2006. Modelling drying shrinkage of cement - stabilised crushed rock. *Proceedings of the Institution of Civil Engineers - Construction Materials*. 159(2):65–75.

Chen, J.J., Thomas, J.J. & Jennings, H.M. 2006. Decalcification shrinkage of cement paste. *Cement and Concrete Research*. 36(7):801–809.

CSIR. 2015. *TRH13: Cementitious Stabilization of Road Materials*.

Domone, P. & Illston, J. 2010. Durbaility of Concrete. In 4th ed. Oxon: Spon Press *Construction materials: Their nature and behaviour*. 184–187.

EdInformatics.com. 1999. *Surface Tension and Capillary Action*. [Online], Available: https://www.edinformatics.com/math_science/surface_tension_capillary_action.htm [2017, December 03].

Freeman, T.J. & Little, D.N. 1998. *Develop maintenance strategy selection procedures for pavements incorporating semi-rigid or chemically stabilized layers*. Texas.

Freeme, C.R. 1984. *Symposium on Recent Findings of Heavy Vehicle Simulator Testing,*

ATC 194 NITRR.

George, K.. 1968. Shrinkage Characteristics of Soil-Cement Mixtures. *Highway Research Record, No. 255*. (January):42–57.

George, K.P. 1969. Cracking in Pavements Influenced by Viscoelastic. P roperties of Soil-Cement. *Highway Research Record*. 263:47–59.

George, K.P. 1990. Characterization and Structural Design of Cement-Treated Base. *Transportation Research Record*. 1288:78–87.

Halsted, G.E. 2010. Minimizing Reflective Cracking in Cement-Stabilized Pavement Bases. In Nova Scotia *Pavement Maintenance and Preservation Session*.

Holt, E.E. 2001. *Early age autogenous shrinkage of concrete*. Vol. 446. Espoo.

Houben, L.J.M. 2008. *Model for transversal cracking in non-jointed plain concrete pavements as a function of the temperature variations and the time of construction*. Delft.

Irwin, G.R. 1957. Analysis of Stress and Strains Near the End of a Crack Traversing a Plate. *Journal of Applied Mechanics*. 24:361–364.

Johannes, H. & Rensburg, J. Van. 2015. Crack Distributions and Characteristics of Continuously Reinforced Concrete Pavements. Stellenbosch University.

Jung, Y. su, Zollinger, D.G., Hooi Cho, B., et al. 2010. *Subbase and Subgrade Performance Investigation and Design Guidelines for Concrete Pavement*. Texas.

Li, X. 2014. Shrinkage Cracking of Soils and Cementitiously-Stabilized Soils: Mechanisms and Modeling. Washington State University.

Ma, B., Wen, X., Wang, M., et al. 2007a. Drying Shrinkage of Cement-Based Materials Under Conditions of Constant Temperature and Varying Humidity. *Journal of China University of Mining and Technology*. 17(3):428–431.

Ma, B., Wen, X., Wang, M., et al. 2007b. Drying Shrinkage of Cement-Based Materials Under Conditions of Constant Temperature and Varying Humidity. *Journal of China University of Mining and Technology*. 17(3):428–431.

Mbaraga, A.N. 2015. Shrinkage characterisation, behavioural properties and durability of cement-stabilised pavement materials. University of Stellenbosch.

Molenaar, A.A.A. 2007. *Deign of Flexible Pavments*. Netherlands, Delft.

Molenaar, A. & Van Niekerk, A.A. 2002. Effects of gradation, composition, and degree of compaction on the mechanical characteristics of recycled unbound materials. *Transportation Research Record:Journal of the Transportation Research Board*. January(1787):73–82.

Morris, P.H. 2005. Plastic Cracking of Concrete - The Roles of Osmotic and Matric Suctions. *6th International Congress, Global Construction: Ultimate Concrete Opportunities*. 1:407–415.

Mukherjee, D. 2014. Determination of Variation of Soil Characteristics due to Lime Stabilisation. *International Journal of Civil Engineering and Technology*. 5(9):976–6308.

Neithalath, N., Pease, B., Moon, J.-H., et al. 2005. Considering Moisture Gradients and Time - Dependent Crack Growth in Restrained Concrete Elements Subjected to Drying. *Concrete Composites and Structures*. January:279–290.

Netterberg, F. & Paige-Green, P. 1984. *Carbonation of lime and cement stabilized layers in road construction*. Pretoria.

van Niekerk, A.. & Huurman, M. 1995. *Establishing Complex Behaviour of Unbound Road Building Materials from Simple Material Testing, Laboratory for Road and Railroad Research*. Dleft.

Van Niekerk, A.A. 2002. Mechanical Behavior and Performance of Granular Bases and Sub-bases in Pavements. DUP Science.

NIST/SEMATECH. 2013. *e-Handbook of Statistical Methods*. [Online], Available: http://www.itl.nist.gov/div898/handbook/ [2017, November 09].

Norling, L.T. 1973. Minimizing reflective cracks in soil-cement pavements: a status report of laboratory studies and field practices. *Highway Research Record*. 442:22–33.

Owens G. 2012. *Fundamentals of concrete*. Second ed. Midrand : Cement and Concrete Institute.

Paige-Green, P. 2008. A Reassessment of Some Road Material Stabilization Problems. *Proceedings of the 27th Southern African Transport Conference (SATC 2008)*. (July):125–134.

Paige-Green, P. 2016. Durability of Cemented Materials. In Stellenbosch *Pavement Materials 1: Granular and Lightly Cemented Materials*.

Penev, D. & Kawamura, M. 1993. Estimation of the spacing and the width of cracks caused by shrinkage in the cement-treated slab under restraint. *Cement and Concrete Research*. 23(4):925–932.

Poon, C., Qiao, X. & Chan, D. 2006. The cause and influence of self-cementing properties of fine recycled concrete aggregates on the properties of unbound sub-base. *Waste Management*. 26(10):1166–1172.

Rululuza, B. 2011. The Use of Gypsum Blocks to Measure Suction Pressure in Relation to Grading of a Crushed Base Material. University of Stellenbosch.

SANRAL. 2014a. Chapter 10: Pavement Design. In 2nd ed. South Africa: South African National Roads Agency SOC Ltd *South African Pavement Engineering Manual*. 1–140.

SANRAL. 2014b. Chapter 2: Pavement Composition and Behaviour. In 2nd ed. South Africa: South African National Roads Agency SOC Ltd *South African Pavement Engineering Manual*.

SANRAL. 2014c. *Chapter 3: Materials Testing*. Second ed.

SANS 3001. 2014. *Civil engineering test methods Part GR57: Determination of the initial stabilizer consumption of soils and gravels*.

Semugaza, G. 2016. Comparative Shrinkage Properties of Pavement Materials Including Recycled Concrete Aggregates With and Without Cement Stabilisation. Stellenbosch University.

Silva, R. V, De Brito, J. & Dhir, R.K. 2014. Properties and composition of recycled aggregates from construction and demolition waste suitable for concrete production. *Construction and Building Materials*. 65:201–217.

Strauss, P.J. & Van der Walt, N. 1989. Stress absorbing membranes and flexible asphalt overlays to prevent reflection cracking at joints or cracks in stiff pavements. In Swaziland *5th Conference on Asphalt pavements for Southern Africa (capsa 89)*. 31–35.

Tawine, J.F. 2017. The Use of Chemical and Strength Tests for Evaluating the Self-Cementing Action of Recycled Concrete Aggregate. Stellenbsoch University.

Tazawa, E. ichi, Miyazawa, S. & Kasai, T. 1995. Chemical shrinkage and autogenous shrinkage of hydrating cement paste. *Cement and Concrete Research*. 25(2):288–292.

Theyse, H.., De Beer, M. & Rust, F.C. 1996. Overview of South African Mechanistic Pavement Design Method. *Transportation Research Record*. 1539(1):6–17.

TMH1. 1986. *Standard Methods of Testing Road Construction Materials*.

TMH 9. 1992. *Pavement Management Systems: Standard Visual Assessment Manual for Flexible Pavements*. Pretoria: Department of Transport.

TRH13. 1986. *Technical Recommendations for Highways 13: Cementitious Stabilizers in Road Construction*. Pretoria: Department of Transport of Republic of South Africa.

TRH14. 1985. *Technical Recommendations for Highways 14: Guidelines for Road Construction Materials*. Pretoria: Department of Transport of Republic of South Africa.

TRL. 2003. *Literature Review: Stabilised Sub-Bases for Heavily Trafficked Roads*. Philippines.

Western Cape Goverment. 2016. *No Title*.

Winston, P.W. & Bates, D.H. 1960. Saturated Solutions For the Control of Humidity in Biological Research. *Ecology*. 41(1):232–237.

Worrell, E., Price, L., Martin, N., et al. 2001. Carbon dioxide emissions from the global cement industry. *Annual review of energy and the environment*. 26(1):303–329.

Xuan, D. 2012. Cement Treated Recycled Crushed Concrete and Masonary Aggregates for Pavements. Wuhan University of Technology.

Van Zyl, E.B. 2015. Influence of Specimen Geometry and Grading Curve on the Performance of an Unbound Granular Material. (March):223.

Appendices

Table A - 1: UCS strength, bulk density and moisture contents

Material	UCS Strength [kN]	UCS Strength [Mpa]	Average [Mpa]	Standard Deviation	Moisture [%]	Bulk Density [kg/m3]	Average Bulk density [kg/m3]
	29.0	3.7				2482	
ANDE - C2	25.3	3.2	3.6	0.3	5.55	2500	2493
	29.5	3.8				2499	
	44.8	5.7				2506	
ANDE - C4	36.2	4.6	5.3	0.6	5.49	2504	2505
	44.3	5.6				2506	
	28.5	3.6				2445	
ANDE - G2	23.9	3.0	3.5	0.4	5.73	2462	2457
	28.9	3.7				2463	
	50.9	6.5				2465	
ANDE - G4	49.8	6.3	6.5	0.1	5.40	2464	2465
	52.0	6.6				2465	
	33.1	4.2				2464	
HORN - C2	30.4	3.9	4.2	0.3	5.99	2463	2470
	34.6	4.4				2482	

	54.6	6.9				2470	
HORN - C4	51.7	6.6	6.4	0.7	5.50	2470	2469
	44.5	5.7				2466	
	37.2	4.7				2242	
RCA.U - C0	36.3	4.6	4.9	0.4	11.14	2221	2236
	41.6	5.3				2245	
	65.5	8.3				2219	
RCA.U - C2	31.1	4.0	7.7	0.8	11.50	2230	2232
	56.2	7.2				2248	
	7.9	1.0				2260	
RCA.E - C0	8.0	1.0	1.1	0.2	12.07	2262	2263
	10.8	1.4				2268	
	72.1	9.2				2292	
RCA.E - C2	69.9	8.9	8.7	0.5	10.80	2277	2282
	64.0	8.1				2277	

Table A - 2: ITS strength, bulk density and moisture results

Material	ITS Strength [kN]	ITS Strength [Mpa]	Average [Mpa]	Standard Deviation	Moisture [%]	Bulk Density [kg/m3]	Average Bulk density [kg/m3]
ANDE - C2	7.0	0.9	0.90	0.07	5.3	2493	2571
	6.9	0.9				2590	
	8.3	1.1				2590	
	7.1	0.9				2591	
	7.2	0.9				2591	
ANDE - C4	16.0	2.0	1.80	0.13	5.2	2595	2592
	13.7	1.7				2595	
	14.1	1.8				2591	
	13.2	1.7				2591	
	14.3	1.8				2585	
ANDE - G2	6.7	0.9	0.80	0.08	5.7	2504	2497
	6.8	0.9				2504	
	6.4	0.8				2501	
	5.7	0.7				2501	
	6.6	0.8				2488	
	7.7	1.0				2488	
ANDE - G4	16.1	2.0	2.00	0.24	5.5	2541	2545
	14.3	1.8				2541	
	13.5	1.7				2541	
	14.4	1.8				2549	
	14.4	1.8				2549	
	14.4	1.8				2549	
	19.2	2.4				2546	
	16.8	2.1				2546	

HORN - C2	10.9	1.4	1.10	0.15	5.5	2506	2505
	8.3	1.1				2506	
	8.7	1.1				2498	
	9.2	1.2				2498	
	8.4	1.1				2508	
	7.2	0.9				2508	
	7.8	1.0				2508	
HORN - C4	15.5	2.0	2.00	0.14	5.5	2493	2504
	17.9	2.3				2493	
	16.1	2.0				2494	
	16.2	2.1				2494	
	15.6	2.0				2526	
	14.7	1.9				2526	
RCA.U - C0	6.2	0.8	0.82	0.03	11.1	2205	2211
	6.7	0.9				2182	
	6.4	0.8				2246	
RCA.U - C2	13.3	1.7	1.69	0.06	11.5	2224	2224
	13.7	1.7				2222	
	12.7	1.6				2225	
RCA.E - C0	0.9	0.1	0.11	0.00	12.1	2279	2257
	0.8	0.1				2257	
	0.9	0.1				2234	
RCA.E - C2	17.9	2.3	2.44	0.15	10.8	2292	2292
	19.4	2.5				2292	
	20.3	2.6				2292	

Note: There are more Hornfels and Andesite ITS samples as they were the first materials tested and many repeats were made for surety.